Rec'd 8/8/66

DESIGN OF AN AUTOMATED STELLAR PROPER MOTION MEASURING SYSTEM

By James S. Newcomb
George E. Zenk
Anton E. LaBonte

Prepared by the Aerospace Research Department of Control Data Corporation under Purchase Order F8711 issued by the University of Minnesota under prime contract NSR 24-005-062

for

NATIONAL AERONAUTICS AND SPACE ADMINISTRATION

Period covered: July 1, 1965 through June 30, 1966

TABLE OF CONTENTS

LIST OF FIGURES

LIST OF FIGURES (concluded)

LIST OF TABLES

DESIGN OF AN AUTOMATED STELLAR PROPER MOTION MEASURING SYSTEM

By James S. Newcomb
George E. Zenk
Anton E. LaBonte

SUMMARY

This report presents the design for a scanning system for measuring the stellar proper motions recorded on pairs of star plates of the same regions of the sky taken a decade apart for the National Geographic-Mount Palomar Observatory Sky Survey. The laser beam-rotating prism scanner is described and its resolving power in detecting the faintest stars now detectable by "blink machine" methods is evaluated. The functions and properties of the electronic signal processing and automatic gain control systems are presented. A computational program by which stellar proper motions may be identified and documented is set forth.

I. INTRODUCTION

Stellar proper motion is the movement of certain stars with reference to "fixed" stars. Proper motion is a characteristic of stars relatively close to the earth. Stars which have proper motions and are faint--of about tenth to twentieth magnitudes--are of especial interest because information about their distance, color, and brightness can supply clues to the understanding of the important process of stellar evolution.

Proper motions are measured by direct comparison of the positions of images of stars or pairs of star plates taken ten or more years aprart. The usual measurement is a two step process. First, a highly skilled observer locates a proper motion by rapid alternation of his field of view between the two star plates whose fixed star fields match. This is called "blinking" the pair of star plates. The next operation is the measurement of the proper

motion using an accurately calibrated measuring microscope. The proper motions are measured with respect to nearby fixed stars of comparable magnitude.

Automation of the proper motion survey depends on the development of two systems: (1) a scanner capable of measuring rapidly and accurately all of the images of the pairs of star plates, and (2) a data processing system capable of reconstructing star images from the scanner data, recognizing and documenting the proper motions. The present "blink machine" plus measuring machine operation takes over 100 working hours to document one plate pair; the scanning and data reduction systems described in this report reduce the time required by a factor of about forty.

This report summarizes the design and analysis efforts on the Automated Proper Motion Survey subcontract from the University of Minnesota under NASA contract NSR 24-005-062 for the year July 1, 1965 to July 1, 1966.

The aims for the year's efforts have been as follows:

(1) to develop the basic design concepts for the complete automatic system from scanning machine to computer computation,

(2) to design and fabricate the star plate scanning machine,

(3) to fabricate an engineering test model of the scanning machine on which the design parameters can be tested, and

(4) to design and fabricate the detection electronics for the scanning machine.

The design concepts set up for the complete system are shown in Figure 1. In the operation labeled Step 1, the x and y coordinates of each star on each plate, measured to $\pm$ 1 micron, are recorded on two magnetic tape units, one to each plate. The stars are located by a scanning spot microdensitometer whose primary light is that from an He-Ne laser at 6328 angstroms. Each time the scanning spot encounters a star image, signal gates transmit the x and y positions to the tape unit through a buffer. The buffer is necessary to absorb "bursts" of measurements coming faster than the tape can handle them.

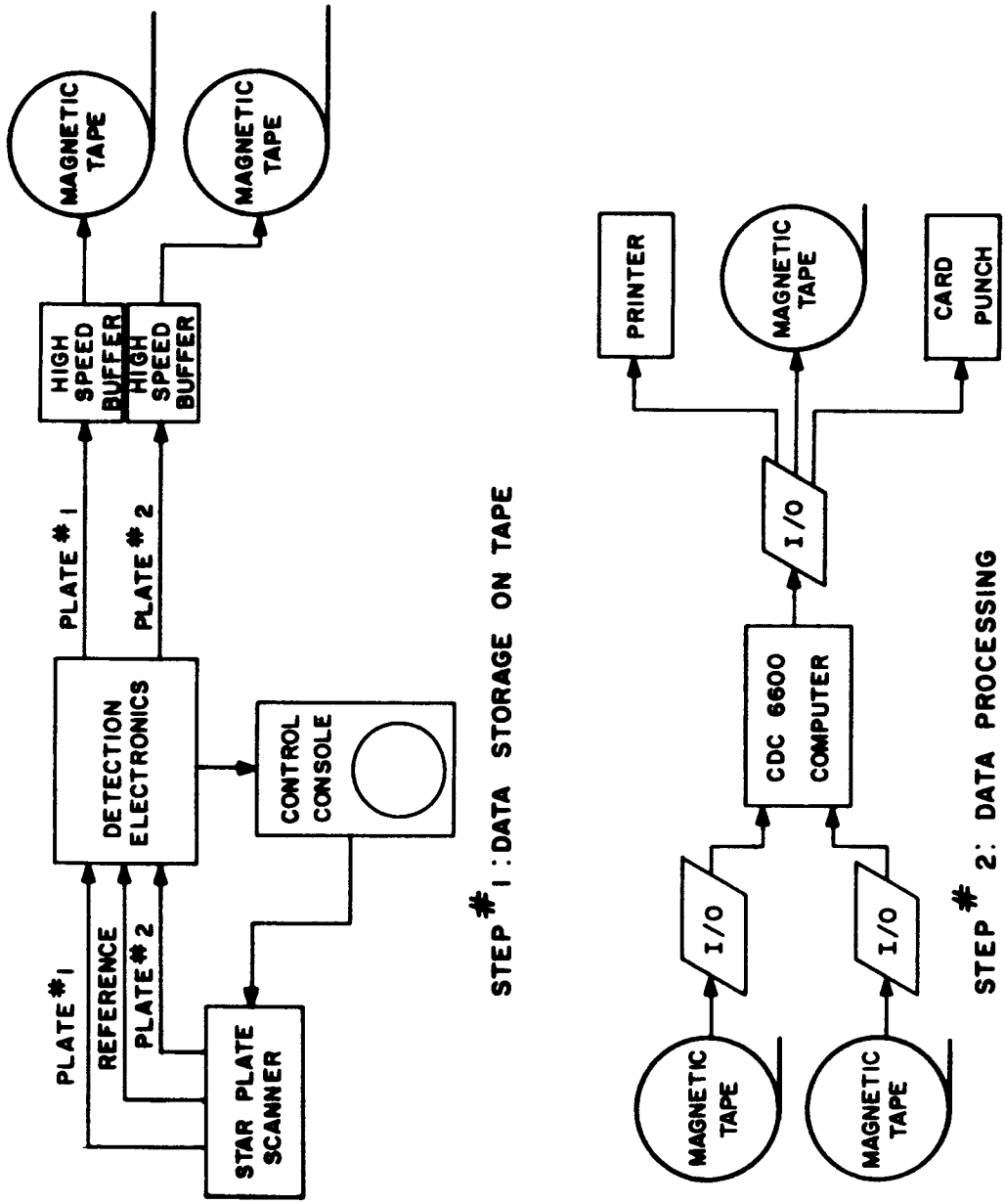

Figure 1: Automation of Stellar Proper Motion, Block Diagram

The control console provides visual scanning displays, alignments and scanning controls for human supervision of the scanning operation.

The detection and documentation of the proper motion stars is accomplished in Step 2 of Figure 1. The data processing consists of the following operations.

(1) The star transits, giving the plate coordinates of each star image, are grouped so that all transits associated with a given star are linked in computer memory locations.

(2) Each linked group is analyzed to obtain the location (in plate coordinates) of the center of the star.

(3) Coordinate transformation of star locations on one plate is performed by the computer to bring the stars on one region of one plate into precise alignment with stars on the other plate.

(4) Star images not alignable by these transformations will be considered proper motion stars and their location and motion will be documented in both plate coordinates and celestial coordinates.

(5) It should be noted that throughout the detection, recording, and computation sections of this system screening techniques--analog, digital, and visual--will be used to reject transits caused by dirt, scratches, or plate flaws.

(6) The proper motions documented by the computer can be recorded on computer printout, punch cards, or magnetic tape.

II. OPTICAL SCANNING SYSTEM

A. Purpose of System

The functions of the optical scanning system are (1) to provide scanning spots moving in synchronization across the two star plates and one reference reticle, and (2) to provide efficient light collection systems to transmit the light passing through the three surfaces to the three photomultipliers.

The scanning motion is provided by the passage of light through a continuously rotating octagonal prism. A transparent prism was chosen for this purpose rather than a mirror prism because the change in path length for the beam passing through the prism as it rotated was less than that of a mirror prism system having the same scan length, thus reducing the change in scanning spot size as the prism rotates.

The scanning beam must be divided into three beams having the same motion on the three surfaces they scan. This is accomplished by two beam splitting cubes and three right angle prisms. A compensating block of glass is necessary in one of the beam paths to equalize the total glass path for the three beams.

B. Engineering Test Model of Optical Scanning System

The final optical scanning system design is the result of extensive testing of many different system elements on an engineering test model built for that purpose. The model was built to provide an 8 millimeter scan length; this length was dictated by the availability of a one inch octagonal prism. The prism cluster splitting the scanning beam in two was assembled from commercially available prisms and beam splitting cubes. The star plates were mounted parallel to each other in holders adapted from the Riddell blink machine. The holders were mounted on a carriage fitted to a Gaertner optical bench. The carriage was moved along the optical bench by a ten thread per inch lead screw driven by a variable speed drive. The entire assembly was mounted on a heavy cast iron table to increase the rigidity of the system. The prism was rotated on a long shaft with an angle encoder coupled to the other end. A belt and pulley coupled the shaft to a synchronous motor drive. The shaft was driven at 3600 and 1800 revolutions per minute for the tests. In operation, the plates moved horizontally past the vertically scanning spot, scanning a "stripe" 8 millimeters wide and as long as the restriction of the equipment on the central post containing the rotating prism, the prism cluster, the converging lens and focussing controls would permit. The laser was mounted on the table and aimed at the rotating prism through a hole bored to the plate holder support. A schematic of the optical system for one of the test setups is shown in Figure 2. The purpose of the angle encoder is to provide one reference pulse per revolution of the prism. This pulse is used to trigger the sweep of the oscilloscope and present a display based on a constant relationship between the individual prism faces and their location on the screen.

A general view of an early test setup is shown in Figure 3. In this test, the laser beam used was nominally 2 millimeters in diameter, and is shown in the center of Figure 3 between the laser and the moving support for the star plates. The storage tube oscilloscope and the video control system were used to provide a visual display of the scanned area.

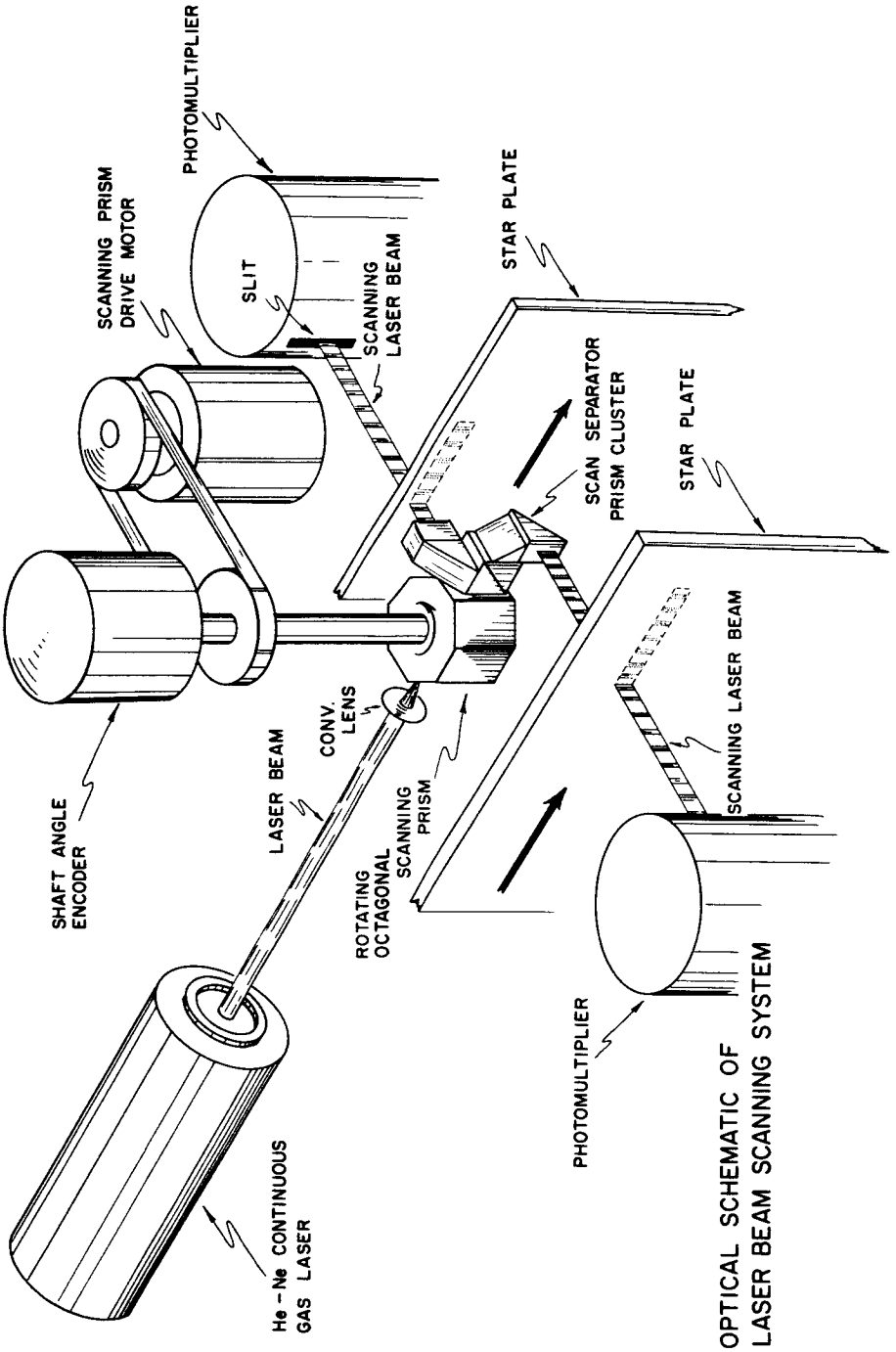

Figure 2: Optical Schematic of Laser Beam Scanning System

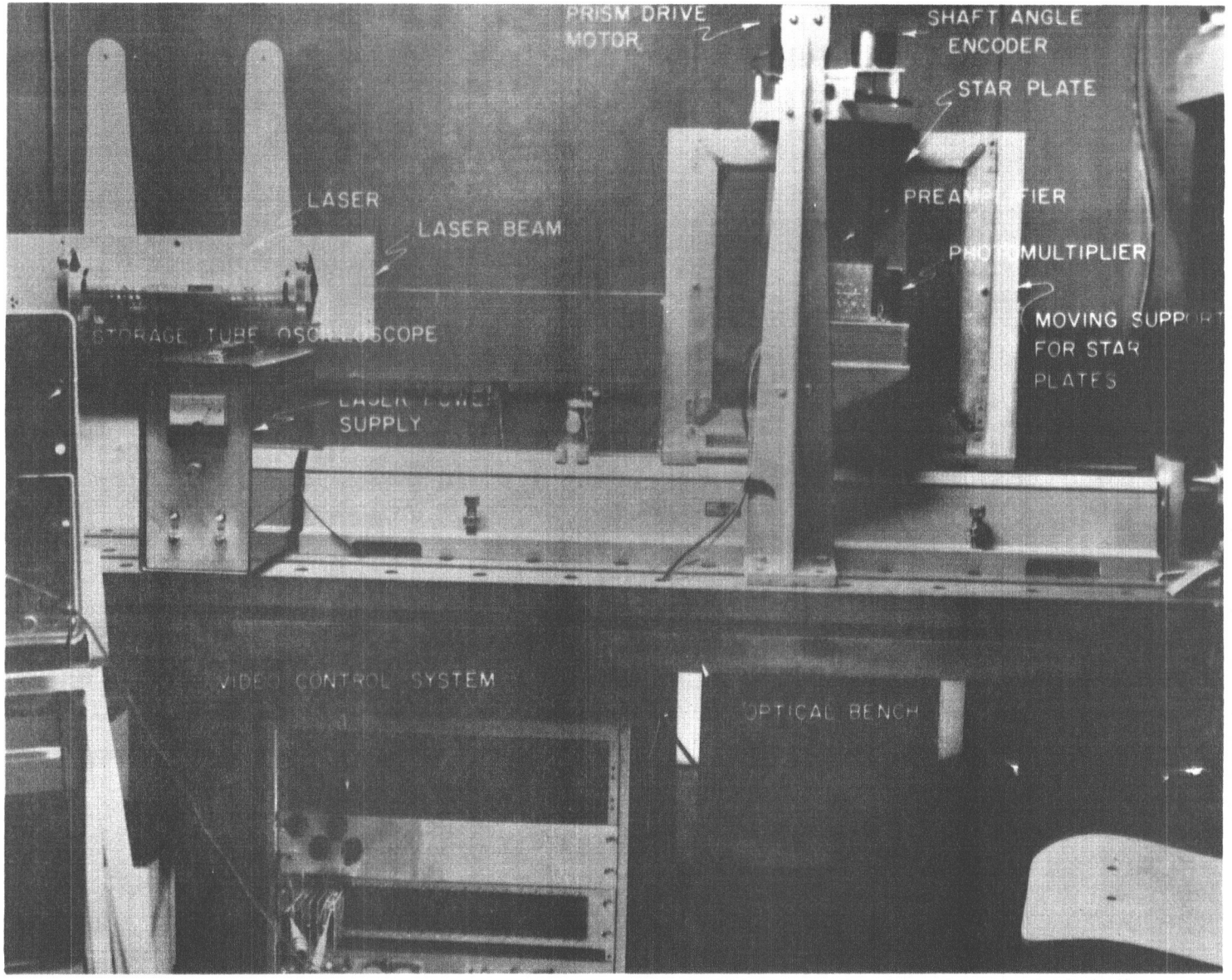

Figure 3: General View of Engineering Test Model of Scanning System

A more detailed photograph of the scanning and detecting system for the test setup is shown in Figure 4. The laser beam enters from the left and is given a scanning motion by the rotating prism. The scan separator prism cluster splits the beam into two beams scanning the star plates vertically. The light balancing filters, neutral density continuously variable filters, were used to compensate manually for the difference in fog level between the two plates. The star plates are not shown in place in this photograph; they are mounted in the two spaces between the prism cluster and the light balancing filters. The rotating prism shown here is the one inch commercially available prism producing an 8 millimeter scan.

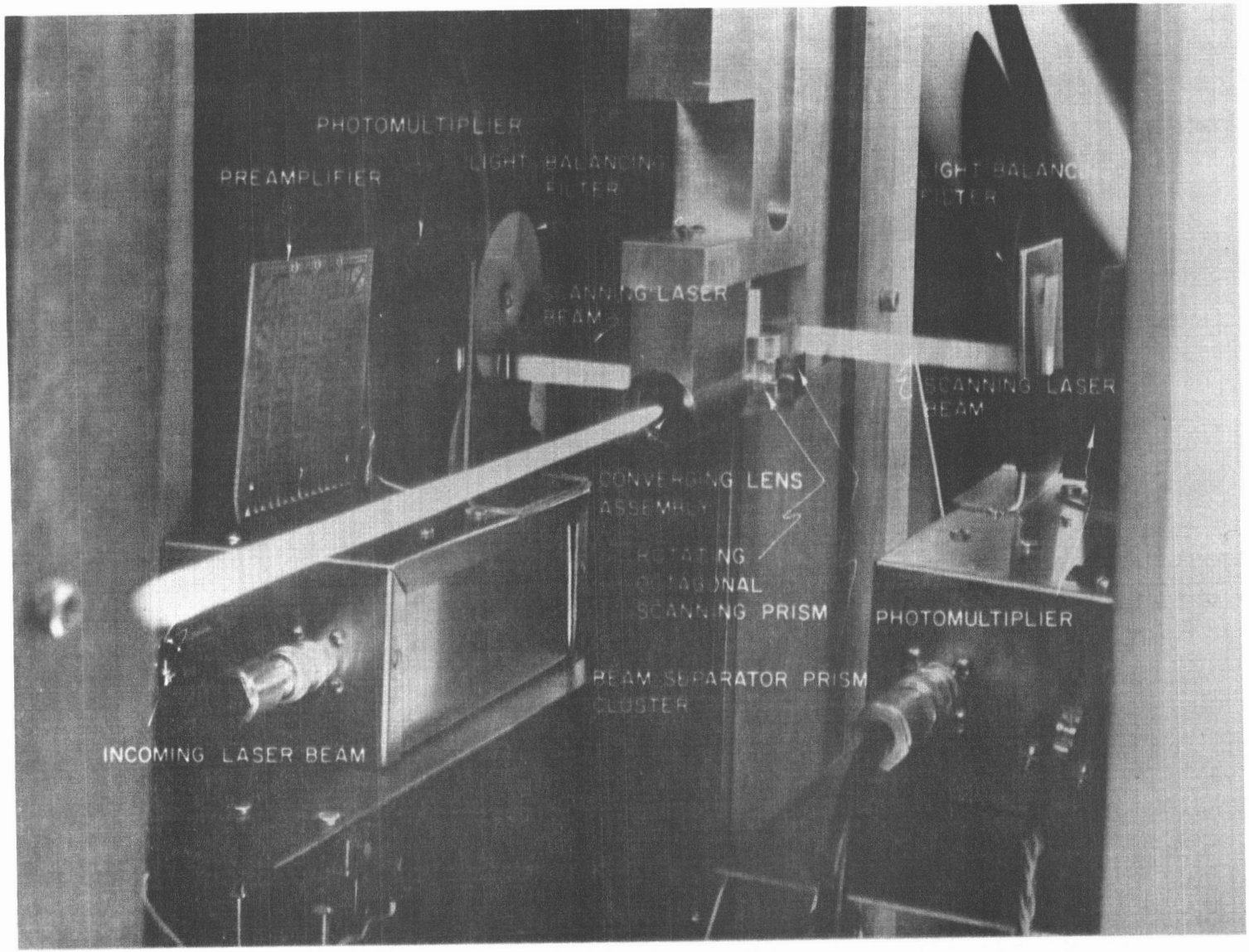

Figure 4: Detail of Engineering Test Model Scanning System

C. Scanning Spot Size

Of all the system parameters affecting the resolution of the scanning system, the physical size of the scanning spot was shown both analytically and experimentally to be the most critical. In addition, the available spot size depends on basic design factors such as the scan length and beam size. Hence, the optical design considerations were evaluated in the final analysis by their influence on the minimum spot size, since the smaller the spot size, the better the resolution will be.

A. E. LaBonte has calculated the theoretical variation of detected transmittance as a spot of varying size scans an opaque round image. The details of the calculation are shown in Appendix A. The resulting curves are shown in Figure 5. The curves are presented in essentially the same manner as they would be observed on the oscilloscope screen as the spot scans through the center of the image. The curves shown neglect the effect of diffraction and the gradual increase of density of star images toward the center. In curves for $d_s/d_i > 1$, note that light "leaking" around the edges of the image when the spot is larger than the image reduces the maximum height of the curve.

When the opaque circular star image is replaced by a star image whose transmittance profile matches measured values, curves calculated by LaBonte (shown in Appendix A) result--as are shown in Figure 6. These curves are for a fixed image size (90 microns) and a variable spot size. Note the smoothing effect on the curves resulting from the more realistic image structure.

Both Figures 5 and 6 show that the spot size should be kept to a minimum for the effective resolution to be usable. The images for which the system is designed range from about 18 microns to about 300 microns in size and 10 to 20 in red magnitudes. Therefore, a spot size between 10 and 20 microns would detect the star images reliably without degradation of the image. Since the beam size of the laser being used is nominally 2000 microns, a converging lens is necessary to reduce the size of the beam, as shown in Figure 2. The lens

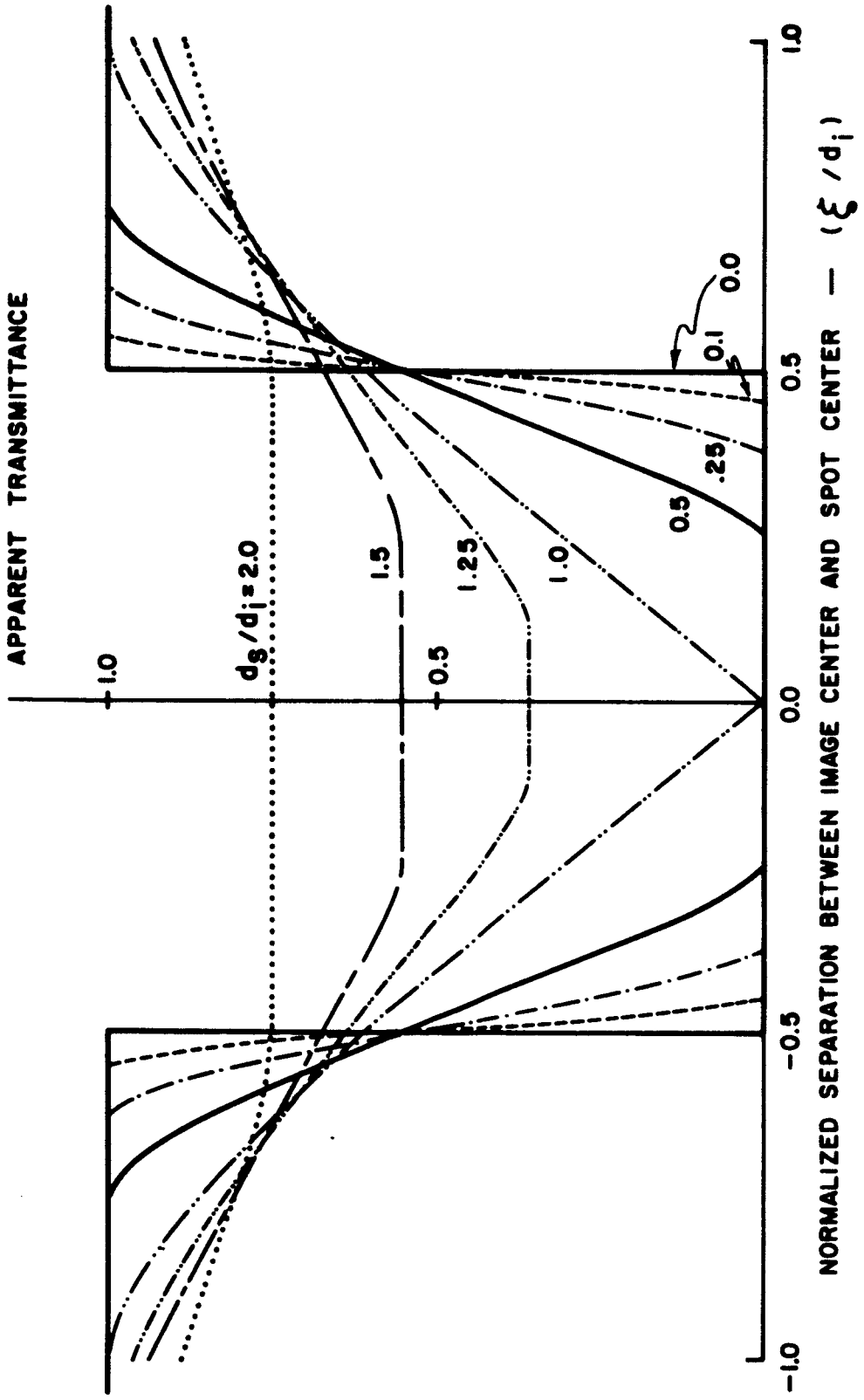

Figure 5: Apparent Transmittance Profiles for an Opaque Circular Image. The image (diameter d_i) is "seen" by a circular spot (diameter d_s) which scans through the image center. See Appendix A for details.

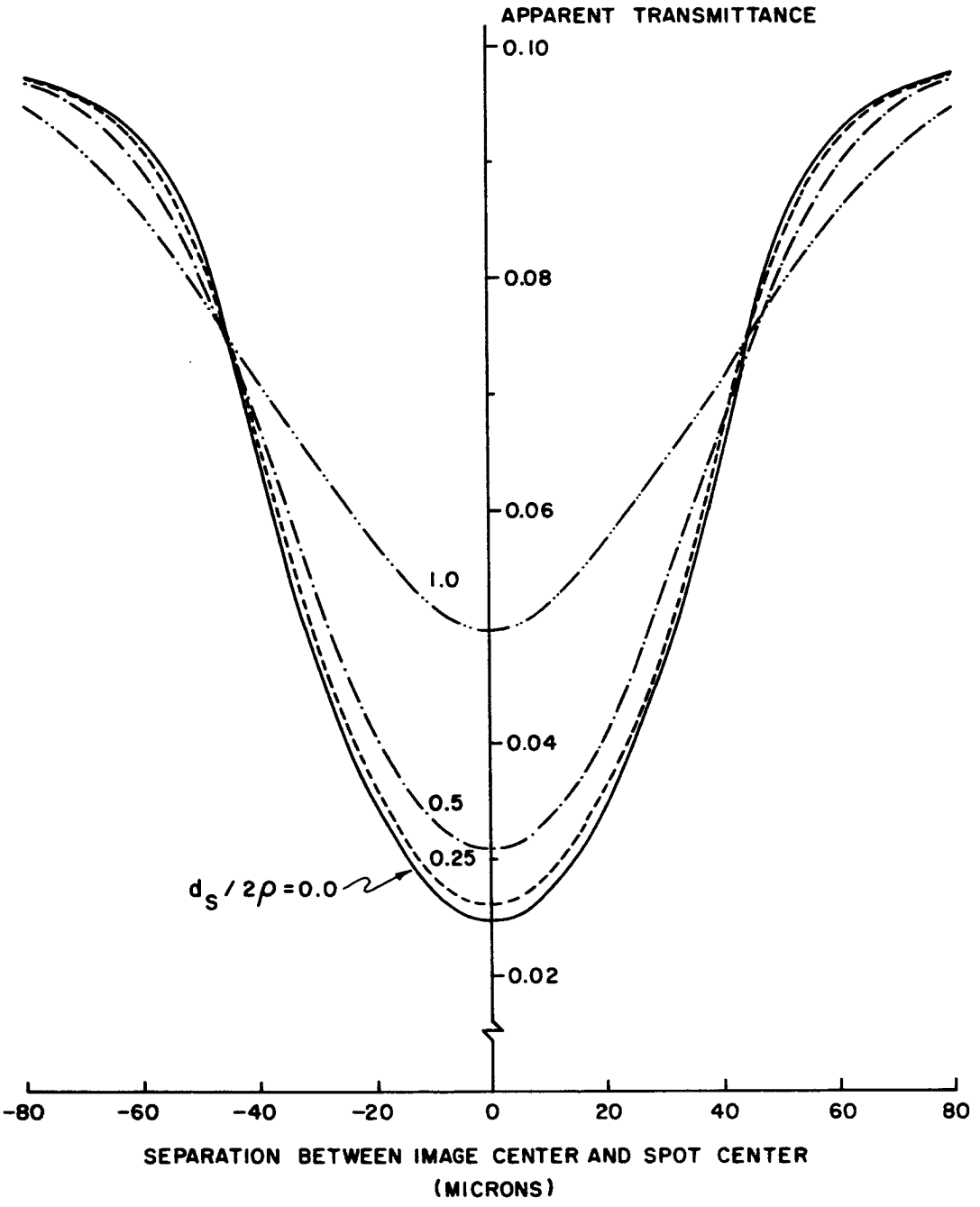

Figure 6: Apparent Transmittance Profiles of a "Star" Image. The star (radius ρ) is "seen" by a circular spot (diameter d_s) which scans through the image center. The results have been matched approximately to those obtained experimentally for the image of an 18^{th} magnitude star on a new original plate taken by Luyten. See Appendix A.

must be located on the laser side of the rotating prism for the image formed at the focal point of the lens to have a scanning action. Thus, the minimum focal length of the converging lens selected must be equal to the optical path from the laser side of the rotating prism to star plate, including the necessary clearances between the rotating and stationary optical elements.

The size of the rotating prism is determined by the length of the scan to be produced by its rotation. The length of scan is in turn determined by the speed of plate processing and the maximum rate of horizontal travel of the plate. In the design of the lead screw advance machine, the manufacturer specifies that the maximum rate of carriage advance is six millimeters per second in the measuring direction; further, the measurements can take place in only one direction. The carriage can be returned in the other direction at the maximum rate of six millimeters per second.

The scans are designed to occur at five micron intervals along the x (horizontal) axis. Hence, the maximum scan rate will be

$$\frac{\text{6000 microns per second}}{\text{5 microns per scan}}$$

or 1200 scans per second. Since, for an octagonal prism, eight scans occur per revolution, this requires that the prism rotate at 9000 revolutions per minute at its maximum scanning rate. At six millimeters per second, one pass of the scanner in the x direction would take one minute to cover the 360 millimeters of plate length. For the n horizontal passes (stripes) needed to cover the whole plate, the return passes would make the total number of traverses equal to $2n - 1$. For a total scanning time of 35 minutes, 18 stripes will be needed. For a total width of plate of 360 millimeters, a single scan length in the y direction of 20 millimeters will be sufficient to cover the whole plate in 18 stripes. The thickness of the prism needed to produce a 20 millimeter scan in the y direction can be calculated with the aid of Figure 7.

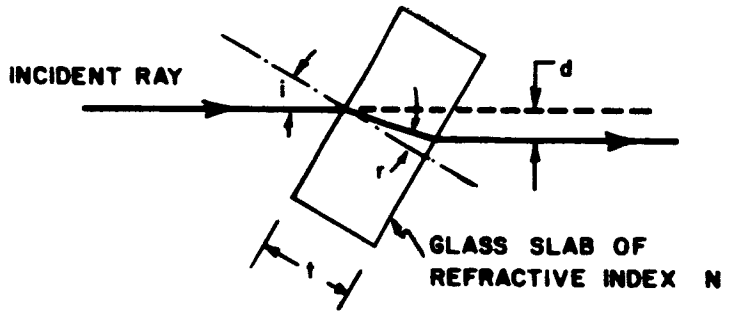

i = angle incident ray makes with normal

r = angle refracted ray makes with normal

t = thickness of glass

d = displacement of beam

$$d = \frac{t \sin (i - r)}{\cos r} \qquad \frac{\sin i}{\sin r} = N$$

Figure 7: Displacement of a Beam of Light in a Glass Slab

When the parallel sided glass plate is an octagonal prism, i becomes the angle of rotation of the prism from the normal to the prism face. The maximum displacement will occur for the maximum incident ray angle, or $22^{\circ}30'$. The maximum total displacement of the beam is given by

$$\text{total } d_{max} = \frac{2t \sin (22^{\circ}30' - r)}{\cos r}$$

For the BSC-2 glass of which the prism is made,

$$N = 1.5094,\ r = 14^{\circ}49.3',\ d_{max} = 20.74 \text{ millimeters.}$$

The prism thickness of 75 millimeters was chosen to provide for an overlap between scans plus a small "dead time" in the scanning system for the insertion of the x coordinate into the data. Allowing a nominal clearance of ten millimeters between the rotating and stationary optical parts, the optical

path between the converging lens and the star plates is 156 millimeters. This is the minimum focal length the converging lens must have in order to form the scanning spot in the plane of the star plate.

In the practical construction of the laser, divergence of the laser beam from parallelism occurs. This divergence, θ_d, is the result of normal diffraction spreading of a beam of light from an aperture plus the contributing errors of mirror placement and construction tolerances. The manufacturer's specification of beam divergence for the two millimeter diameter laser beam is 10^{-3} radians. The diffraction contribution for a two millimeter circular aperture is given by θ_d' (radians) $= \frac{1.22\lambda}{a}$, where a is the diameter of the aperture in millimeters, and λ is the wavelength used, 6.328×10^{-5} millimeters. The θ_d' contributed by diffraction is 3.86×10^{-5} radians, or about four percent of the total divergence. The minimum spot size attainable by a perfectly corrected converging lens of f millimeter focal length is the product, $s_{min} = f\ \theta_d$.

For a focal length of 156 millimeters, this gives a minimum spot size of 156 microns. Though this spot size is an appreciable reduction from the beam diameter, the design objective of 20 microns could not be realized without further manipulation of the design parameters. Since f and λ are both fixed by system requirements, the spot size was reducible only by increasing the diameter of the original laser beam, the quantity a in θ_d' (radians) $= \frac{1.22\lambda}{a}$. This was accomplished by the use of a 10X beam expander supplied as an accessory to the laser by the laser manufacturer. The beam expansion was produced by passing the laser beam through a two lens system consisting of a short focal length entrance lens, a very small aperture, and an exit lens, aspheric and diffraction limited, having a focal length ten times that of the entrance lens, producing a beam expansion of ten, or a nominal beam diameter of 20 millimeters. Applying this new value of beam diameter to the spot size equation, s_{min} becomes 15.6 microns, an acceptable spot size.

However, it should be noted that the minimum spot size can be attained only with a lens so perfectly corrected as to be diffraction limited in its operation. Tests on the engineering test model with commercially available lenses have confirmed the detection capability and the limitations of this large spot size.

In order to reduce the sensitivity of the detection system to spot size and the variation of spot size during a single scan, a special light collection system was devised. A schematic view of the light collection system for one star plate is shown in Figure 8. In this drawing, D represents the diameter of the projection of the spot size on the converging lens number 1; S' represents the effective diameter of the scanning spot on the star plate; and A is the actual physical diameter of the aperture placed in front of the photosensitive surface of the photomultiplier. The effect of the light collection system is to limit the effective spot size to a fraction of the aperture size A.

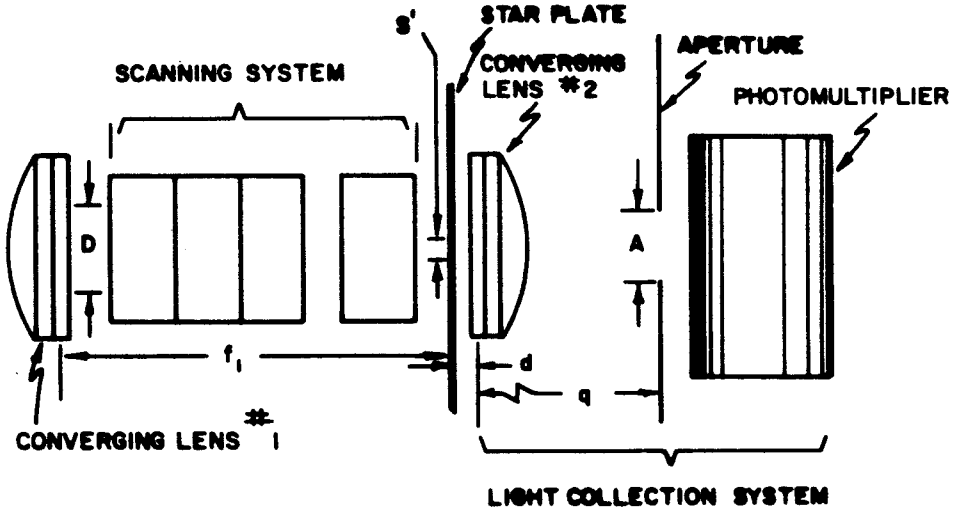

Effective spot size: $S' = \frac{d}{q} A$

Position of aperture: $\frac{1}{q} = \frac{1}{f_2} - \frac{1}{f_1+d}$

Scanned aperture on converging lens #1: $D = \frac{f_1+d}{q} A$

Figure 8: Light Collection System

In this system the aperture A in Figure 8 is placed a distance q from the converging lens number 2, such that a real image of the converging lens number 1 is formed on the aperture. This image remains stationary while the rotating prism turns; the aperture, when reduced to a size smaller than the size of the image of the lens, effectively screens the scanning spot and transmits to the photomultiplier only the part of the spot passing through the aperture. Thus, the effective spot size is determined by the aperture diameter and the ratio of d to q, as shown in Figure 8. The actual spot size is determined by converging lens number 1 as explained above. While this light collection system relieves the converging lens number 1 of the necessity of producing a very small spot, excessive spot size reduces the intensity of light of the scanned area, as well as decreasing the image contrast for small star images.

The relationships of the three scanning beams, the star plates, and the reference reticle are shown in an optical schematic of the final design system, Figure 9. In this design each light path in the light collection systems passes to the aperture down a hollow tube which also supports the scanning mechanism. The laser, the three photomultipliers, and their apertures are all located in the support structure into which the light collecting tubes are mounted. All of the mirrors shown in this schematic are first surface mirrors flat to 1/4 wavelength. The reticle with spot position measuring grid has precise graduations at right angles to the scan direction. The spacing of the lines is such that the position of the spot can be located to an accuracy of one micron.

Figure 10 is an exploded view of the scan separator prism cluster showing the assembly which separates the converging laser beam into three beams. The beam projected upward in the drawing has fifty percent of the intensity of the original laser beam; the other two beams have 25 percent. The added intensity on the upper beam is needed to adequately penetrate the normal fog level on the original plates. This fog level is much higher on

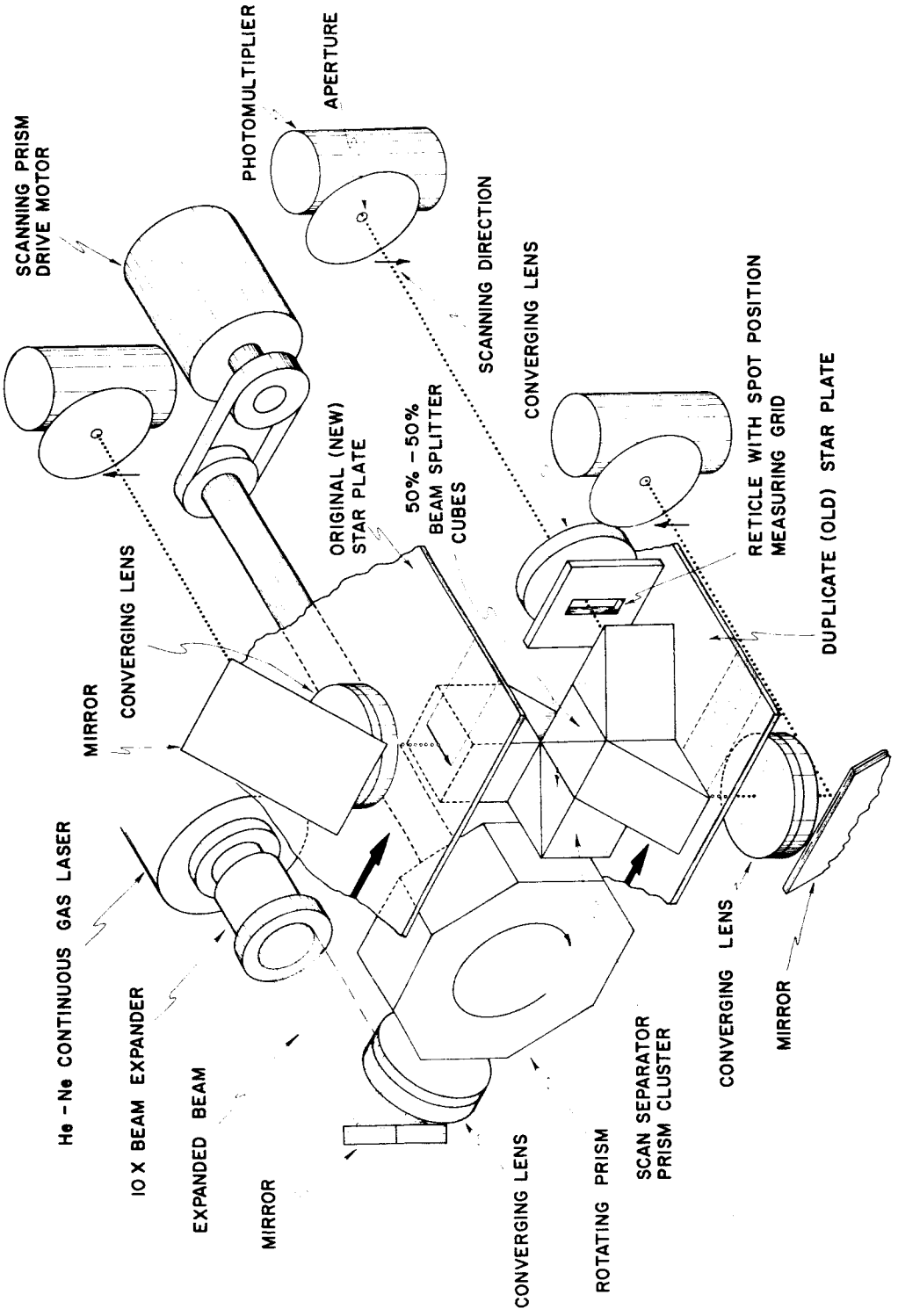

Figure 9: Optical Schematic of Star Plate Scanning Apparatus

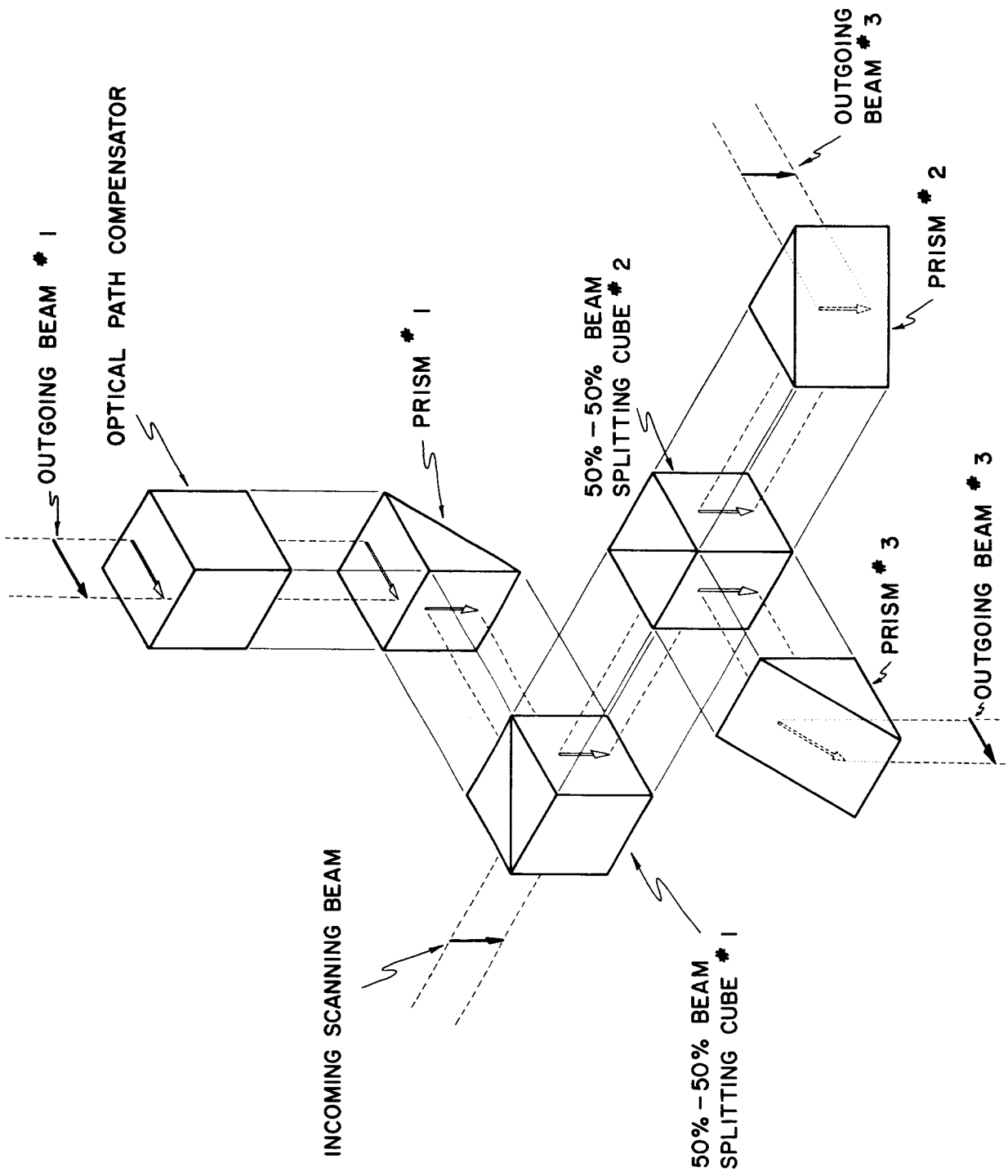

Figure 10: Exploded View of Scan Separator Prism Cluster

the original plates than it is on either the duplicate plates or the reticle.

In the actual design of the section of the system shown in Figure 8, f_1 = 156 millimeters, f_2 = 130 millimeters, d = 16 millimeters. For these values, the value of q becomes 525 millimeters. At this distance, the reduction of the aperture size A to the effective spot size S' becomes

$$S' = \frac{16 \text{ millimeters}}{525 \text{ millimeters}} \times A = .0305 \text{ A.}$$

The scanned aperture of converging lens number 1 becomes

$$\frac{172 \text{ millimeters}}{525 \text{ millimeters}} \times A = .328 \text{ A.}$$

For an aperture of 0.5 millimeter, an effective aperture of 15 microns would result, with a scanned aperture of .164 millimeter. In the final design of the system, photographic type diaphragms having continuously variable aperture sizes will be used. The variable diaphragm controls used on the engineering test model have proved invaluable in balancing the resolution of the spot with the fog level of the plate.

D. Design of Converging Lens Number 1

The function of this lens is to form the smallest possible spot of light from the expanded laser beam on the star plate. Two factors tend to increase the spot size when off the shelf lenses are used, making advisable a lens designed especially for this application. These factors are (1) the presence in the image space of 69 millimeters of glass, and (2) the change in actual glass path as the beam is deflected for the scanning operation.

Several off the shelf lenses were tested for spot size formation, particularly those used for prism binocular objectives, since their design would include compensation for the glass path of the Porro prism assembly. The spot size was tested by visual and photographic examination. The photographic method was set up as shown in Figure 11.

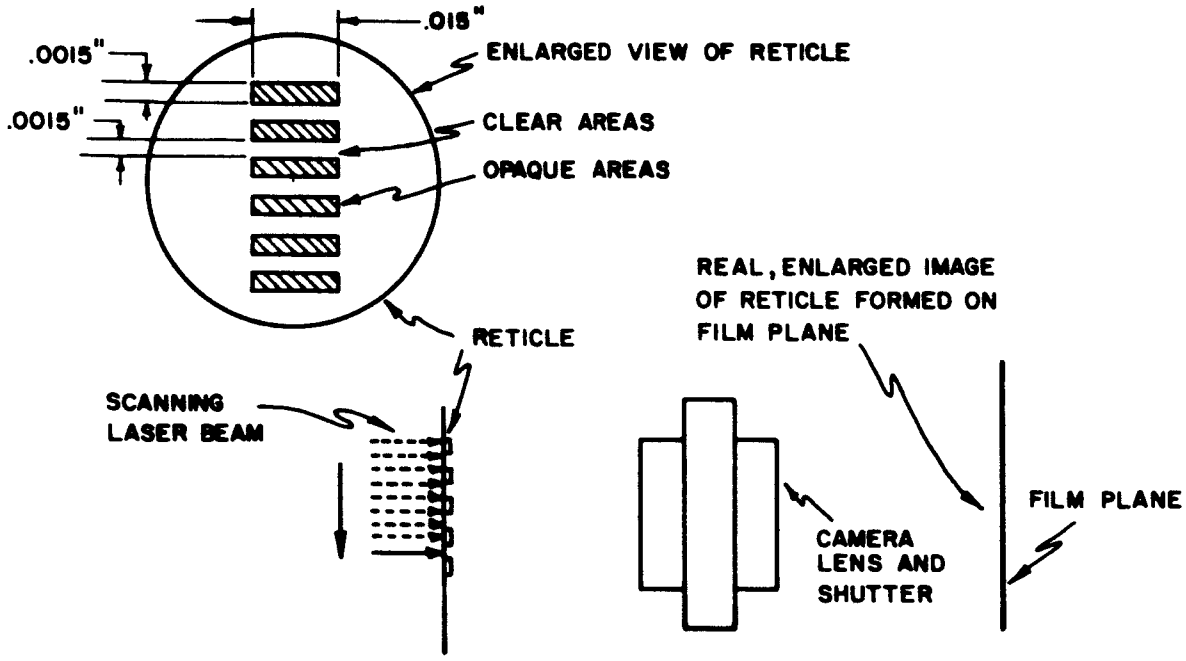

Figure 11: Photographic Measurement of Spot Size Using a Reticle

The photographic exposure was made by a standard shutter on the laser beam while the scanning prism was rotating. The resulting streaks contain several scans. These scans are not quite superimposed because the experimental prism did not mount in a plane exactly normal to the axis of rotation of the drive shaft. Figure 12 shows two exposures with two lenses of differing focal lengths and apertures. In each case the "spot" size refers to the width of the streak on the plate for a single scan. The dark "comb" crossing the beam is the pattern of the reticle shown in Figure 9. Each measurement shows, as did other similar measurements, that the measured spot size was always greater than the diffraction limit.

A computer ray tracing program was used to evaluate the optical parameters of a lens capable of forming a spot with (1) minimum size throughout the scan and (2) minimum change of size from the center of the scan to either edge. Additional requirements imposed were those of simplicity--the simplest lens with the smallest possible number of elements to reduce both internal reflections and cost.

Designs were evaluated for several scan lengths and beam sizes. A simple converging meniscus lens with its convex face toward the laser was found to produce minimum spot size for a laser beam two millimeters wide with a ten millimeter scan. Doubling the scan length increased the path length of the laser beam through the system by a factor of 1.5 from 104 millimeters to 156 millimeters. This, plus the expansion of the diameter of the laser beam by a factor of ten made a meniscus lens inadequate for spot formation.

The final design used a cemented doublet to give a flat focal field over the whole scan. Rays entering the lens parallel to the principal axis at distances of up to 17 millimeters from the center of the lens were traced through the rotating prism and the scan separator prism cluster. The intersections of these rays with the axial ray was used to determine the spot size in the plane of the star plate. A graph of the radii of spots formed by rays

A. Streak for spot size measurement. Lens focal length 124mm. Beam diameter 17mm. Spot size 23 microns.

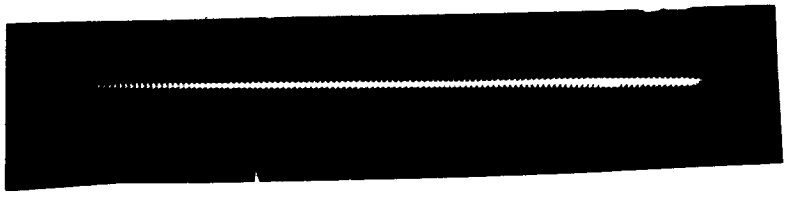

B. Streak for spot size measurement. Lens focal length 147mm. 10X expanded laser beam. Spot size 20.5 microns.

Figure 12: Measurement of Spot Size. Dark bars across the scan are the reticle described in Figure 9. Photographs show several scans not quite superimposed, due to the wobble in the experimental prism mounting.

entering the lens at various distances from the center of the lens is shown in Figure 13. These spot radii were calculated solely from geometrical considerations, and do not include diffraction disk calculations. The height of the entrance ray giving a 15 micron spot is shown on the graph to be about 4.6 millimeter radius, or 9.2 millimeter diameter. This is the theoretical maximum scanned aperture on converging lens number 1, shown as dimension D in Figure 8, which would result in a spot size not exceeding 15 microns for 22 degrees of prism rotation either side of the nornal to the prism face.

In the final design, however, the maximum scanned aperture, D, is shown to be .328 A. For a 15 micron effective spot size, the aperture A would be 1/2 millimeter. The scanned aperture D would be only .164 millimeter in diameter, including diffraction effects; hence, the variation of spot size with prism rotation at that aperture would be very small. Thus, although the variation of spot size with prism rotation is large for light entering the outer portions of lens number 1, the effective spot size deals only with the central portions of the image and changes little with prism rotation. A further enhancement of this property occurs because the intensity of the laser beam is not uniform across the beam, but a Gaussian distribution, with the greatest intensity at the center. This has the effect of increasing the number of rays entering the system near the axis of the lens and decreasing the number of rays entering near the margin of the lens.

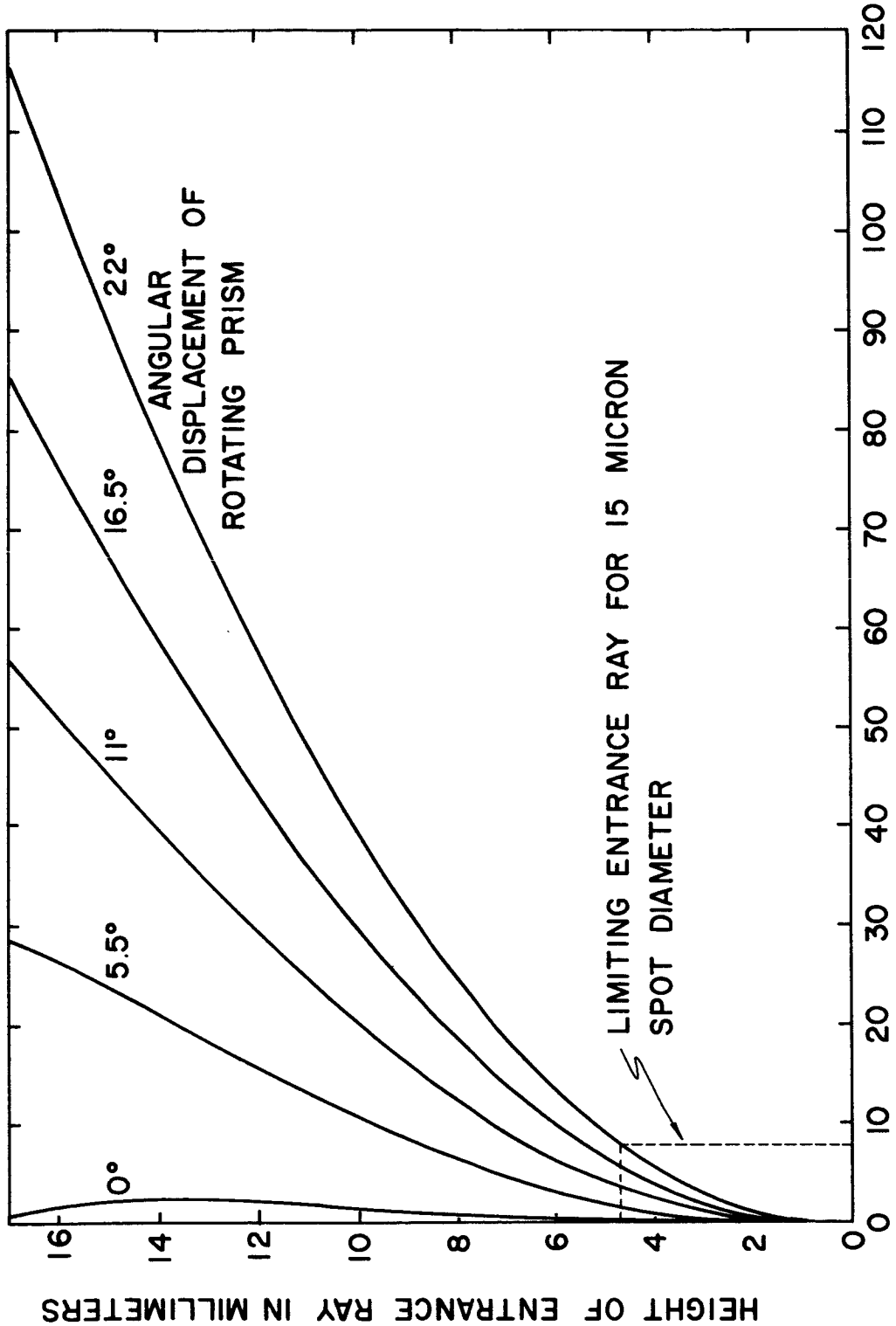

Figure 13: Results of Computer Ray Trace Used to Design Converging Lens Number 1. Spot radius on the star plate for rays entering converging lens number 1 at various distances from the center of the lens.

III. SIGNAL ELECTRONICS

A. Introduction

The function of the Signal Electronics portion of the system is to convert the information in the three intensity modulated laser beams into pulse-position modulated electrical signals. This portion of the system supplies various gates, control signals, and video signals to the computer interface and control and display consoles. A simplified functional block diagram of the basic image data flow is shown in Figure 14.

The laser beam is passed through a rotating prism that causes it to scan, then split into three parts. Each of these sub-beams is focused at the surface of a photographic plate. Two of the plates contain images of approximately coincident star fields. The third plate is a Ronchi ruling. The modulated laser beams are detected by light sensors. The electrical outputs of the light sensors for the two star plate channels are monitored by image detectors that determine the presence or absence of a star image in the laser beam. The outputs of these detectors are two gates: Star Plate 1 Image Gate, and Star Plate 2 Image Gate. The output of the Ronchi ruling* light sensor is used for two purposes. The first is to provide a pulse as the beam passes over each ruling. The position of the beam at any instant may be determined by counting these pulses. The pulse count is then compared with the occurrence of a star image gate to locate the image position on the star plate. The second use of the ruling sensor output is to measure the laser beam intensity. This is accomplished by detecting the signal when the beam is in the clear interval between rulings. The signal representing beam intensity is fed to the two star plate image detectors. This enables them to determine the presence or absence of an image on the basis of an absolute modulation index, or transmittance. In summary, the three basic outputs of the Signal Electronics are (1) Star Plate 1 Image Gate, (2) Star Plate 2 Image Gate, and (3) Spot Position Pulses.

* Note: This is the device referred to in the previous sections as the reticle.

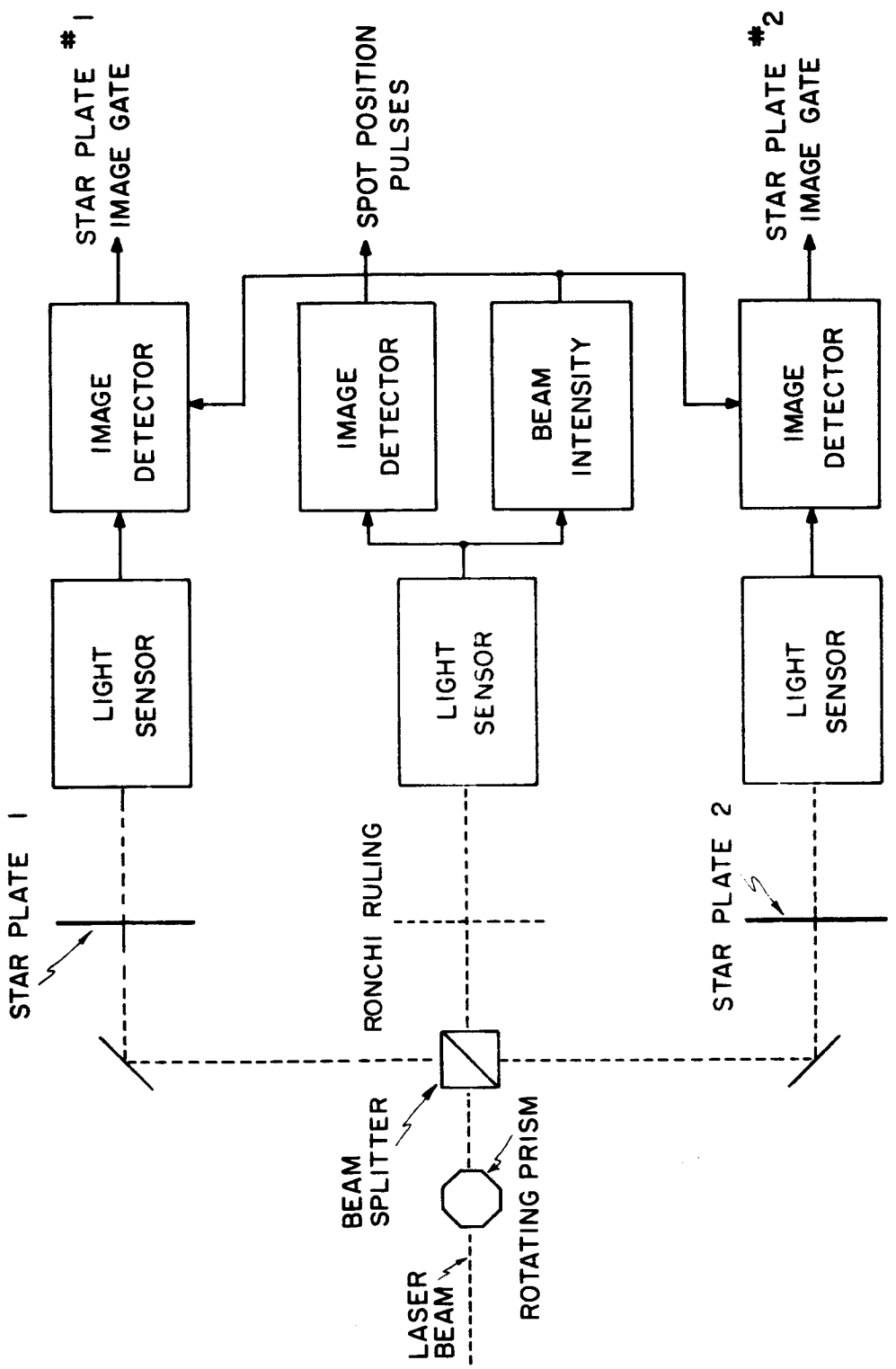

Figure 14: Signal Electronics Image Data Flow

B. Functional Block Diagram

A more detailed block diagram of the Signal Electronics is shown in Figure 15. Application of automatic gain control to the photomultiplier tubes is indicated here, along with the use of a common video level reference voltage for all three channels. The function of the various blocks will be discussed with reference to the idealized video and level detector waveforms shown in Figure 16.

1. Photomultiplier

The photomultiplier tube used in this system is the 1P21. It is supplied by two dynode bleeder chains; one of which is connected to an intermediate dynode 6 and the other to the remaining electrodes. This permits gain control of the tube by varying the voltage on dynode 6. The tubes are operated at relatively high photocathode currents, yielding signal-to-noise ratios in excess of 100.

2. Video Amplifier

The video amplifiers are basically wide-band d.c. amplifiers. Their purpose is to provide a low-impedance, high output current capability reproduction of the video voltage at the photomultiplier load resistor.

3. Automatic Gain Control and Video Level Reference

Automatic gain control of the photomultiplier tube output or video level is required for two primary reasons. They are:

(a) to enable the system to operate within the dynamic range of the photomultiplier and amplifier, and

(b) to establish a set voltage that represents the "no image" signal or maximum light transmission.

The considerations that determined the Automatic Gain Control philosophy are as follows.

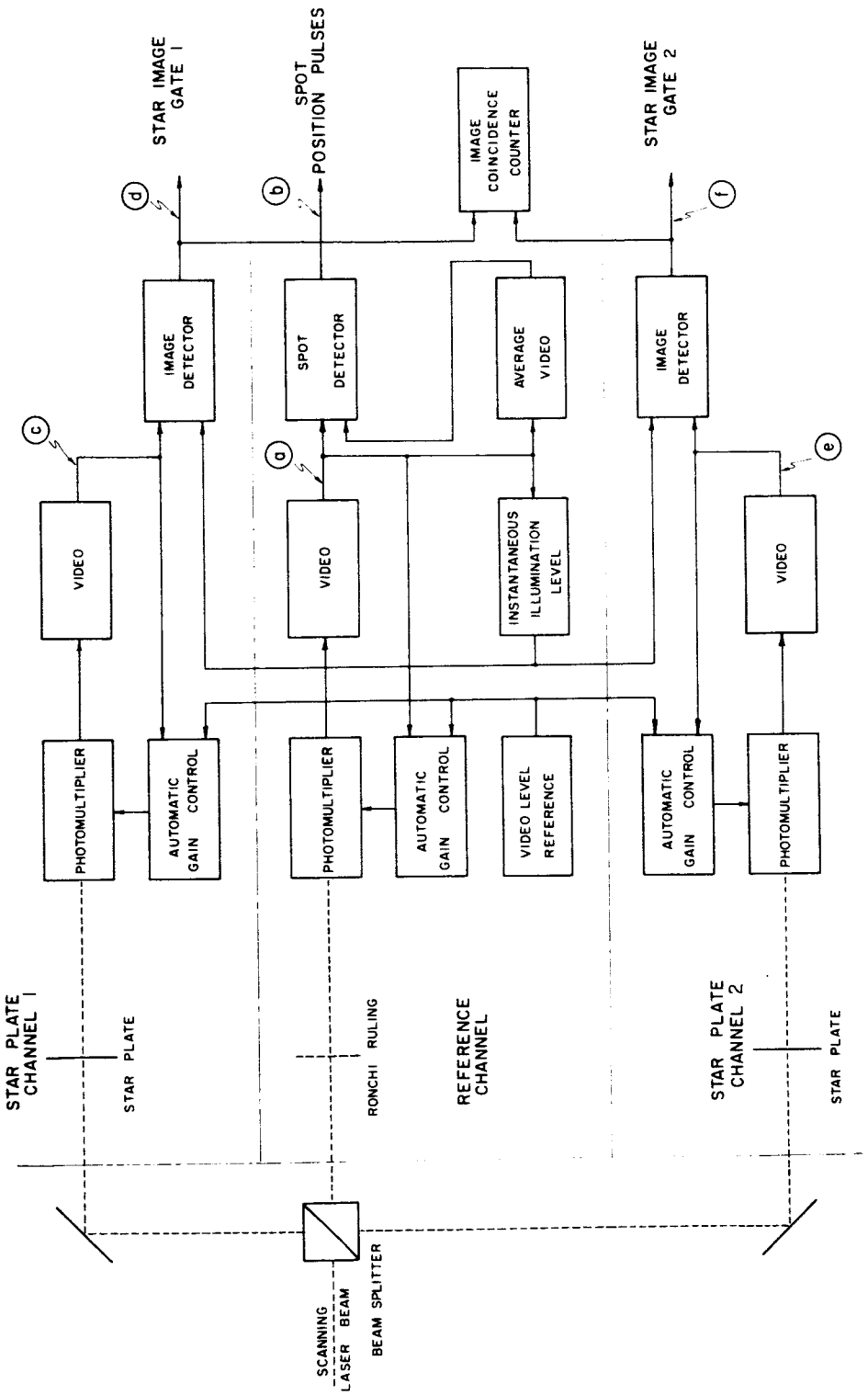

Figure 15: Automatic Proper Motion Survey Signal Electronics

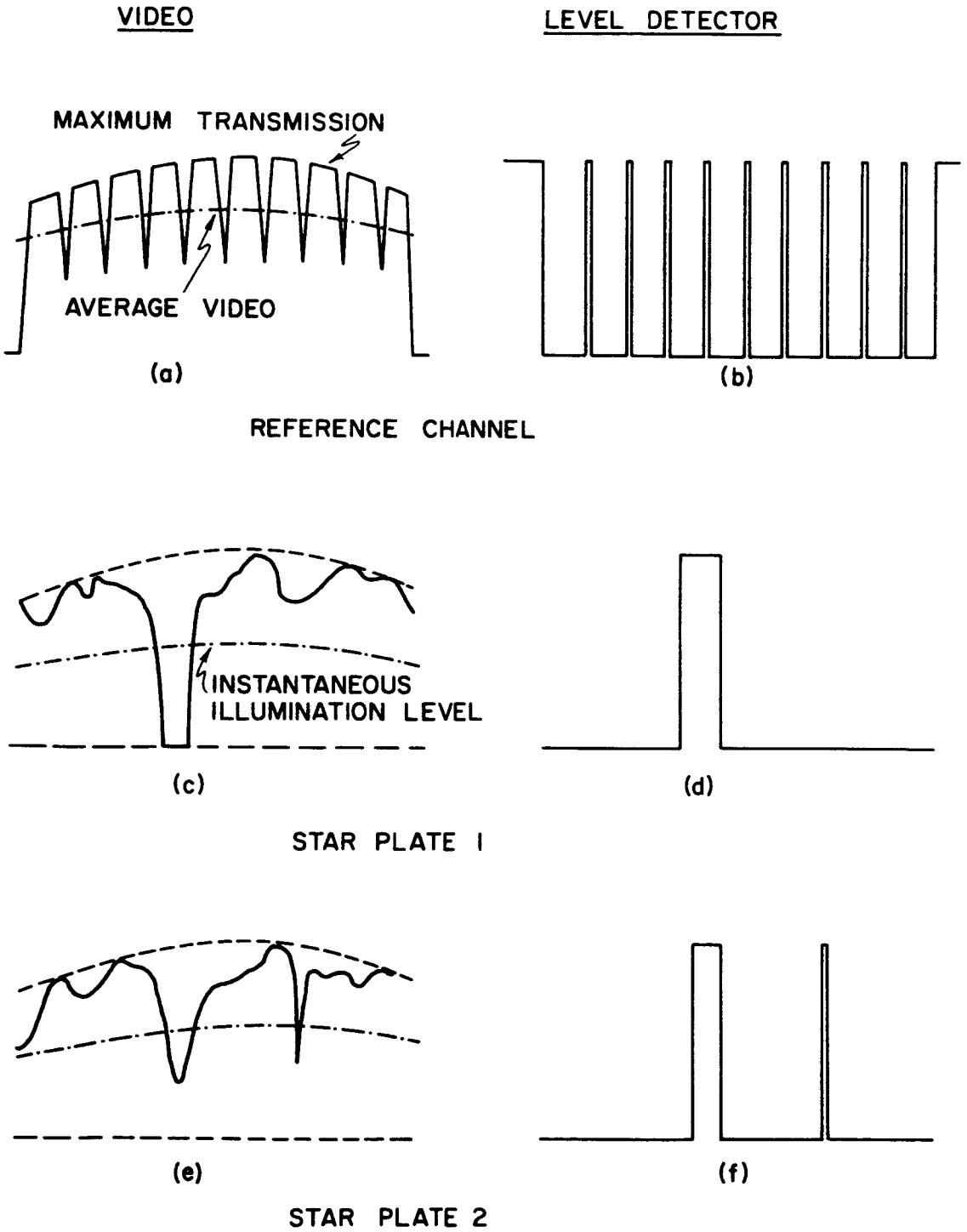

Figure 16: Idealized Waveforms Occurring at Lettered Reference Points in Figure 15

The intensity of the laser sub-beams will vary during the scan, roughly as shown by the dotted maxima lines in Figures 16a, c, and e. The beam splitter design is such that the relative variation between channels should be nearly identical; i.e., the ratio of light intensity between any two channels should be a given constant at any point in the scan. It would be very desirable to AGC the photomultiplier tubes so that the nominal output for "maximum transmission" through the plate is a known, constant voltage throughout the scan. This could be done for the reference channel, where the signal is a series of sharp, closely spaced dark areas interspersed with relatively wide areas of open emulsion (Figure 16a). The character of the video modulation on the star plates, however, is completely random and a large image could depress its level for an appreciable portion of any given scan. This obviates direct measurement of the maximum transmission level on a continuous basis during the scan. Any corrections applied to the instantaneous value of video must be done essentially open-loop, either by means of a predetermined function or by using the measured instantaneous peaks in the reference channel. The latter approach has been chosen and will be discussed under Instantaneous Illumination Level. The Automatic Gain Control action is now determined by measuring the peak of the dotted maximum transmission curves (whenever it is present during a scan), and setting the photomultiplier gains so that this voltage is equal for all three channels. This facilitates implementation of the image detectors, and will be discussed later. All three Automatic Gain Control channels are supplied with a Video Level Reference voltage obtained from a zener reference diode-amplifier source in the reference channel.

4. Instantaneous Illumination Level

The Instantaneous Illumination Level voltage is obtained by measuring and smoothing the voltage level between rulings on the reference channel. This voltage follows quite accurately the dotted maximum transmission curve and also represents the maximum transmission curves for the two star plate channels, within the accuracies of the Automatic Gain Control level and beam splitter. The Instantaneous Illumination Level voltage provides the threshold for the

Image Detectors to be discussed next.

5. Image Detectors

The Image Detectors are level detectors (Schmitt triggers) that compare the video and instantaneous illumination level voltages. When the video falls below a pre-set percentage of the illumination level, the trigger changes state. This generates the Star Image Gate (Figure 16d, f).

6. Average Video and Spot Detector

The Average Video Circuits measure the minimum and maximum values of the modulation on the reference channel, and average them. This voltage is used as the threshold for the Spot Detector.

The Spot Detector contains a Schmitt trigger that compares the reference video and average video voltages, and generates spot position gates, (Figure 16b). These gates are shaped and clipped, resulting in a series of narrow pulses that denote passage of the spot over the beginning of a bar on the ruling. These are the Spot Position Pulses.

7. Image Coincidence Counter

The image coincidence counter is a coincidence gate, coupled with a counting circuit. It is intended to be used as an aid to plate alignment.

C. Circuit Performance

This section will explain the functions and performance of the prototype Signal Circuits in somewhat greater detail. A series of oscilloscope photographs showing system waveforms has been made, with inputs from the experimental scanner. These will be cross-referenced to the detailed functional block diagrams in Figures 17, 18, and 19. Circuit schematic details will be added where appropriate. In the following discussion, sections 1 through 3 cover the photomultiplier, video, and Automatic Gain Control circuits. These "front end" boxes are identical for all three channels.

1. Photomultiplier Tube and Dynode Bleeder

A 1P21 photomultiplier tube is used as the laser beam sensor in all three channels. This tube contains a photocathode, nine dynodes, and an anode. The gain of the tube may be adjusted by varying the high voltage supply, or by modulating various combinations of dynodes. In this system the high voltage is varied manually on each tube to set its operating point within the automatic gain control range. The output is then maintained at precisely the desired level by the automatic gain control circuits, which modulate the voltage on dynode 6.

A schematic of the photomultiplier-dynode bleeder circuitry is shown in Figure 20. It is noted that two dynode bleeder chains are used, one of which supplies dynode 6 and the other supplies the remaining dynodes. The anode current is returned to ground through a load resistor located in the preamplifier. The signal voltage is developed across this resistor. The curve of tube gain versus dynode 6 voltage contains maxima and minima (Figure 21). Therefore, in order to prevent transition or switching type instabilities in the automatic gain control loop, the voltage range through which dynode 6 is varied must be restricted to a monotonic portion of this curve. This is accomplished by means of the two clamping diodes connected between dynode 6 and selected points on the main bleeder. These are normally back-biased.

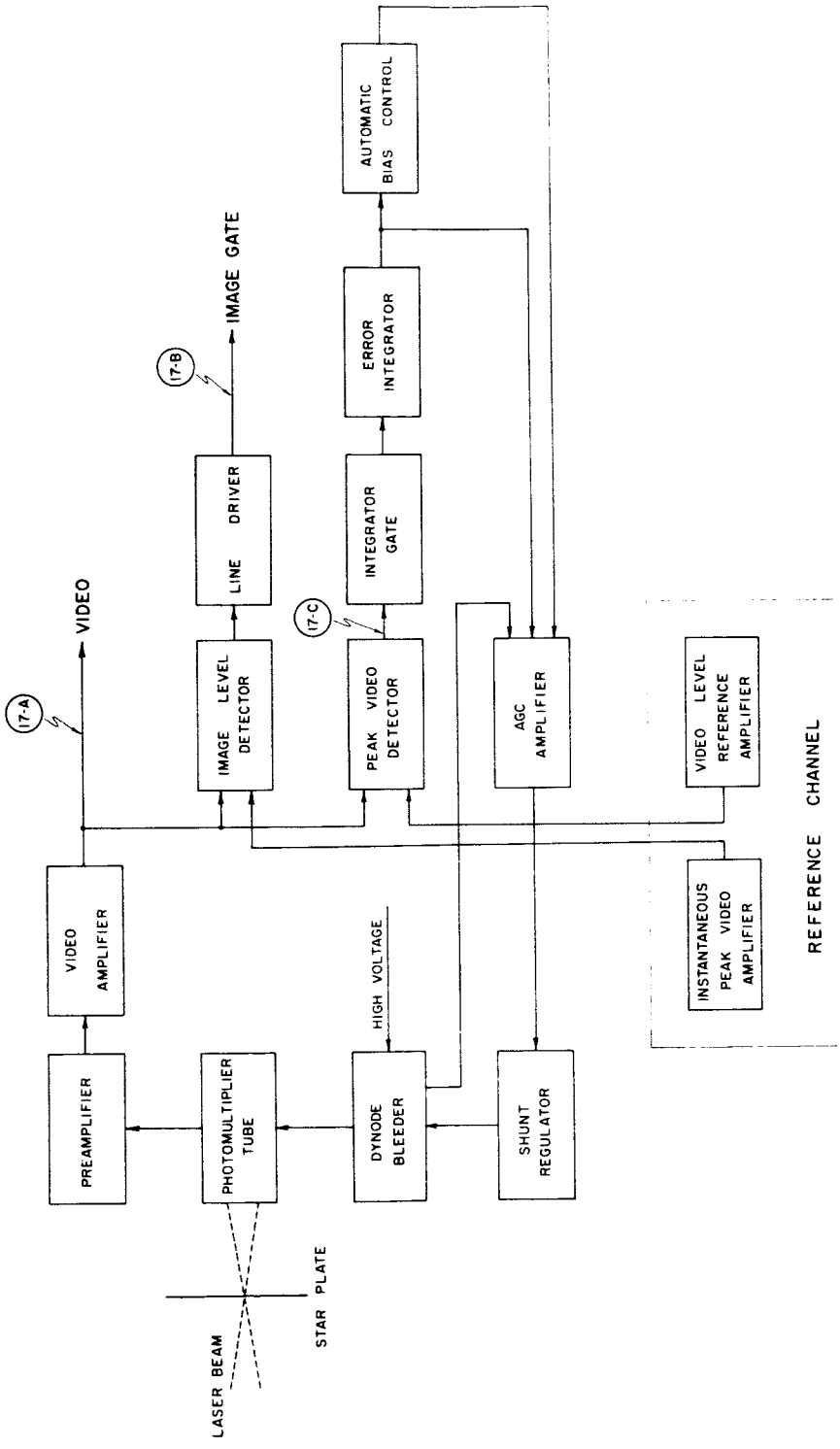

Figure 17: Star Plate Channel

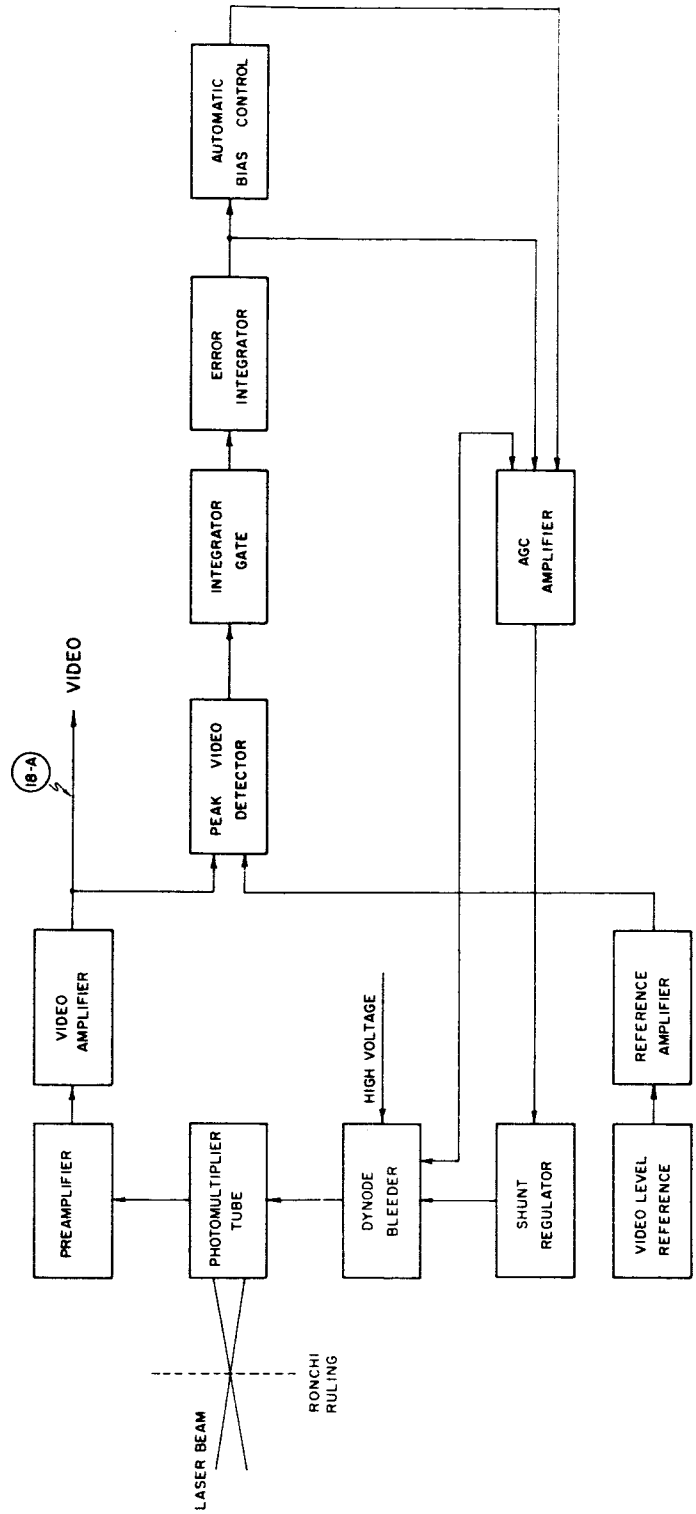

Figure 18: Reference Channel Video and AGC Circuits

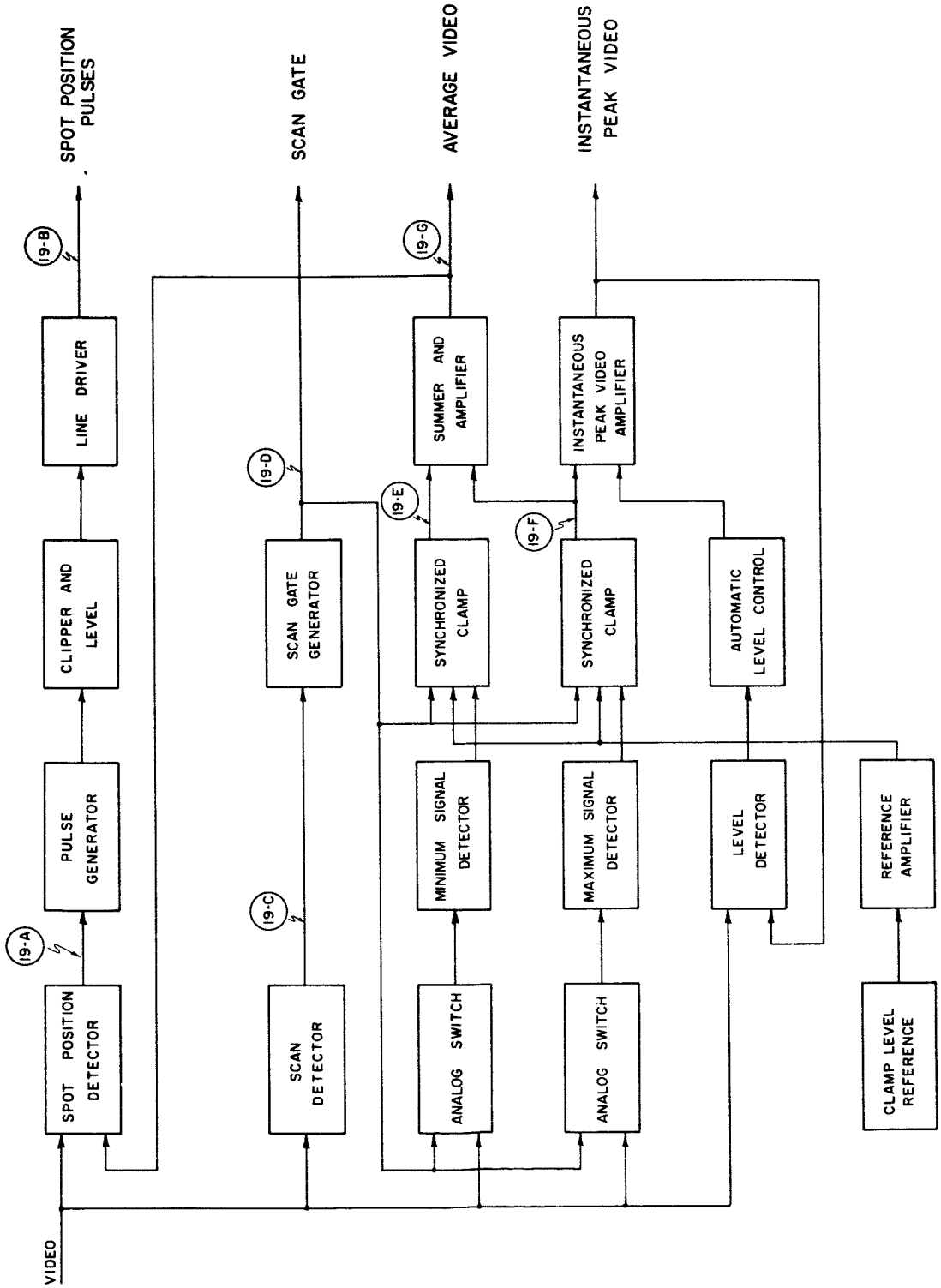

Figure 19: Reference Channel Pulse and Data Circuits

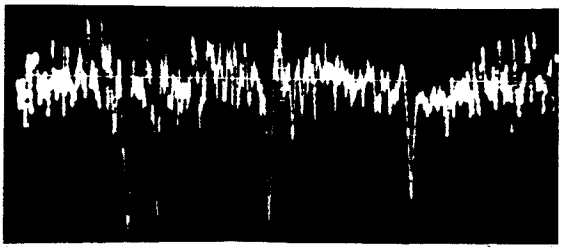

A	H	V
Star Plate Video	.5ms/div	1 volt/div

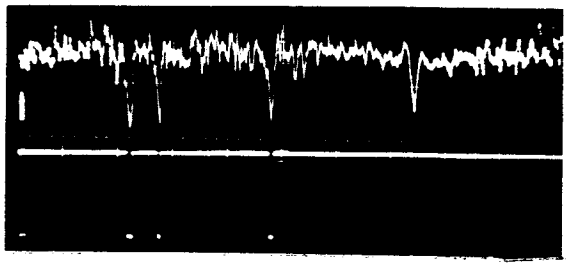

B	H	V
Star Plate Video	.5ms/div	2 volts/div
Image Detector	.5ms/div	2 volts/div

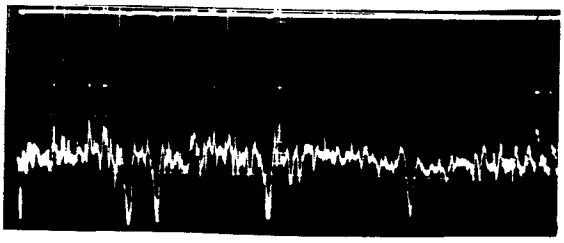

C	H	V
AGC Level Detector	.5ms/div	2 volts/div
Star Plate Video	.5ms/div	2 volts/div

Oscilloscope Waveforms Illustrating Figure 17

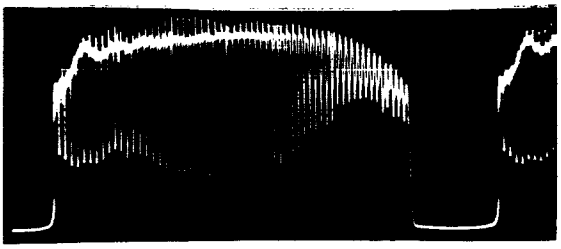

A	H	V
Reference Video	.5ms/div	1 volt/div

Oscilloscope Waveforms Illustrating Figure 18

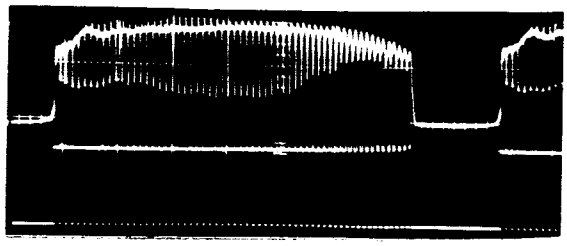

A H V
Reference Video .5ms/div 2 volts/div
Spot Position Detector .5ms/div 2 v/div

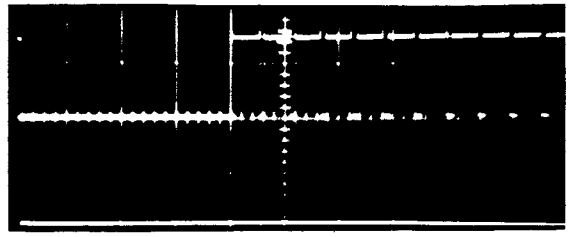

B H V
Spot Position Detector .1ms/div 2 v/div
Spot Position Pulses .1ms/div 5 v/div

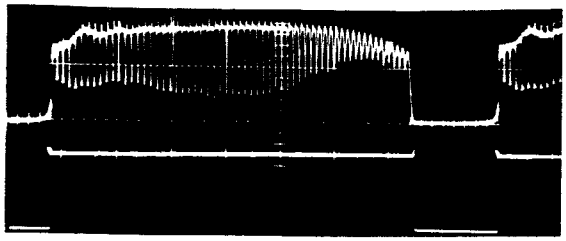

C H V
Reference Video .5ms/div 2 volts/div
Scan Detector .5ms/div 2 volts/div

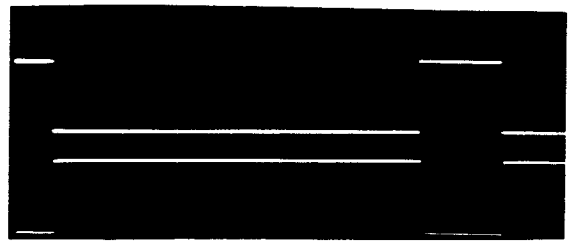

D H V
Negative Scan Gate .5ms/div 5 volts/div
Positive Scan Gate .5ms/div 5 volts/div

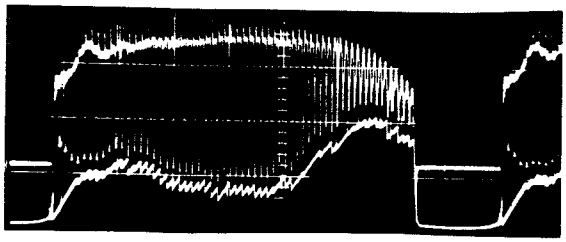

E H V
Reference Video .5ms/div 1 volt/div
Minimum Video .5ms/div 1 volt/div

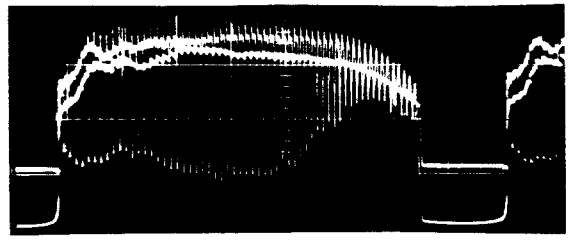

F H V
Reference Video .5ms/div 1 volt/div
Minimum Video .5ms/div 1 volt/div

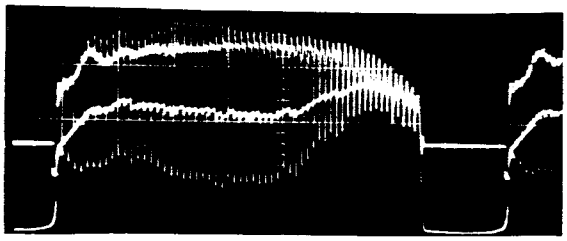

G
Reference and Average Video
H--.5ms/div V--1 volt/div

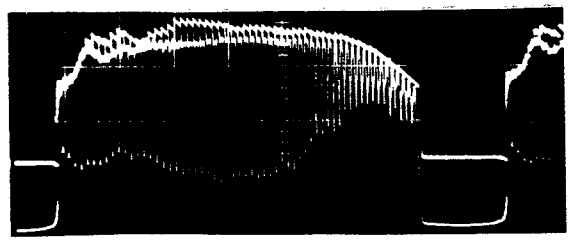

H
Reference and Instantaneous Peak Video
H--.5ms/div V--1 volt/div

Oscilloscope Waveforms Illustrating Figure 19

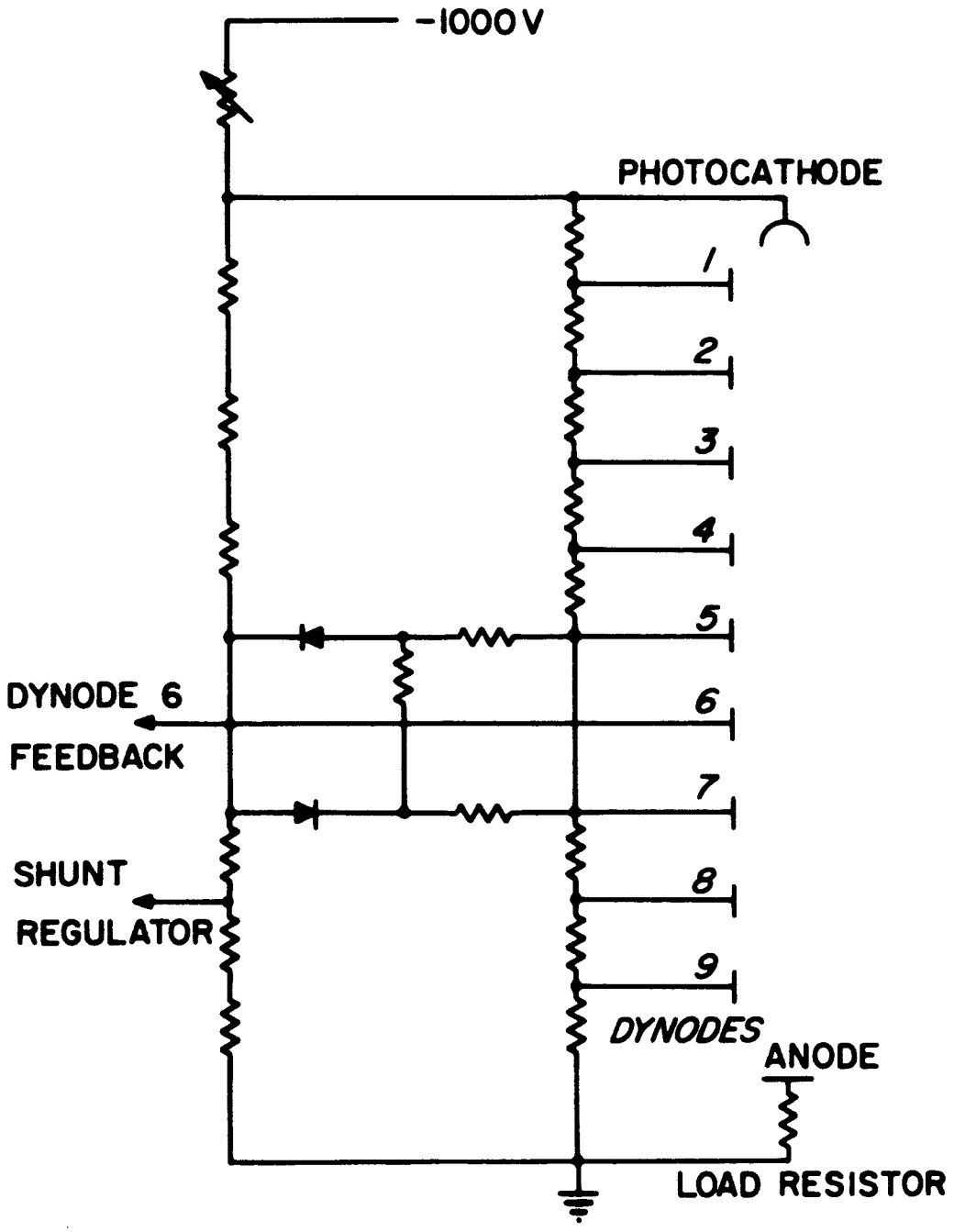

Figure 20: Photomultiplier and Dynode Bleeders

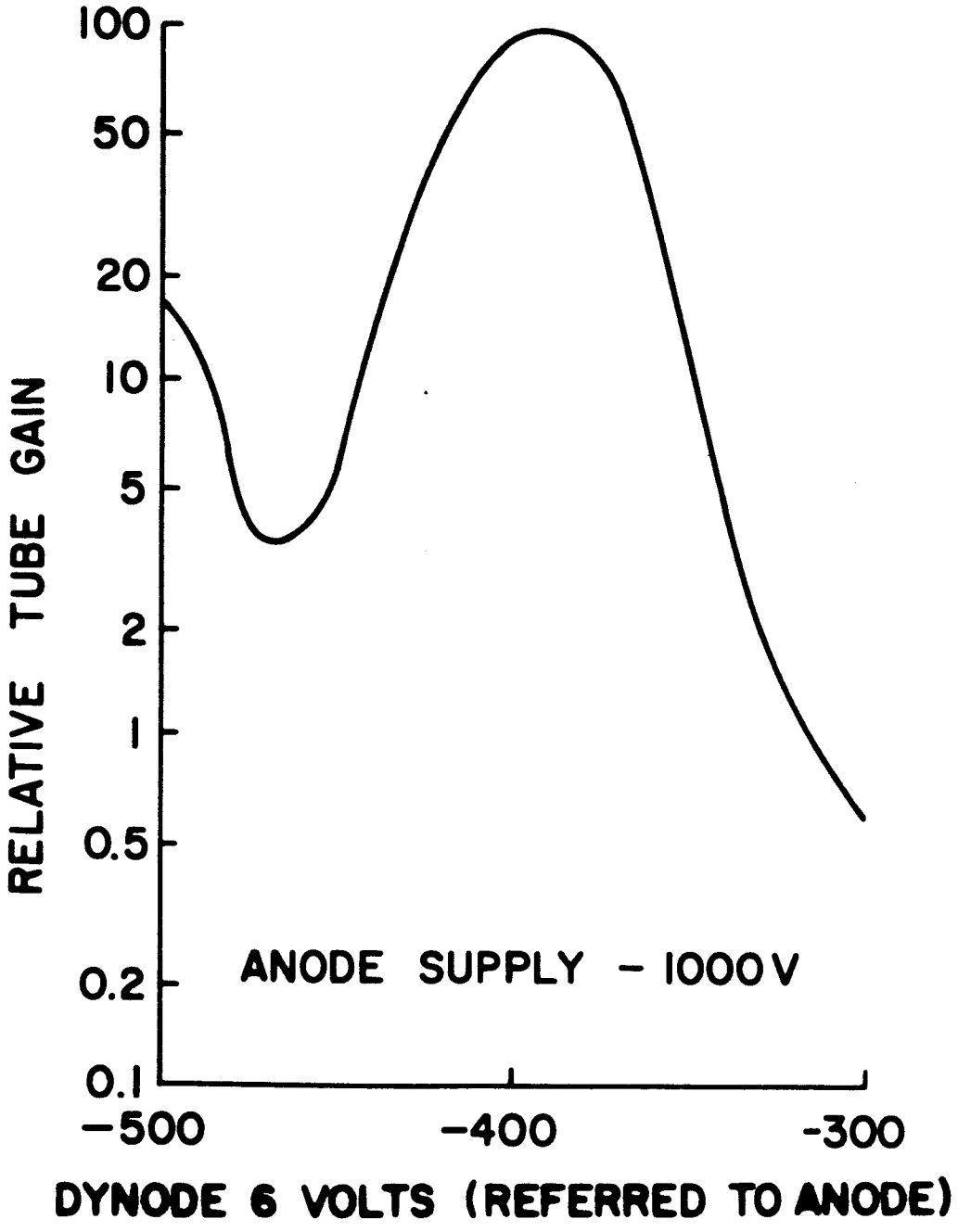

Figure 21: 1P21 Photomultiplier Gain Versus Voltage Applied to Dynode 6

Their function is to clamp dynode 6 at a potential referenced to the main bleeder if it is attempted to modulate it beyond the limits of the selected range.

2. Preamplifier and Video Amplifier

The preamplifier and video amplifier are essentially wide-band d.c. amplifiers. The preamplifier has a high input impedance to avoid loading effects on the photomultiplier load resistor. Its output impedance and current capability permit it to drive the cable connecting the photomultiplier assembly to the console containing the remainder of the electronics. The video amplifier provides a very low impedance, high current capability source of voltage. This is required to obtain maximum speed and accuracy from the image detectors.

3. Automatic Gain Control Circuits

The forward loop of the Automatic Gain Control circuits consists of the photomultiplier, preamplifier, and video amplifier. The feedback loop is implemented by the peak video detector, integrator gate, error integrator, automatic bias control, Automatic Gain Control amplifier, and shunt regulator. The operation of each element of the feedback loop is as follows.

a. Peak Video Detector

This is a level detector, or Schmitt trigger. The inputs are the video voltage, and the video level reference voltage. Whenever the video voltage exceeds the reference voltage, the trigger output changes state. This initiates corrective action in the Automatic Gain Control loop.

b. Integrator Gate

The integrator gate functions as a buffer between the peak video detector and the integrator gate. When the detector is switched, indicating high video, it drives a pre-set amount of current into the integrator. When the detector is not operated, it appears as an open circuit to the integrator input. This

permits the integrator to act as a holding circuit when there is no video error input.

c. Error Integrator

The error integrator is an operational amplifier with capacitive feedback. It has two inputs. One is the error gate from the integrator gate. The other is a bias, or "run-down" current. The bias current is adjusted so that the Automatic Gain Control level will decrease at a given rate. This sets the maximum rate at which the Automatic Gain Control will follow video that is decreasing in peak value. The maximum rate at which the Automatic Gain Control level will increase is set by the current from the integrator gate. This sets the slewing rate of the Automatic Gain Control integrator.

d. Automatic Bias Control

The automatic bias control circuit has two functions. They are (1) to extend the dynamic range of the error integrator, and (2) to provide low pass filtering for the automatic gain control loop.

The automatic gain control action in this system is obtained by regulating the voltage on dynode 6, as previously explained. This is done by comparing the current from a feedback resistor from dynode 6 with the current from the automatic gain control circuits. The automatic gain control range indicated on Figure 21 is for dynode 6 voltages between -400 and -425 volts. This means that the automatic gain control input current will consist of a large bias component (to obtain -400 volts) plus a small signal current. This dynamic range is difficult to obtain in practice with a simple integrator.

The automatic bias control circuit, connected to the output of the integrator, supplies the bias component of the automatic gain control voltage. It does this by measuring the error integrator output and comparing it with a reference voltage. If the integrator output is offset from the reference, the bias will change gradually until the integrator is operating in the center of

its range. By this means, the integrator dynamic range may be utilized to furnish only the small signal portion of the total automatic gain control current.

The automatic bias control circuit is also an effective low pass filter. This action smooths the rapid changes in integrator output that occur when the automatic gain control error detector switches on the video peaks.

e. Automatic Gain Control Amplifier and Shunt Regulator

The automatic gain control amplifier is a high gain operational amplifier that sums the automatic gain control input and dynode 6 feedback currents. Its output drives the shunt regulator. This is a high voltage, small signal PNP transistor. The collector of the shunt regulator is connected to an intermediate point on the dynode 6 bleeder chain. The shunt regulator drives the voltage at dynode 6 over the required automatic gain control range.

4. Image Level Detector and Line Driver

The image level detector is a fast Schmitt trigger. It compares the output of the star plate video amplifier with the instantaneous peak video voltage. Whenever the video modulation is greater than a pre-set percentage of the reference channel peak video, the detector signals the presence of an image on the plate.

Since the output current capability of the image detector is limited, a buffer or line driver is used between it and the interface equipment. As many as three line drivers may be connected to one trigger.

The preceding sections have dealt with the star plate channel electronics. These circuits also comprise the video and automatic gain control portion of the reference channel. The following sections will discuss the pulse and data circuits in the reference channel.

5. Spot Position Detector

The spot position detector is a fast Schmitt trigger identical to the image detectors in the star plate channels. Its inputs are the reference channel video and the average video voltage. The average video is internally generated in the reference channel, and represents the point midway between the peaks of the video "comb" generated by the Ronchi ruling. The spot position detector triggers when the video modulation is greater than the average video voltage. This generates a gate equal to the half-height width of the teeth in the video comb.

6. Pulse Generator, Clipper and Level, and Line Driver

The pulse generator is fed by the spot position detector output. It is a transistor with an inductor for a collector load. Very sharp pulses of opposite polarity are generated across the inductor at turn-on and turn-off of the spot detector. The clipping and level circuit clips off the negative pulses and sets the level of the positive pulses down from the collector potential to d.c. The line driver is a buffer which provides a spot position pulse output with high current capability.

7. Scan Detector and Scan Gate Generator

The scan detector is a Schmitt trigger. Its purpose is to detect the beginning and end of the laser beam motion across the Ronchi ruling. Its inputs are the reference channel video and a fixed bias voltage. The threshold of the scan detector is set midway between zero output (no light) and the bottom of the reference video comb. This generates a gate that begins when the video indicates the presence of the beam and ends when the video again falls to zero at the end of the ruling.

The scan gate generator is fed from the scan detector. It generates positive and negative (scan and not scan) gates. These gates are used as control signals.

8. Average Video Circuits

The average value of the reference video voltage is used as the bias input to the spot position detector. This voltage is obtained by detecting the maximum and minimum values of the reference video comb, filtering, and combining them to obtain the arithmetic mean.

The maximum signal is obtained as follows: An analog switch, gated by the scan gate, passes video during the interval that the beam is scanning the Ronchi ruling. The gated video is peak detected and filtered by a data-holding circuit with a relatively short time constant. The time constant is chosen to permit the peak video to follow variations in the beam intensity during the scan. The maximum signal value is clamped to a predetermined value between scans by the synchronized clamp. This minimizes the transient that occurs at the beginning of the scan. The minimum signal is obtained in an analogous manner.

The filtered maximum and minimum signals are combined in an amplifier with a gain of one-half. The resulting output is therefore the average of the two voltages. This is used as the threshold for the spot position detector.

9. Instantaneous Peak Video

An important function of the reference channel is to provide an output that accurately represents the instantaneous laser beam intensity. This is accomplished by the instantaneous peak video amplifier.

The output of the maximum signal detector is an accurate reproduction of the reference video peaks, with a shift to d.c. level due to a series of uncompensated base-emitter voltages in the circuitry. This difference in level is measured by a level detector that compares the output of the instantaneous peak video amplifier with the video voltage. If the video peaks exceed the instantaneous value, the detector triggers and charges a data hold in the automatic level control circuits. The output of the automatic level control is

fed to the instantaneous peak video amplifier, increasing its effective d.c. offset. This feedback loop maintains a very tight control on the level of the measured video peaks.

The instantaneous peak video voltage, which accurately represents the laser beam intensity, is used as the threshold voltage for the image detectors in the star plate data channels.

D. Experimental Displays

Two experimental displays have been constructed, utilizing standard laboratory oscilloscopes as indicators. A functional block diagram of these displays is shown in Figure 22. One uses a storage tube to present a magnified replica of an area on the star plate as seen by the laser beam. This is accomplished by providing a raster scan for the picture format, and intensity modulating the electron beam with the image detector transitions. The spot position pulses from the Ronchi ruling may be superimposed on the display to provide a reference scale. Figure 22A shows a typical stored image, with the scale indicated in the center. The second display uses a linear horizontal sweep, with the video voltage from a star plate channel on the vertical channel. The display is intensity modulated by the image level detector. A photograph of this display is shown in Figure 22B. The following sections discuss the functions of the blocks in Figure 22 in greater detail.

1. Star Plate Image Display

The star plate image display shows a "picture" of a small area on the star plate as seen by the image detector. This is essentially a plot of an isophot, or equal image density contour, for any given detector level setting. The display requires three signals, two to generate the raster scan, and one to intensity modulate the storage tube. These signals are:

(a) horizontal sweep--generated in the scope and triggered manually,
(b) vertical sweep--scan gated, and
(c) intensity modulation--amplified image detector output.

The functions of the blocks in this display are as follows:

Video/Sweep and Video/Sweep Delay Multivibrator

These are two adjustable duration one shots. The delay multivibrator determines the beginning of the vertical sweep. It may be set to occur at any desired time after the scan detector operates. The video-sweep multivibrator determines the total duration of the sweep, and may be adjusted to

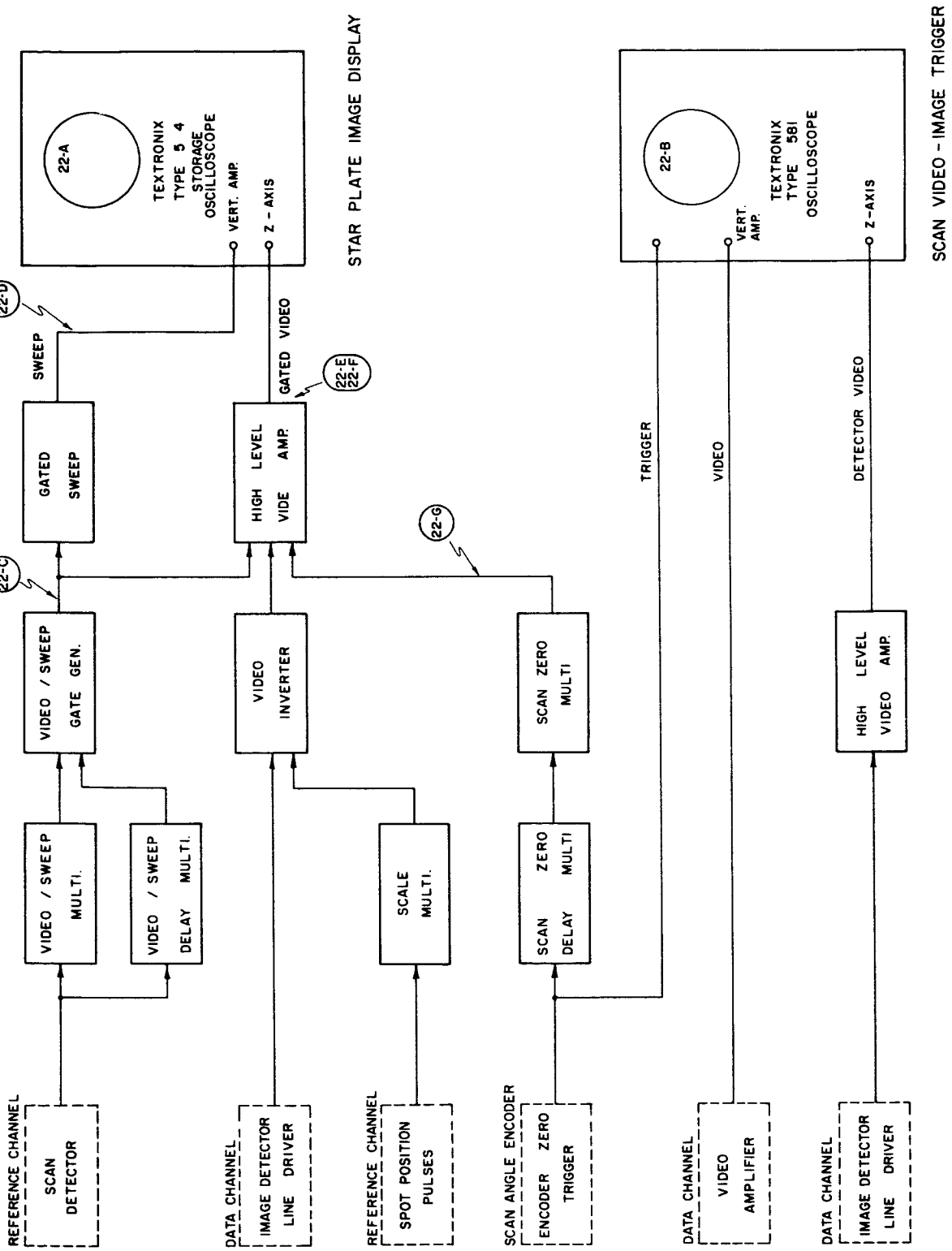

Figure 22: Experimental Display

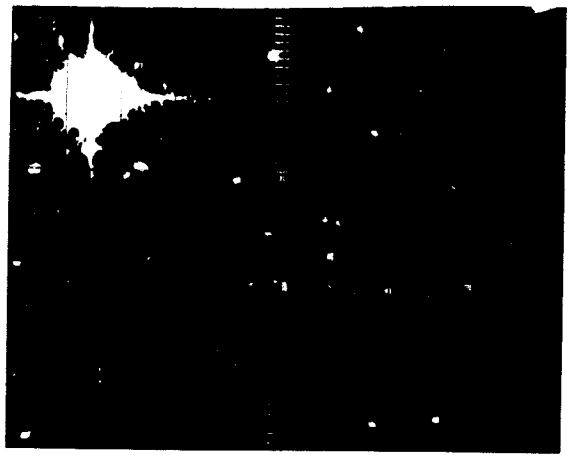

A
Star Plate Image Display
Oscilloscope Storage Tube
Reference Ruling Spacing, 100 Microns

B
Star Plate Video Display Image Detector
Intensity Modulation Trigger Setting
40% transmission

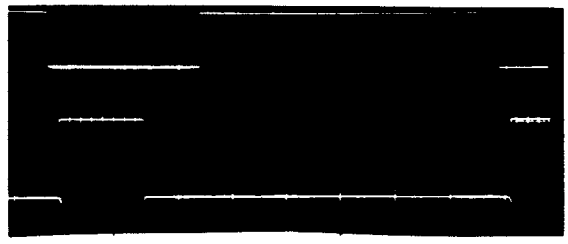

C H V
Scan Detector .5ms/div 2 volts/div
Neg. Video/Sweep Gate .5ms/div 10 v/div

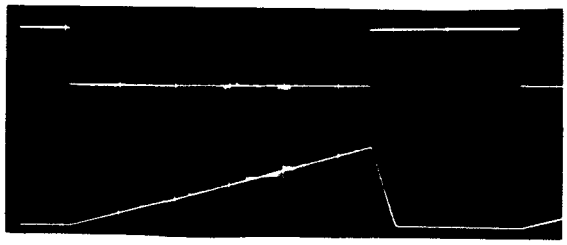

D H V
Neg. Video/Sweep Gate .5ms/div 10 v/div
Gated Sweep .5ms/div 2 volts/div

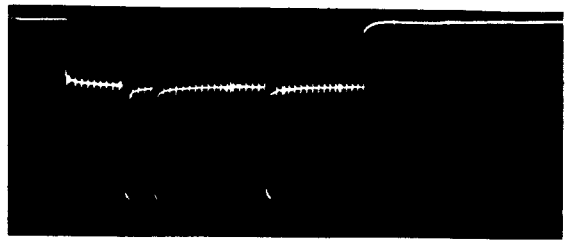

E H V
High Level Video .5ms/div 10 volts/div
(no scale pulses)

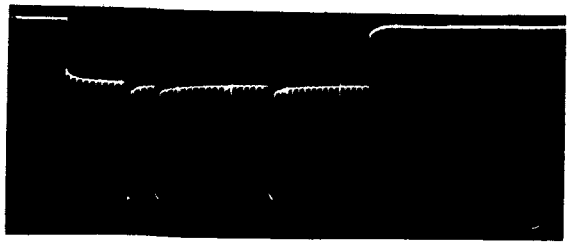

F H V
High Level Video .5ms/div 10 volts/div
(with scale pulses)

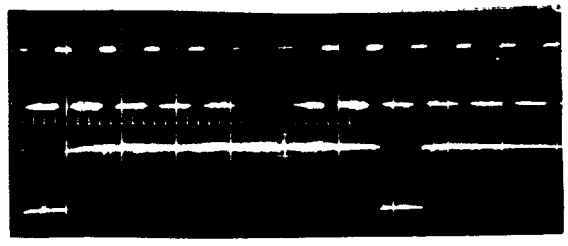

G H V
Neg. Video/Sweep Gate .5ms/div 10 v/div
Scan Zero Gate .5ms/div 10 volts/div

Oscilloscope Waveforms Illustrating Figure 22

cover any portion of the scan. It is also triggered by the scan detector.

Video/Sweep Gate Generator

The video/sweep gate generator is a pulse coincidence circuit and gate generator. It generates gates of both polarities. The gates occur in the interval between the end of the delay one-shot period and the end of the video/sweep one-shot period. The video/sweep gates are the basic control waveforms for the sweep and video unblanking circuits.

Gated Sweep

The gated sweep is essentially a clamped integrator that generates a triangular waveform. The sweep duration is controlled by the video/sweep gate, and the retrace time depends on the current sink capability of the gating circuits. The sweep is applied to the vertical amplifier of the storage oscilloscope.

Scale Multivibrator

The scale multivibrator is an adjustable period one-shot. It is triggered by the spot position pulses. The output pulse width of the scale multivibrator is adjusted to provide the desired line width for the scale on the display.

Video Inverter

The video inverter acts as a summer for the image detector signals and the scale multivibrator output. It is used to drive the high level video amplifier.

High Level Video Amplifier

The high level video amplifier provides the z axis modulation for the storage oscilloscope. It is a gated amplifier with a gain of ten. The signal input is the mixed image detector video, scale multivibrator signal from the video inverter. The control signals are the video/sweep gate and the scan

zero gate. Both gates must be present to permit the amplifier to operate.

Scan Zero Delay and Scan Zero Multivibrators

These two multivibrators are variable-length one-shots. They are used to provide a gate that will select one of the eight scans generated for each scan prism rotation. The scan zero delay multivibrator is triggered by the zero pulse from a shaft angle encoder on the scan prism drive shaft. The scan zero multivibrator is triggered by the trailing edge of the scan zero delay pulse. The scan zero gate length is therefore equal to the scan zero multivibrator output pulse length, and its position with respect to the scan is determined by the delay multivibrator setting. The scan zero gate is somewhat longer than the sweep/video gate, and is set so that it brackets the chosen scan.

2. Scan Video-Image Trigger Dispaly

The primary purpose of this display is to provide a convenient method of monitoring the image detector threshold setting. It may also be used to observe the quality of the star plate video signal. The display requires three signals:

(a) trigger--used to initiate the horizontal sweep--obtained from the scan encoder zero trigger,

(b) video--vertical channel signal--obtained from the star plate video amplifier, and

(c) detector video--z axis modulation--derived from the star plate image detector.

The trigger and video signals are self-explanatory. The detector video is obtained as follows.

High Level Video Amplifier

The purpose of the high level video amplifier is to amplify the star plate image detector output. This signal is applied to the z axis input of the display scope. The resulting display is a trace of the video waveform with the peaks of the star pulses intensified. The level at which the intensification begins and ends is the image detector threshold setting.

IV. MECHANICAL CONFIGURATION OF STAR PLATE SCANNING MACHINE

The machine on which the scanning of the star plates occurs serves three basic functions:

(1) to provide lead screws for accurate measurement of distances on orthogonal coordinates,

(2) to provide accurate ways for planar motion along accurately orthogonal coordinates, and

(3) to provide support for the star plates and the optical scanning system.

An overall view of the measuring machine with the scanning head mounted on it is shown in Figure 23.

A. The Measuring Machine

The measuring machine is the x and y coordinate measuring portion of the Moore Measuring Machine Model #3, modified to suit the 14 inch measurement travel requirements. The standard machine has 18 inches of x travel, but only 11 inches of travel in the y direction. The machine was modified to accommodate the longer travel, and a longer lead screw was substituted for the standard lead screw. Both lead screws are of three millimeters per revolution pitch, and are driven by three speed synchronous motors. The instantaneous positions of the two lead screws are reported by identical shaft encoders. These encoders give 3000 equally spaced pulses per revolution of the lead screws, plus a reference pulse once per revolution. Connected to suitable counters, they will indicate the position of the star plate holder carriage to one micron accuracy. The maximum speed of carriage movement at which the manufacturer will guarantee accuracy is six millimeters per second. Measurements must be made in one direction of carriage travel only. The drive motors provide continuous motion along the x axis for measurement and carriage return, and stepwise motion along the y axis after each x axis traverse has been completed. Each step along the y axis is the nominal length of the optical scan, or 20 millimeters. Eighteen steps will be needed to scan the 360 millimeter plate. The drive motors have three windings for three speeds.

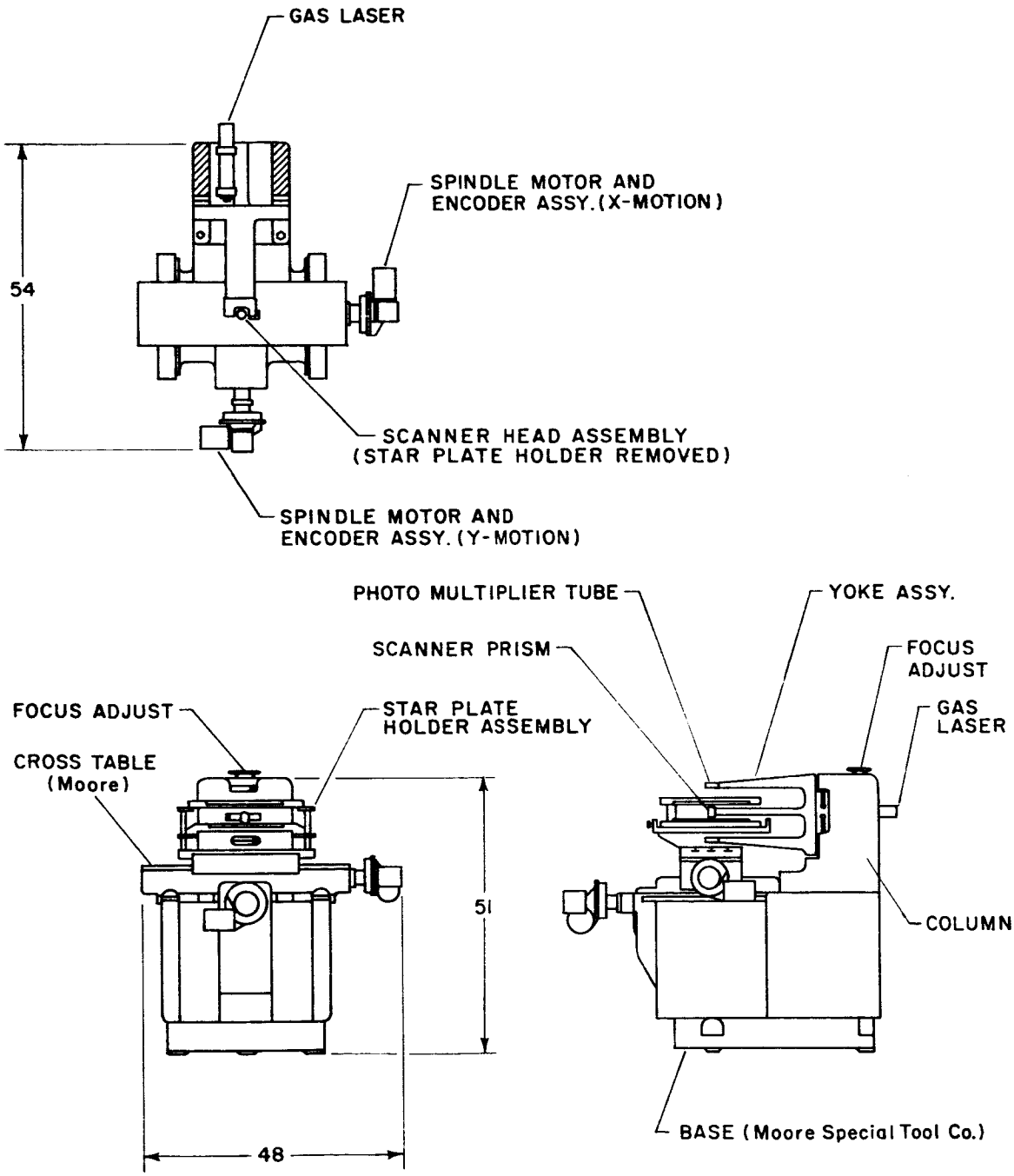

Figure 23: Proper Motion Survey Machine

The three motor speeds, when passed through a gear reducer, result in x axis star plate motions of 6 millimeters per second, 3 millimeters per second, and 1.5 millimeters per second.

B. The Optical Scanning System Mechanical Configuration

The structure supporting the optical scanning system is a casting mounted on the column at the rear of the measuring machine. A center arm projects between the star plates. This center arm supports the converging lens #1, the rotating scanning system, the scan separator prism cluster, the reference reticle, and the motor driven focusing mounts for the converging lens #1 and the reticle. Two other arms project from the column; one over the top of the upper star plate, and one below the lower star plate. These two arms hold the light collection systems for the upper and lower plates, and return the light to the housing after it passes through each of the two star plates. The adjustable apertures and photomultipliers for both star plates and the reticle are all located within the casting, receiving light from the hollow tubes of the yoke assembly. The helium-neon gas laser is also housed within the casting. Focusing the optical system is accomplished by the following controls: (1) converging lens #1 is focused by the slow speed threaded mount holding the lens and driven by a small reversible motor, (2) the reticle is physically moved along an axis normal to the measuring plane, and (3) the three arm yoke is tilted slightly on a flat spring pivot located parallel to the x axis and on the edge of the casting nearest the star plates. This action changes the relative position of the scanning head and the two star plates. This adjustment may be either by handwheel or remotely by motor. In all three cases, the final judgement of best focus is the appearance of the signal trace on the oscilloscope. All motor controlled motions will be provided with limit switches.

C. X and Y Control Systems

The electromechanical motion control systems are shown in Figure 24. The system for control of the table is the x axis control and is used for scanning and carriage return. The cross slide control is the stepwise motion for y axis. The motor-clutch combination provides the stepping motion; the second motor provides the slewing for return to the original or "home" position. The "lock" is an electrically actuated clamp to maintain the y position during an x traverse.

D. Plate Alignment Controls

Before the measurement of the pair of star plates begins, the fixed stars on the two plates must be aligned as nearly as possible. This alignment can involve both rotational and translational relative displacements between the two plates. The drive systems needed for these adjustments are shown in Figure 25. In the star plate scanning machine, the translational adjustments are provided by remote control of the stepper motors on the orthogonal displacement controls on the lower plate. Rotational displacement is provided by a remote control of a stepper motor rotating the upper star plate holder in its housing. The controls for these motors, the focusing motors, the scan and stepwise y axis motors are all located at the control console.

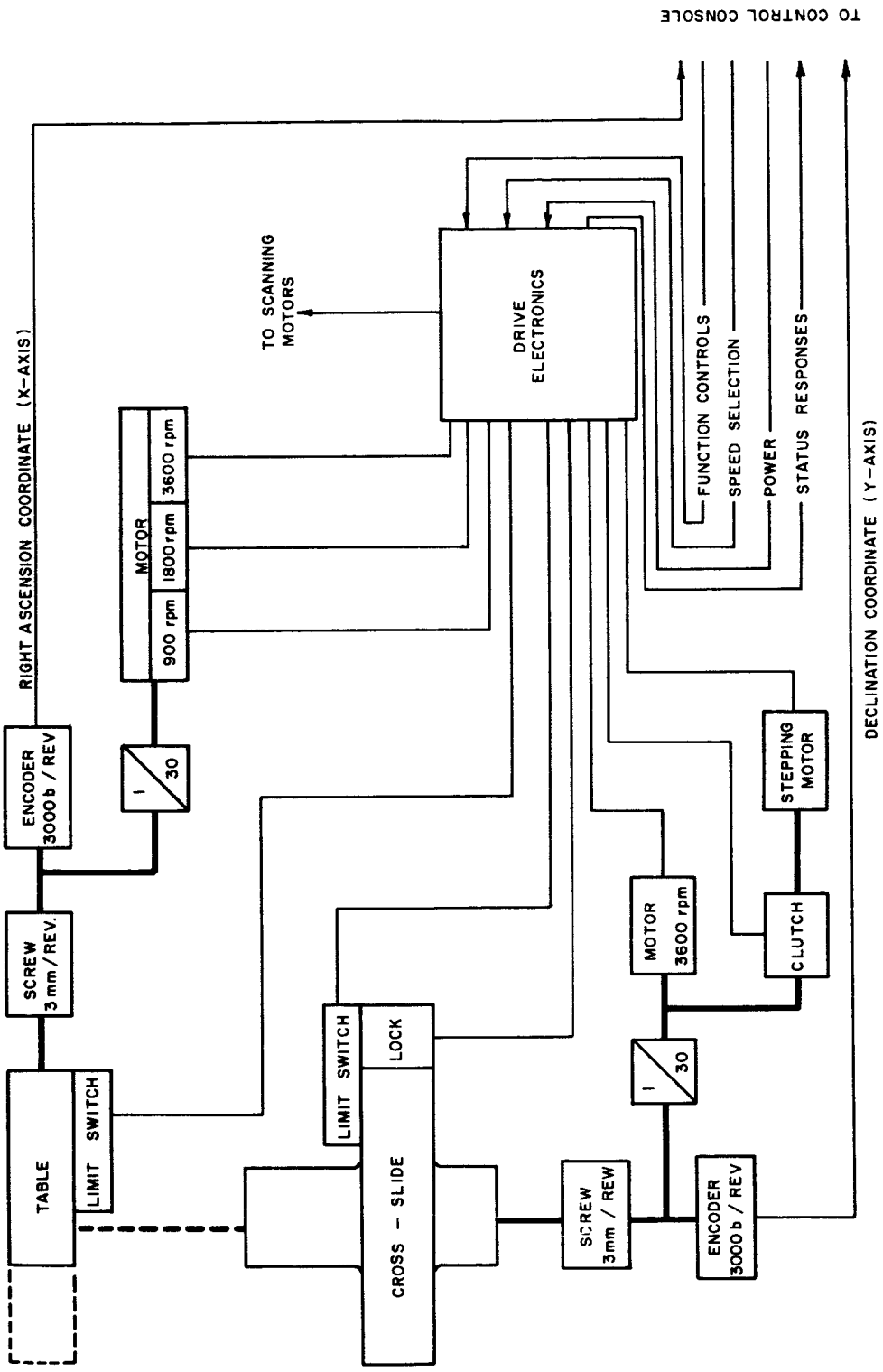

Figure 24: Star Plate Comparator Block Diagram

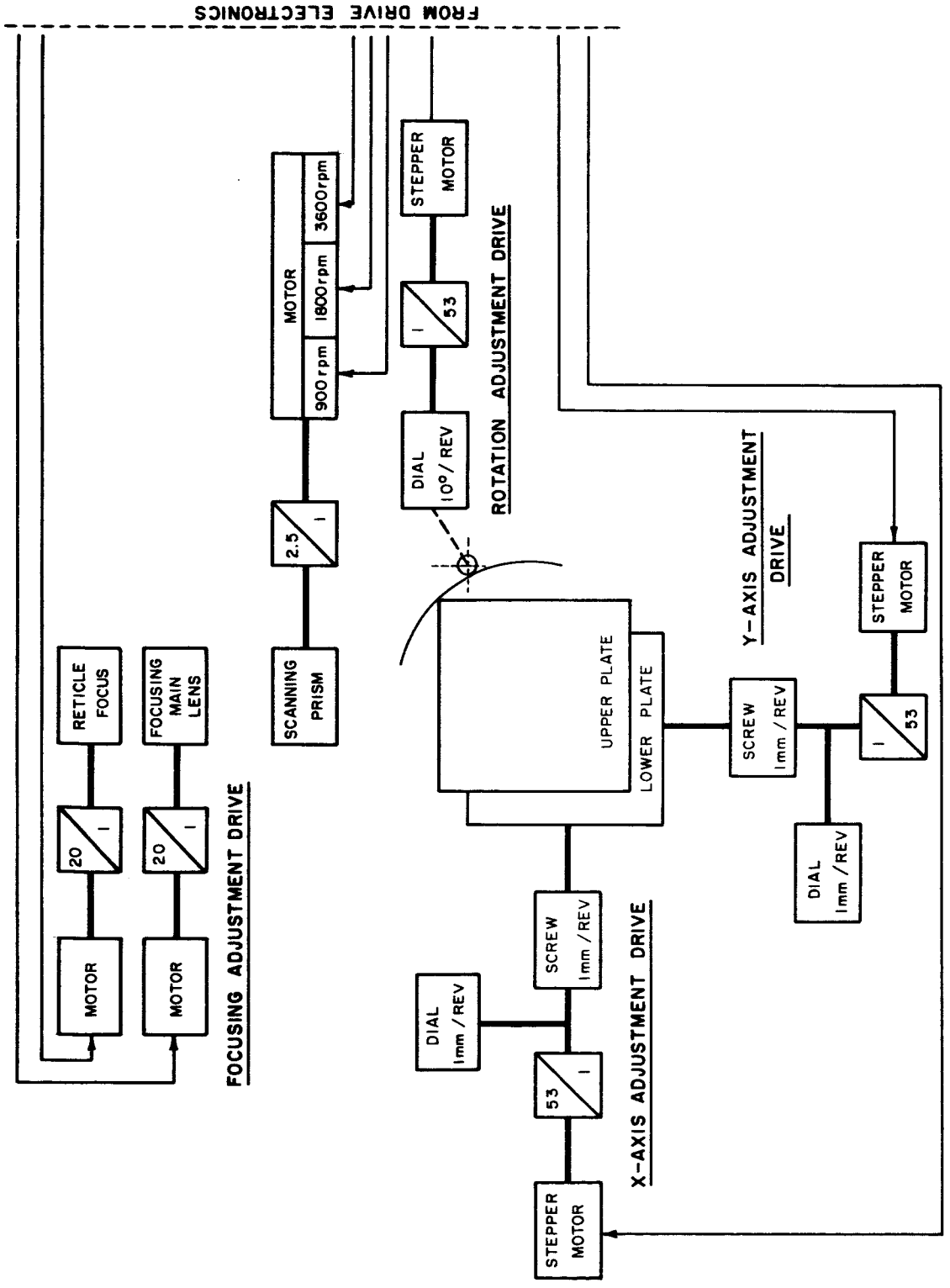

Figure 25: Plate Adjustment and Focusing Drive Block Diagram

E. A Measurement Laboratory Arrangement

A tentative arrangement of the equipment necessary to execute the first step in the proper motion measurement, that of transferring the star plate measurements onto two tapes, one for each star plate, is shown in Figure 26. The scanning machine will be located in a separate room with extensive provisions for maintaining a clean, temperature and humidity stable environment. During actual operation, human intervention will be needed only in changing star plates. All other routine operations, such as plate alignment, initiate and stop the scanning, and focusing, will be done by remote control from the console, with visual monitoring of results by means of magnified star plate displays, meters, and other devices. It is expected that forced air cooling will be required for the tape units and associated electronics in the control room as well.

F. Accuracy of Measuring Machine

The foundation of the accuracy of the scanning systems rests primarily on the accuracy of the measuring machine. The specifications for this accuracy are as follows:

Table travel (x axis) accuracy:

Greatest error in any one inch: 0.38 micron

Greatest error in entire motion: 2.00 microns

Cross slide (y axis) accuracy:

Greatest error in entire motion: 2.00 microns

Geometry of machine:

Orthogonality of x-y axes: 0.51 micron in 10" x 10" travel

Straightness of table travel: 0.64 micron

Straightness of cross slide travel: 0.64 micron

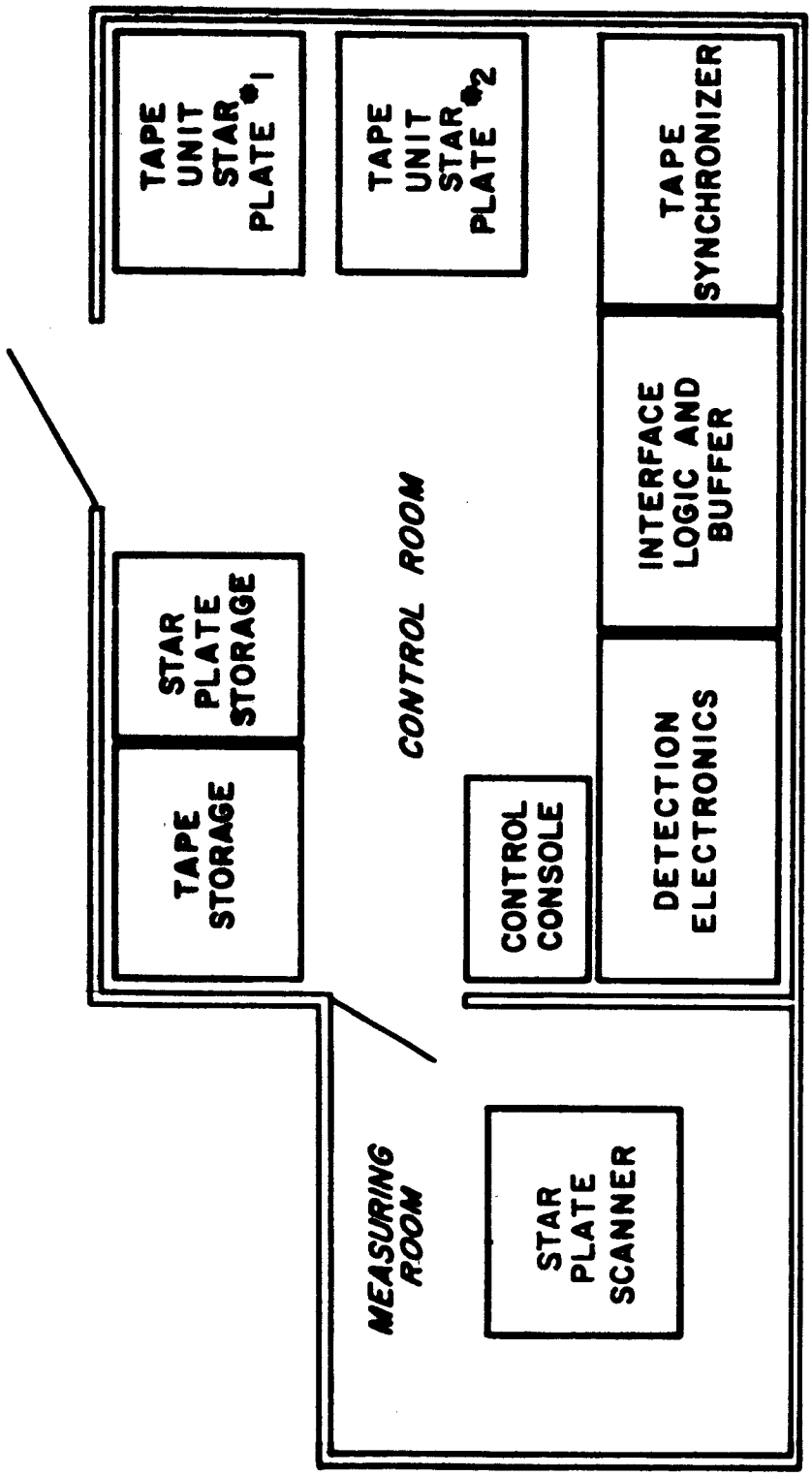

Figure 26: Star Plate Measuring Laboratory

V. DATA COLLECTION AND REDUCTION

The Automatic Proper Motion Survey as presently conceived will be a two step operation, that is, data will be collected by a hybrid system involving high speed core memory and magnetic tape units, and the data will be processed later on a high speed digital computer; possibly the University of Minnesota Control Data Corporation 6600 Computer. The primary reason for not operating on line with a high speed computer was the inefficient use made of the computer time resulting in high cost per computation. This inefficiency arises from the time required to remove one set of star plates and to mount and align another set while still connected to the computer, as well as the time required to return the carriage from the end of a stripe. The following are descriptions of the various stages of the operating system. The steps set forth for programming for the high speed digital computer are tentative.

A. Data Format

Before considering the system for the proper motion survey, some terminology and the data format will be defined. As now defined, the machine will scan the pair of plates in several strips, where each strip will now be defined as a "stripe". The distance from the edge of the plate to the bottom of a given stripe is defined as Y_s. Hence, during any stripe, this measurement shall be a constant. Figure 27, then, goes one step farther by showing the scanning within the stripe. Only one image is used for clarity. The stripe will be approximately two centimeters in height with the length of a plate being 356 millimeters. The laser beam will be moved from bottom to top by a rotating prism. The distance between each scan Δx shall be a fixed known quantity, and hence defined within the computer program.

In actuality, the scan beam is tilted due to the continuous motion on the x-axis lead screw. However, this will be corrected within the program. When the beam intercepts an image on the star plate, a "transit" occurs. For this transit we need to know the x and y coordinates of the beginning of transit of the image, and the duration of the transit. The beginning is called

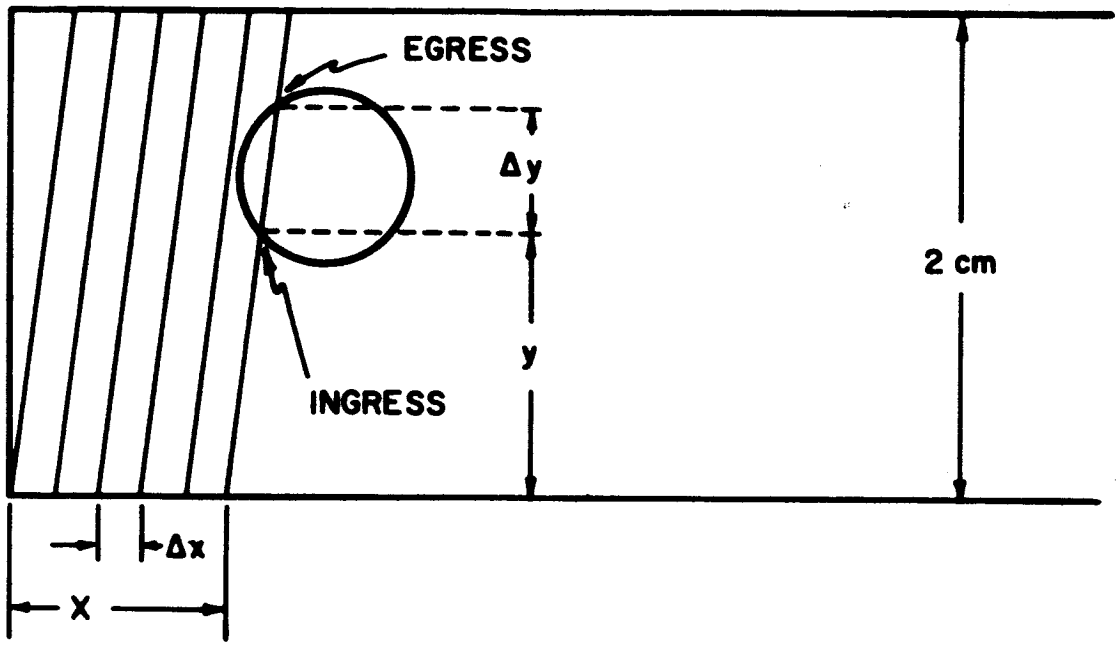

Figure 27: Typical Transit in Stripe

"ingress" and the end called "egress". At ingress, the x measurement from the beginning of the stripe and the y measurement from the bottom edge of the stripe are created. At egress, Δy is created, a measure of the duration of the transit or width of image. Table I gives a summary of all the measurements discussed above and the number of bits necessary to give a one micron accuracy for each.

After many discussions on data format, the following operational requirements were devised: Before the scanning of a stripe is commenced, a request will be sent to the star plate interface for the present value of Y_s, since this is constant for the entire stripe. The operator will control the beginning of scanning for each stripe. It has been suggested, for ease and increased speed in programming, that there be some simple way to detect the transition from one scan to the next. Therefore, at the beginning of each scan the quantity x shall be written and remain the same for all transits within

that scan. The bit which denotes the x measure for a transit shall be the uppermost bit (a one) of the data word for branching on the sign (0 = + and 1 = -) within the computer program. Y_s and x measurements come from the respective lead screw, therefore, each lead screw shall have a 3000 count per revolution angle encoder plus an 8-bit revolution counter.

TABLE I

SUMMARY DESCRIPTION OF DATA WORDS		
Symbol	Description	Number of Bits
Y_s	Distance from edge of plate to bottom of stripe--8-bit revolution counter 3000 count/revolution angle encoder	20
y	Width of transit = 1 millimeter or less	10
y	Distance from bottom of stripe to beginning of transit	15
Δx	Distance between each scan (center to center)	--
x	Distance from end of stripe to beginning of transit--8-bit revolution counter 12-bit angle encoder	20

The layout of the data format as it will be on magnetic tape is shown in Figure 28. Thus, for each transit a data word of 30 bits is created. Y_s will be contained in an identification record which precedes the data from the stripe.

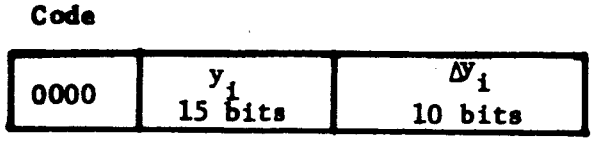

(a) Word Format for Transit

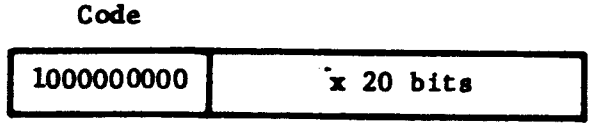

(b) Word Format for x Value

Figure 28: Data Format (30-bit word)

B. Data Collection System and Data Rates

A diagram of the data collection system for one plate is shown in Figure 29. The two registers before the core memory act as a buffer to slow down the data rate for writing into core memory. The core memory presently being considered has a write time of 1.24μs, but data can come at peak rates of one transit every 1μs. Hence, these two primary flip-flop holding registers will give sufficient delay to the data rate for storage to occur without losing any data (i.e., overflow). As the data for a transit enters the first holding register, the tag (a 0) is put in the upper bit to denote a transit. This tag, plus $\bar{y}$ and Δy, are then stored in core memory. From here, data is read out of core, reformatted to 30 bits (as shown previously in Figure 28) and written on magnetic tape. Using a standard Control Data 607 Magnetic Tape Unit 556 bits per inch, 150 inches per second, 7 channels), the system can write a 30-bit word every 60μs. Hence, the ultimate factor in determined data rates is how fast the magnetic tape can accept data. We will now consider this.

Again, let us assume a Control Data 607 magnetic tape transport which has a recording density of 556 bits per inch (frames per inches--frame = six bits and parity and a tape speed of 150 inches per second. This results in a 30-bit data word written in 60μs. If we then assume a record (block of data) of 1024 data words, this uses 9.21 inches of tape plus 3/4 inch for record gap. The total time required to write this block is 6.62×10^{-2} seconds. Dividing this into 1024 data words, 1.55×10^{4} data words can be written on magnetic tape in one second. The three scanning speeds of the plate machine are 1200, 600, and 300 scans per second. Each time a scan begins, an x data word is generated. However, these occur at a fixed, predetermined rate. Subtracting the x rate (or scan rate) from the data words per second, the remaining is the number of transits per second the tape can accept. This can be broken down into transits per scan. The results are shown in Table II.

TABLE II

TRANSITS PER SCAN RATE FOR MAGNETIC TAPE AS A FUNCTION OF SCAN RATE	
Scans Per Second	Transits Per Scan
1200	11.9
600	24.8
300	50.7

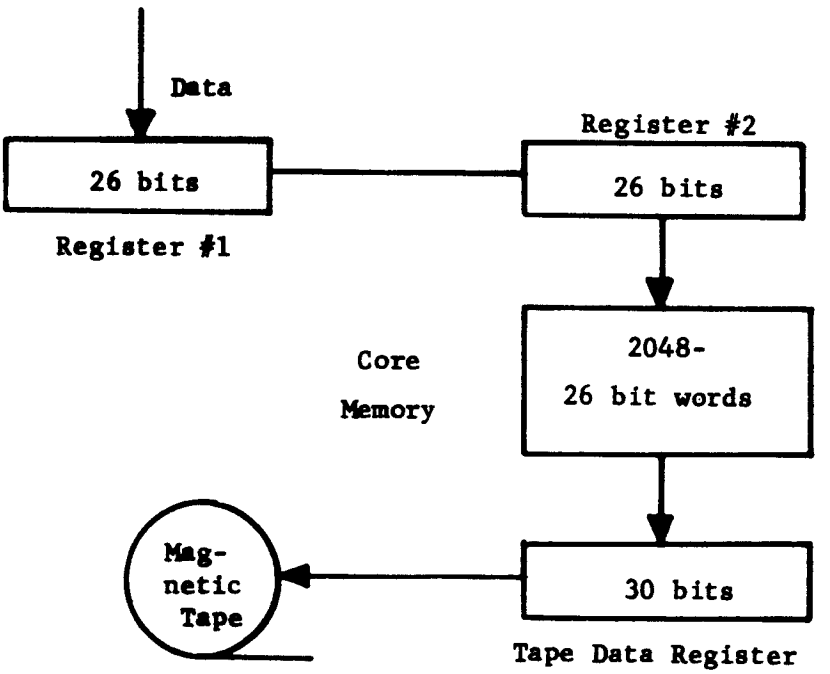

Figure 29: Data Collection System for One Plate

C. Complete Data Processing Program

In order to understand how data from the star plate scanner data tapes will be handled, a flow diagram showing a tentative method is given in Figure 30, and discussed below.

Processing will begin by reading in blocks of data for each plate. The images are then constructed from this data (explained in Appendix B). Having formed all images from both plates, the matching process is initiated over small subsections of each stripe. These subsections are chosen so that they each contain approximately 1000 stars. All stars are matched except perhaps those appearing at the edge of a subsection. These may not match with anything from the other plate because the two subsections are not precisely lined up. Again, if troublesome star pairs appear (difficult to match pairs), they will be temporarily set aside and only those which agree very well will be used to compute a new set of misalignment parameters. Any pairs which are separated by more than some preassigned value (undergone some proper motion) are not used in this computation. These new misalignment parameters are a rotation, a stretch in two dimensions, and a translation in two dimensions. These parameters will be applied mathematically to the stars from the older plate to bring them into coincidence with the images from the new plate. Now the proper motion stars (motions larger than some predetermined small value) can easily be picked out of the collection of all plate stars. Motion stars are then written on a magnetic tape along with all pertinent information such as plate, celestial coordinates, and the magnitude and direction of motion.

Completing one subsection, the program moves on to the next until the complete plate has been considered. A detailed description of the proper motion problem and a method of solution follows.

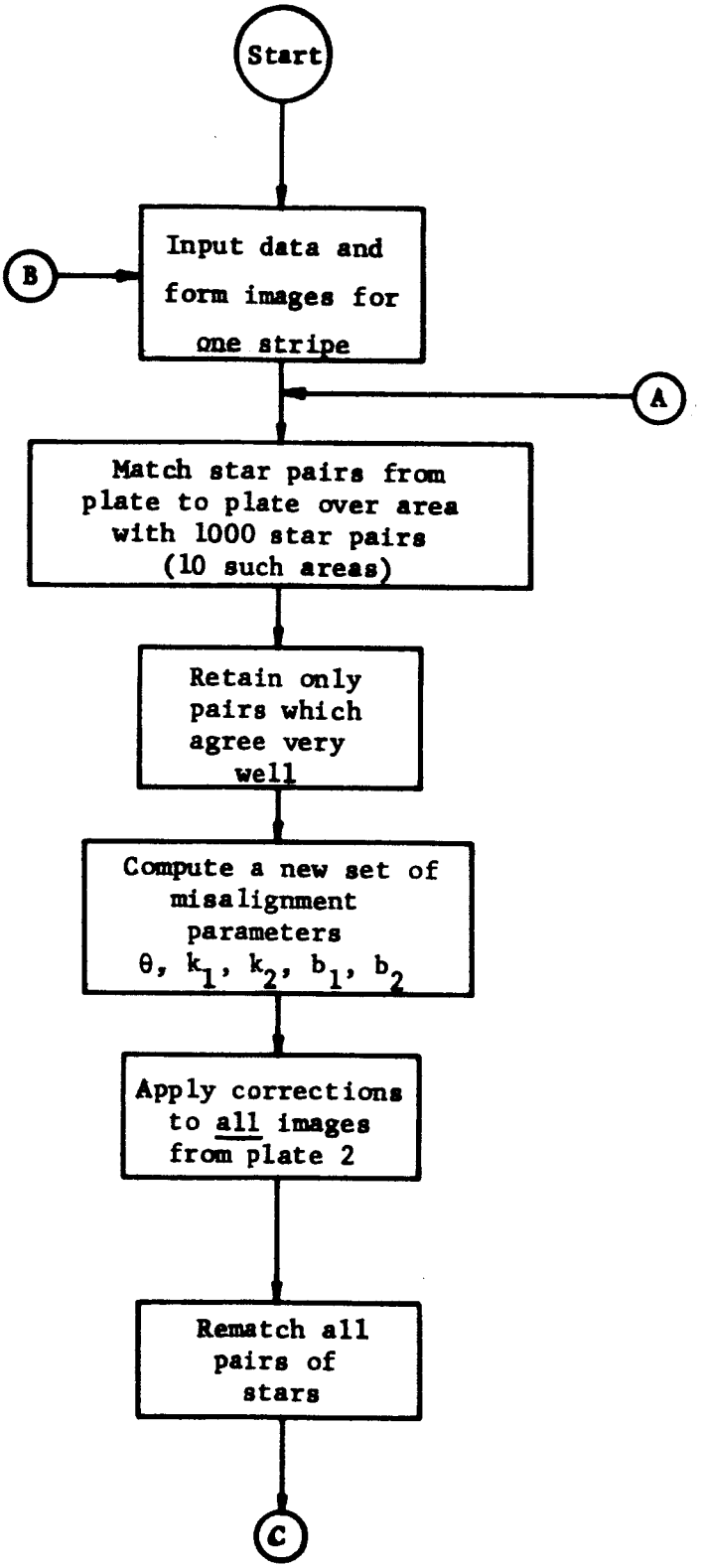

Figure 30: Data Handling--Proper Motion Machine

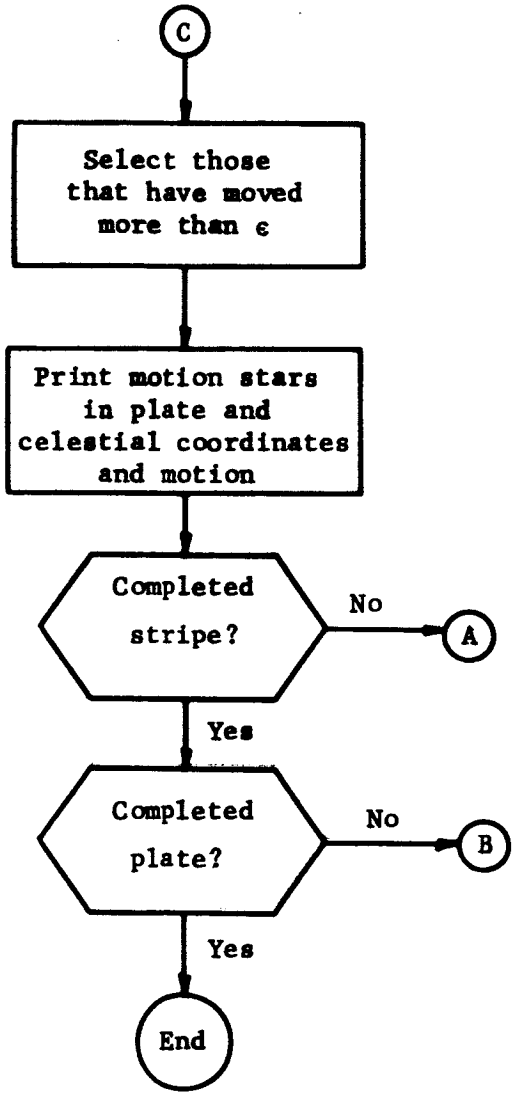

Figure 30 (concluded)

D. Plate Alignment

Let the vectors $\overline{V}$, $\overline{U}$ be the position of a pair of corresponding stars from the newer plate and older plate respectively. Suppose we are able to rotate and translate the older plate in order to align the two stars by a transformation of the form $\overline{V} = A\overline{U} + \overline{B}$, where

$$A = \begin{pmatrix} \cos\theta & \sin\theta \\ -\sin\theta & \cos\theta \end{pmatrix}, \quad B = \begin{pmatrix} b_1 \\ b_2 \end{pmatrix}$$

where θ is a rotation angle and b_1, b_2 are translations in two orthogonal directions to be applied to the $\overline{U}$ coordinate system in order to bring the vectors $\overline{U}$ and $\overline{V}$ into coincidence (no amount of plate adjustment will compensate for a misalignment due to stretching, this will be taken care of mathematically after initial alignment.) See Figure 31. Given a set of $\overline{V}_i$ vectors and their mates $\overline{U}_i$, $i = 1, 2, \ldots, N$, N stars from each plate, find the angle θ and the two translation parameters b_1 and b_2 in order to best align the two plates (all motion as defined here will be applied to plate U, if not, use same magnitudes but change signs and apply to plate V). Note that we only need a single pair of stars in order to find these three parameters, and that if more than one pair is used, there will be no unique solution since the system of equations is overdetermined. For this reason we may consider only a "best" alignment in some sense; in this case, we will choose the least squares sense.

$$\overline{V} = \begin{pmatrix} \cos\theta & \sin\theta \\ -\sin\theta & \cos\theta \end{pmatrix} \overline{U} + \begin{pmatrix} b_1 \\ b_2 \end{pmatrix}$$

We may further assume θ is small, say $|\theta| < 1/2$ degree, then

$$\sin\theta \cong \theta, \quad \cos\theta \cong 1$$

and

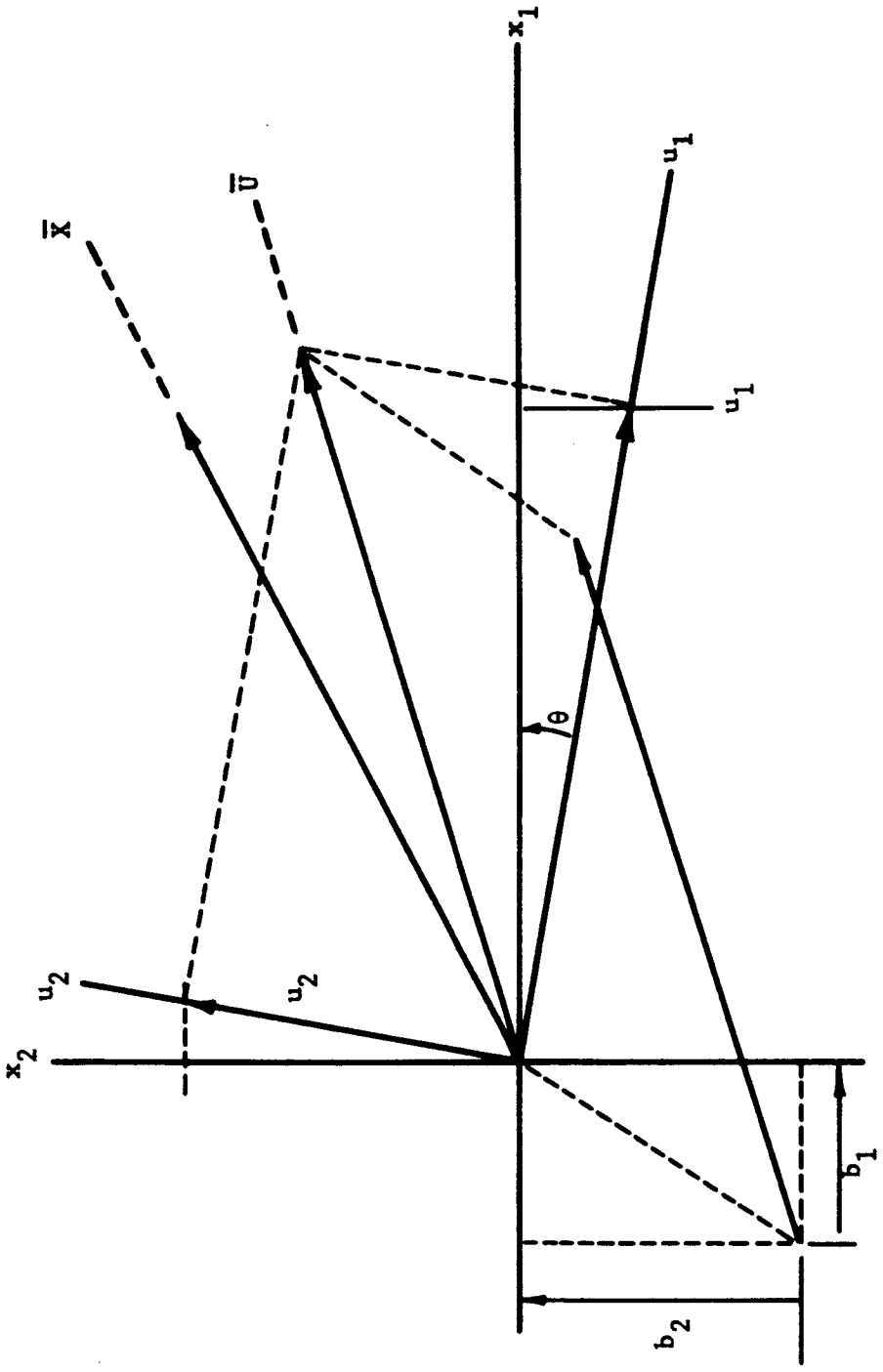

$$x_1 = u_1 \cos\theta + u_2 \sin\theta + b_1$$

$$x_2 = -u_1 \sin\theta + u_2 \cos\theta + b_2$$

Figure 31: The Misalignment Rotation and Translations

$$\overline{V} = \begin{pmatrix} 1 & \theta \\ -\theta & 1 \end{pmatrix} \overline{U} + \begin{pmatrix} b_1 \\ b_2 \end{pmatrix}$$

$$v_1 = u_1 + \theta u_2 + b_1 \qquad v_2 = -\theta u_1 + u_2 + b_2$$

or $$v_1 - u_1 = u_2\,\theta + b_1$$

$$\underbrace{v_2 - u_2}_{\overline{d}} = -u_1\,\theta + b_2$$

$\overline{d} = CW$ where C is the 2 x 3 matrix $\begin{pmatrix} u_2 & 1 & 0 \\ -u_1 & 0 & 1 \end{pmatrix}$

and $W = \begin{pmatrix} \theta \\ b_1 \\ b_2 \end{pmatrix}$

Each star and its mate will produce a vector $\overline{d}_i$ and a matrix c_i. These will be arranged in the vector D and the matrix C as

$$D = \begin{pmatrix} \overline{d}_1 \\ \overline{d}_2 \\ \vdots \\ \overline{d}_N \end{pmatrix} = CW = \begin{pmatrix} c_1 \\ c_2 \\ \vdots \\ c_N \end{pmatrix} W$$

(2N x 1) (2N x 3)(3 x 1)

The least squares best solution is given by

$$W = (C^T C)^{-1} C^T D$$

Note that $C^T C$ is a 3 x 3 symmetric matrix of the form,

$$\begin{pmatrix} u_2^{(1)}, & -u_1^{(1)}, & u_2^{(2)}, & -u_1^{(2)} \ldots u_2^{(N)}, & -u_1^{(N)} \\ 1 & 0 & 1 & 0 \ldots 1 & 0 \\ 0 & 1 & 0 & 1 \ldots 0 & 1 \end{pmatrix} \begin{pmatrix} u_2^{(1)} & 1 & 0 \\ -u_1^{(1)} & 0 & 1 \\ u_2^{(2)} & 1 & 0 \\ -u_1^{(2)} & 0 & 1 \\ \vdots & & \\ u_2^{(N)} & 1 & 0 \\ -u_1^{(N)} & 0 & 1 \end{pmatrix}$$

$$= \begin{pmatrix} \sum_{i=1}^{N} (u_1^{(i)2} + u_2^{(i)2}), & \sum_{i=1}^{N} u_2^{(i)2}, & -\sum_{i=1}^{N} u_1^{(i)2} \\ \sum_{i=1}^{N} u_2^{(i)2} & N & 0 \\ -\sum_{i=1}^{N} u_1^{(i)2} & 0 & N \end{pmatrix}$$

This may be written

$$C^T C = A = \begin{pmatrix} a+b & b & a \\ b & N & 0 \\ a & 0 & N \end{pmatrix} \quad \text{with} \quad a = -\sum_{i=1}^{N} u_1^{(i)2},$$

$$b = \sum_{i=1}^{N} u_2^{(i)2}$$

The determinant

$$p = N^2(-a + b) - N(a^2 + b^2)$$

and the inverse may be written

$$A^{-1} = \frac{1}{p}\begin{pmatrix} N^2 & -Nb & Na \\ -Nb & N(-a+b) - a^2 & -ab \\ Na & -ab & N(-a+b) - b^2 \end{pmatrix}$$

The inverse is well defined except where $p = 0$.

$$N^2(-a + b) - N(a^2 + b^2) \stackrel{?}{=} 0$$

$$Nb - b^2 = a^2 - Na$$

$$a \leq 0$$

$$b \geq 0$$

$$N > 0$$

We have been able to write the inverse of $C^T C$ as a function of the sums a and b and the number of star pairs N. A simple check of the quantities $Nb - b^2$ and $a^2 - Na$ will indicate the condition of the inverse. Note that if the $U_1^{(i)}$ and $U_2^{(i)}$ are near 1, the sums a and b are near N and all the elements of the inverse are of approximately the same size. We will choose the units then according to this criteria.

E. Proper Motion Calculations

Let the proper motion of the i^{th} star be given by the product of a scalar and a direction vector $\epsilon_i \, d_i$. Then if the star plates have been perfectly aligned, the relation between a vector to the same star on the two plates (U plane will be the earlier or older plate, V plane will be the new plate) is

$$\overline{V}_i = \overline{U}_i + \epsilon_i \hat{d}_i \qquad i = 1, 2, \ldots, N \text{ (N star pairs)} \tag{1}$$

However, because the two plates may be misaligned, we may state only that we are able to account for this misadjustment by some transformation of the coordinates of one plate to the coordinates of the other. In general, this transformation may take almost any form, however, for physical reasons, we may assume it to be linear and consist of a combination of a stretch, rotation, and translation. Let the stretch-rotation transformation be given by the 2 x 2 matrix A, and the translation be given by the 2 x 1 vector $\overline{b}$. Then applying these to Equation (1), we have

$$\overline{V}_i = A(\overline{U}_k + \epsilon_i \hat{d}_i) + \overline{b} \tag{2}$$

Now given N corresponding vectors from the two plates we see that there will be 2N + 6 unknown quantities involved, 4 from A, 2 from $\overline{b}$, and 2 from each $\epsilon_i \hat{d}_i$. Suppose, however, that we attempt to solve Equation (2) by setting $\epsilon_i d_i = 0$ and find A', $\overline{b}'$. Then we solve (2) for the proper motion $\epsilon_i \hat{d}_i$, i = 1, 2, ..., N. Next, we temporarily discard those star pairs which appear to have large proper motions and use the remaining pairs to recompute A, and $\overline{b}$. This process may be repeated if necessary until the $\epsilon_i \hat{d}_i$ stabilize (hopefully after two iterations). The parameters of interest then are

$$\mu_i = | \epsilon_i |$$

$$\theta_i = \tan^{-1} \left(\frac{d_{2_i}}{d_{1_i}} \right)$$

A method for testing the above procedure may be considered. Generate a set of vectors $\bar{U}_i$, i = 1, 2, ..., N. Choose a reasonable value for ϵ, say the largest proper motion anticipated. Select a set of proper motions for approximately 1/8 of the star pairs. Choose some A and $\bar{b}$, and form the vectors $\bar{V}_i$ where

$$\bar{V}_i = A(\bar{U}_i + \epsilon_i \hat{d}_i) + \bar{b} \qquad i = 1, 2, \ldots, N.$$

Set $\epsilon_i \hat{d}_i = 0$ and solve for A, $\bar{b}$. Find $\epsilon_i \hat{d}_i$ for i = 1, 2, ..., N and compare with the known proper motion assigned. Note

$$\bar{V}_i = A\bar{U}_i + \bar{b}_i + A(\epsilon_i \hat{d}_i)$$

$$\epsilon_i \hat{d}_i = A^{-1}(\bar{V}_i - A\bar{U}_i - \bar{b}) = A^{-1}(\bar{V}_i - \bar{b}) - \bar{U}_i$$

where A^{-1} is A inverse. Provide an option to continue the process and compare successive motions. Stop the iterative process when the proper motions stabilize.

VI. TESTS AND MEASUREMENTS USING EXPERIMENTAL TEST MODEL

This section presents results of measurements of the performance of optical and electronic components and systems using the engineering test model. These measurements form the basis for the parameters used in the final design of the scanning instrument and the signal electronics.

A. Effect of Closing Aperture on Resolution of System

The purpose of this measurement was to evaluate the effect of aperture size change on the signal-to-noise ratio of the video output. The area scanned was on "old" duplicate "red" plate P322; this region was known as "Selected Area 57". It was chosen for this study because the stars in this region have accurately documented magnitudes; one of the stars measured was listed as $m_{red} = 20.0$ in the photoelectric and visual ranges. In addition to testing whether or not the scanning system can detect a faint star, the effect on the storage tube oscilloscope display of change in the threshold setting shows in the shape of the images of bright stars. The threshold control is a hand-set control which sets the percentage of the illumination level at which the image detector trigger changes state, as discussed in Section III.B.5.

The plate used was a "red" plate duplicate. A 10.5 power microphotograph of the section scanned is shown in Figure 32 with the scan path indicated. A higher power photomicrograph of the $m_v = 20$ star is included to describe the image and grain structure of the plate.

The oscillograms produced by this scan are shown in Figure 33. The oscillograms labeled A were made with the aperture diameter opened wider than the effective width of the photocathode of the 1P21 photomultiplier; hence, both the effective spot size and shape were determined by the photocathode rather than the aperture. Since the sensitivity of the photocathode varies with position on the photocathode, predicting the spot size and shape in this aperture setting is difficult. The lower trace is an expanded sweep showing the $m_v = 20$ star trace in detail. Note that in the upper trace the star

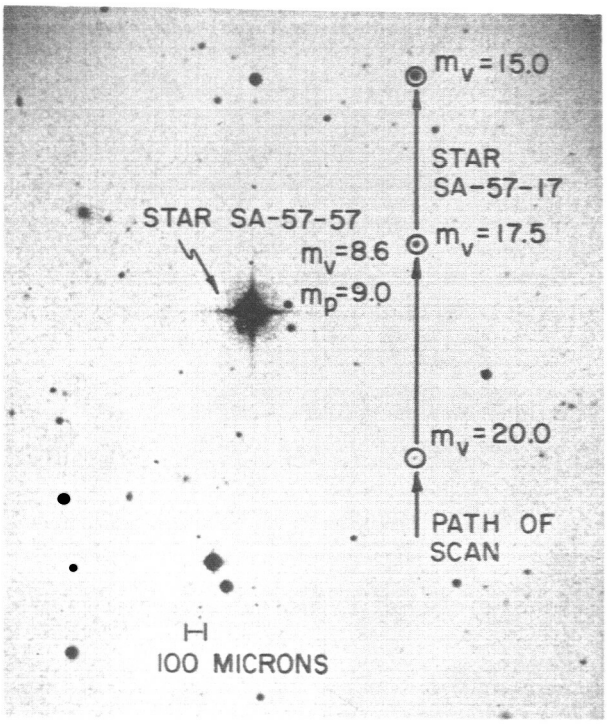

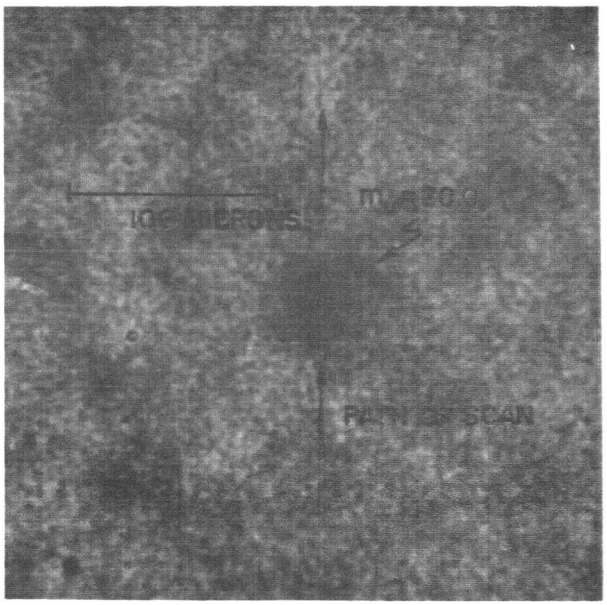

B. 275 x magnification of the 20th magnitude star in the scan

Figure 32: Photomicrographs of SA57 From Plate P322. The coordinates of the ninth photographic magnitude star are: 13 hours, 6.2 minutes right ascension 1950, and 29°39' declination

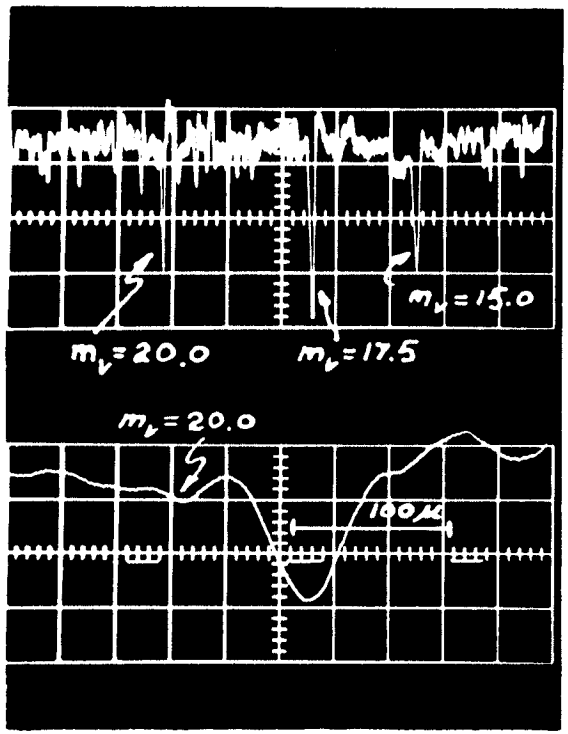

A. Scan with aperture defined by photomultiplier photocathode.
Upper trace: full scan
Lower trace: expanded trace of the m_v = 20 image. Horizontal markers are 100 microns apart

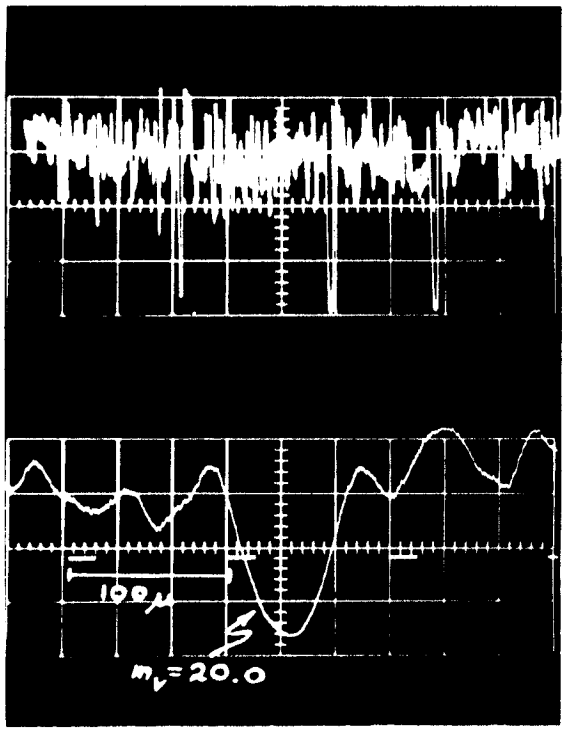

B. Scan with aperture diameter at a minimum.
Upper trace: full scan
Lower trace: expanded trace of m_v = 20 image. Horizontal markers are 100 microns apart

Figure 33: Full Scan and Expanded Scale Oscillograms of SA57 Along the Path Shown in Figure 32

B. Effect of Changing Threshold Level of Image Detector on Number and Shape of Star Images Detected

The purpose of this measurement was to find a threshold setting at which stars of highest magnitude number could be reliably detected without including photographic grain and stars of higher mangitude within the detection limits.

The area selected for scanning was the same as the area used for the previous measurement--SA57. In this case, the stars detected were displayed on the screen of the storage oscilloscope. A microphotograph of the area is shown in Figure 34 with the specific area scanned outlined in black.

Photographs of the display of the star field for various threshold level settings are shown in Figure 35. The threshold level settings are expressed as the percentage of transmission of light less than plate fog level. The lower level, 30 percent, was chosen as being the level at which the $m_v = 20$ star could first be detected; no photographs were taken beyond 55 percent because the number of detected targets that were not usable stars was very large beyond the 55 percent level setting.

Comparison of the $m_p = 9.0$ star in Figures 32 and 34 with the images of this star in Figure 35 show that the apparent shape of the bright star changes as the trheshold level changes. This, as well as many observations on other plates, indicates the value of a threshold level setting of 35 percent to 45 percent for a practical balance between reliability of detection of plate limit stars and detection of excessive numbers of fainter stars and grain clusters.

m_v = 15.0 appears to produce less change in transmission than the smaller star images. This is due to the fact that the scan path did not pass directly through the center of the image, but grazed one side. The lower trace shows the m_v = 20 star on an expanded scale with 100 micron reference markers from the reticle superimposed on the lower trace.

The oscillograms labelled B show the comparative traces with the aperture diameter at its smallest opening. Calculations based on the curves of Appendix A and Figure 6 indicate an effective spot diameter of about 22 microns. Note that changing the aperture size produces several important effects. They are:

(1) increasing the percentage of transmission change for the faint stars with reference to the average fog level, and

(2) increasing the percentage of transmission of the average fog level.

This is the result of the Automatic Gain Control using the peaks of the video signal for reference. With the increase in resolution, the peaks of the grain noise show a wider deviation from the average noise. This results in a depression of the average grain noise from the maximum transmission level. This, in effect, offsets the advantage of higher resolution obtained when the aperture is closed down.

Thus, with automatic gain control referenced to the peak of the grain noise, increased resolution produces little improvement in signal-to-noise ratio. However, this property of the system can be improved by using a time based average grain noise as a reference for the automatic gain control. Work on such an automatic gain control reference is now in progress.

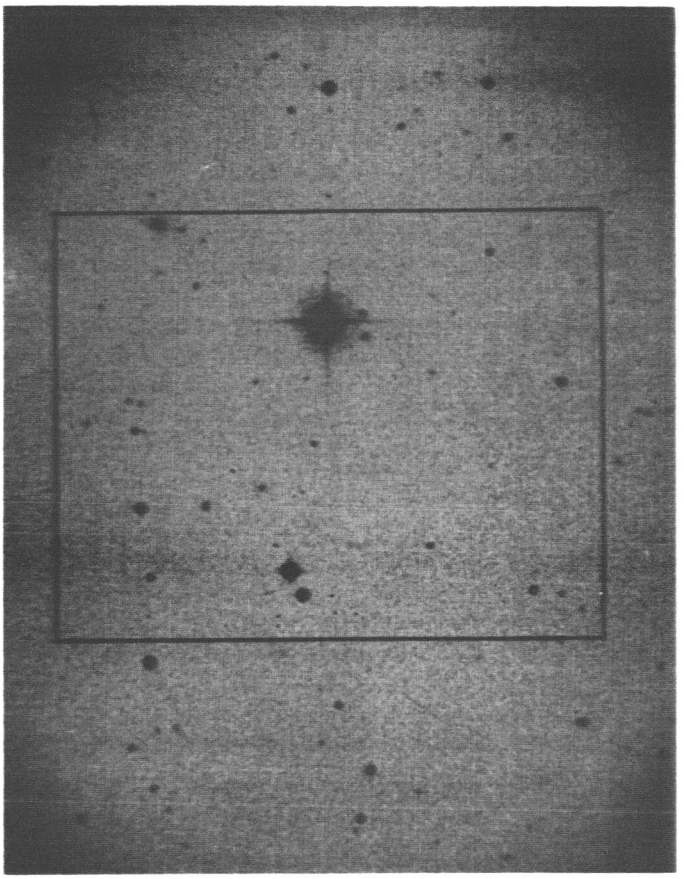

Figure 34: Region of SA57 Used in Evaluating the Effect of Altering the Threshold Level Control. Area displayed in storage tube photographs of Figure 35 outlined in black

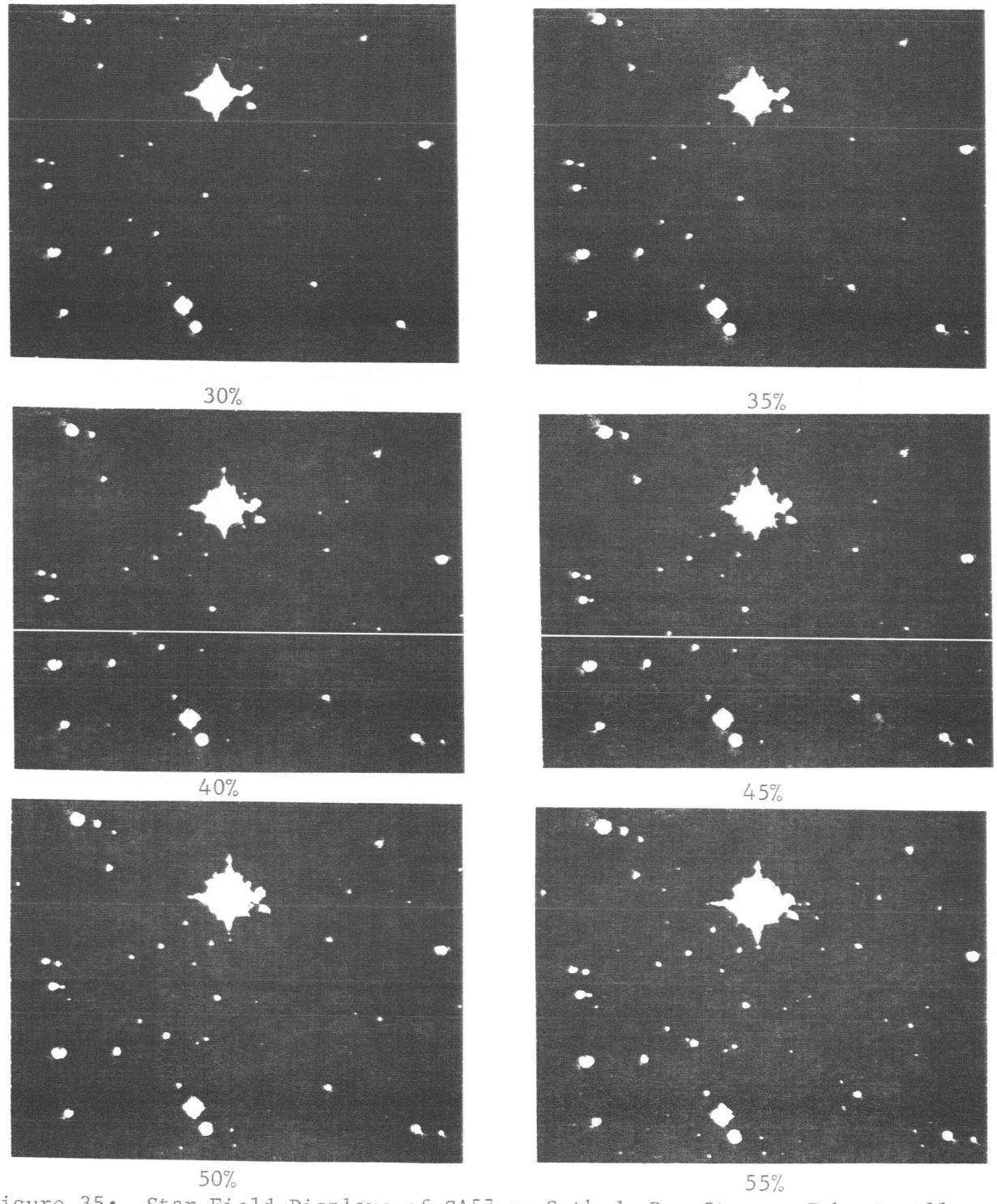

Figure 35: Star Field Displays of SA57 on Cathode Ray Storage Tube Oscilloscope for Various Threshold Level Settings of the Image Detector. Note that the $m_v = 20$ star appears for all settings of threshold level. Level settings are expressed as percentages of film fog level: that is, 100% would detect all stars plus background grain, and zero percent would detect none.

C. Concluding Remarks

The investigations of design parameters of the Automatic Star Proper Motion Scanning System have shown that:

(1) The laser beam-octagonal prism microdensitometer has sufficient resolution to detect images of stars of twentieth magnitude in the present National Geographic-Mount Palomar Observatory Sky Survey star plates.

(2) Analog signal processing electronics have been designed and fabricated to present the star plate measurements to digital data processing equipment in a form such that the data processing equipment can detect and document stellar proper motions.

(3) The design of the Automatic Proper Motion Scanning Machine is complete, based on the results of investigations described in this report.

(4) The design philosophy of the data processing system centered around a two stage operation--measurement to magnetic tape, and magnetic tape to computer and documentation has been worked out.

APPENDIX A

THE EFFECT OF SCAN SPOT SIZE ON IMAGE RESOLUTION

The star plate comparator may be characterized as a multichannel scanning microdensitometer. As such, it is to be expected that the resolving power of the system will depend critically on the effective size of the scan spot relative to the size of the smaller star images. A highly simplified analysis of the interaction between the scan spot and the image is presented below. The goals are twofold. First, a model is to be developed which can be used to estimate spot size from the experimentally observed interaction of the scan spot with a set of images of known characteristics. Second, the general changes in star image transmittance profiles introduced by the use of a scan spot of finite size are to be predicted approximately.

Two major simplifying assumptions have been made. All diffraction effects have been neglected. This would be a serious defect if it were important to match the fine detail of the image profiles obtained with the scanner against those found in this analysis. However, only the general limitations imposed by finite spot size are required here. The mathematical simplifications which result from the use of a first order model without diffraction make it possible to investigate a large number of cases at relatively little cost. The additional assumption is that the scan spot corresponds to a flat field of illumination. This is probably satisfied quite well since the optical collection system in the scanner looks only at the center portion of the total laser beam striking the star plate.

To the unaided eye, the stellar images on plates taken with the 48-inch Schmidt camera at the Palomar Observatory appear both sharp and circular over the entire field of view; this is one of the great advantages of this telescope. However, on a magnified scale, the individual images are "blurred" over a finite region by the astronomical seeing. The grain density distribution in

the images of faint stars is probably two-dimensional Gaussian* (on a scale which is large compared with the size of the individual grains). The transmittance T is related to the local grain density G by the relation

$$\frac{1}{a} \log \frac{1}{T} = G \qquad \text{(A-1)}$$

where a is the average grain cross section. The transmittance profile of a faint star image on an original plate is thus probably of the form

$$T(r) = e^{-a(G_o e^{-r^2/2\sigma^2} + G_B)} \qquad \text{(A-2)}$$

where G_o is the central grain density of the image alone, G_B is the "fog" level density due to the overall background illumination of the night sky, and r is the distance from the center of the image (a circular image is postulated). Equation (A-2) is further complicated in the case of brighter stars where photographic saturation is encountered or in the case of images on duplicate plates where two or more additional photographic processes are involved.

On a still finer scale, the images are simply collections of exposed photographic grains. Investigation on this level (resolution sharper than two or three microns) would result in a wildly discontinuous transmittance as the image is scanned--at least for faint images or near the edges of bright images. In any event, the profiles of actual photographic star images are quite complex and difficult to characterize. Indeed, the experimental information available** for the transmittance characteristics of these images was itself obtained with a densitometer employing a spot of finite size (30 microns

---

* Edward J. Farrell, "Information Content of Photographic Star Images," a paper presented at the 1965 Annual Meeting, Optical Society of America, October 5-8, 1965, Philadelphia, Pennsylvania.

** See Appendix III, a proposal to the National Aeronautics and Space Administration for an Automatic Proper Motion Survey. Department of Astronomy, University of Minnesota.

diameter). Thus, an image of simpler and more precisely described shape would be advantageous for use in evaluating the performance of the scanner.

A. The Apparent Transmittance of an Opaque Circular Image as "Seen" by a Circular Scan Spot

An image whose transmittance has the form of a circular "well" may be characterized by the following equations:

$$\begin{aligned} T(r) &= T_i \qquad r < r_i, \\ &= T_b \qquad r > r_i, \end{aligned} \tag{A-3}$$

where T_i is the transmittance within the image circle and T_b is the background transmittance outside of the images. Here "transmittance" refers to the ratio of transmitted light to incident light for an infinitesimal spot of light; the image is treated as continuous rather than grainy. If $T_i = 0.0$ and $T_b = 1.0$, the image is just a round opaque dot on an otherwise clear field.

If an ideal image corresponding to Equation (A-3) were scanned by a finite spot of light, it is clear that the scan spot would not be occulted discontinuously but would require a finite time to disappear and reappear. Of course, if the spot is larger than the image, it is never completely eclipsed.

If the spot has radius r_s and is centered at a distance ξ from the center of the image (at the origin), the apparent transmittance is just,

$$T_a(\xi, r_s) = \frac{1}{\pi r_s^2} \int\int_{\text{scan spot}} T(r)\, dA_{\text{spot}} \,. \tag{A-4}$$

For the image considered here, this reduces to

$$T_a(\xi, r_s) = \frac{1}{\pi r_s^2} (T_i - T_b)\, A_{com} + T_b \tag{A-5}$$

where A_{com} is obviously just the area of overlap between the spot and the image. A number of cases arise here and these are illustrated in Figure A.1 for $r_s \leq r_i$ and Figure A.2 for $r_s \geq r_i$. The distinction between Ib and Ic (or IIb and IIc) is merely a matter of convenience in the integral evaluation of A_{com}. In Ib and IIb it is easier to evaluate $(\pi r_s^2 - A_{com})$; in Ic and IIc, A_{com} is evaluated directly. The integrations are all straightforward and in many cases, trivial. The results are as follows:

Case I, $r_s \leq r_i$:

$$T_a(\xi, r_s) = T_i, \qquad 0 \leq \xi \leq (r_i - r_s);$$

$$= T_i + (T_b - T_i)\frac{A'}{\pi r_s^2}, \qquad (r_i - r_s) < \xi \leq \sqrt{r_i^2 - r_s^2};$$

$$= T_b + (T_i - T_b)\frac{A}{\pi r_s^2}, \qquad \sqrt{r_i^2 - r_s^2} < \xi < (r_i + r_s);$$

$$= T_b, \qquad (r_i + r_s) \leq \xi;$$

$$A' = \xi\, y_o + r_s^2 \sin^{-1}\frac{y_o}{r_s} - r_i^2 \sin^{-1}\frac{y_o}{r_i};$$

$$A = -\xi\, y_o + r_s^2 \sin^{-1}\frac{y_o}{r_s} + r_i^2 \sin^{-1}\frac{y_o}{r_i};$$

$$y_o = \frac{1}{2\xi}\sqrt{2\, r_i^2\, \xi^2 + 2\, r_s^2\, \xi^2 + 2\, r_i^2\, r_s^2 - \xi^4 - r_i^4 - r_s^4}.$$

(A-6)

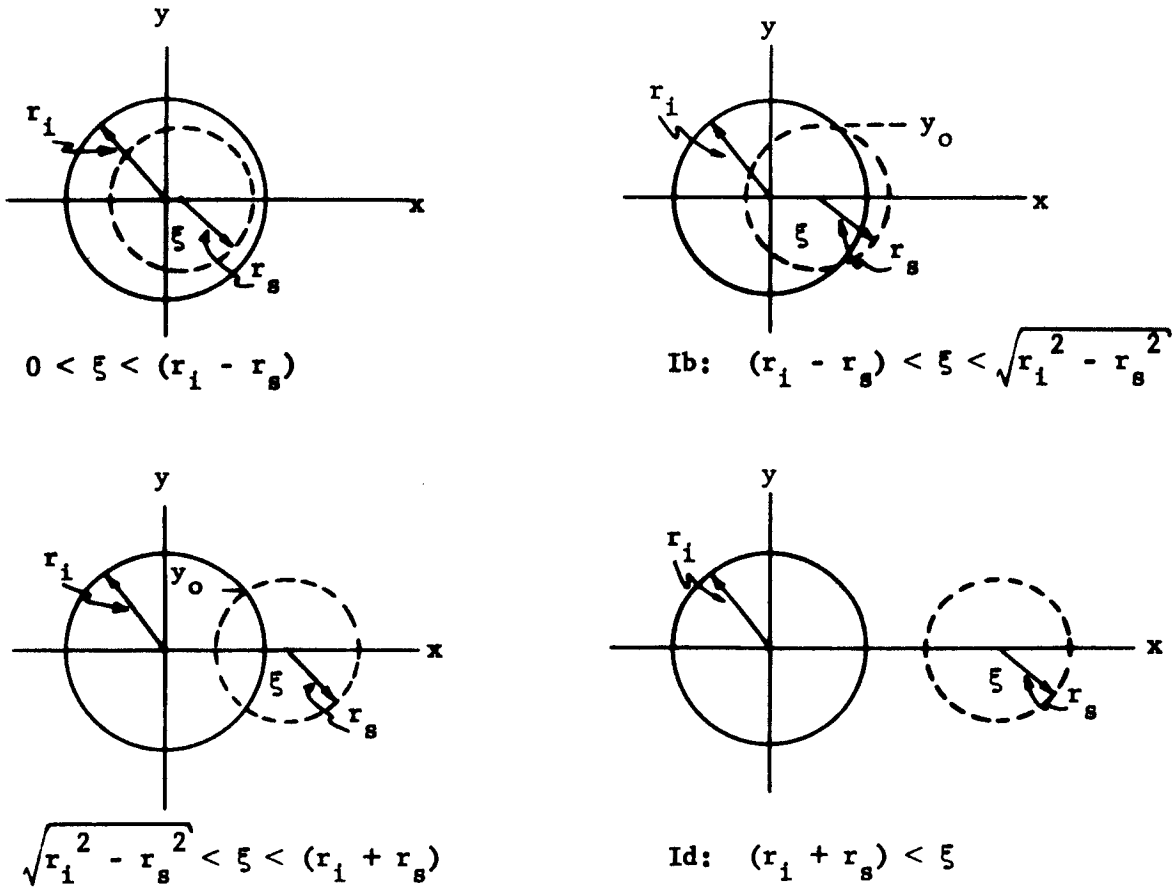

Figure A.1: Geometrical Relations for the Image - Spot Interaction Problem; $r_s \leq r_i$. A circular opaque image of radius r_i (solid circle) is "seen" by a circular spot of transmitted light of radius r_s (dashed circle). The image is centered at (x, y) =(0,0); the spot is centered at (x, y) = (ξ, 0)

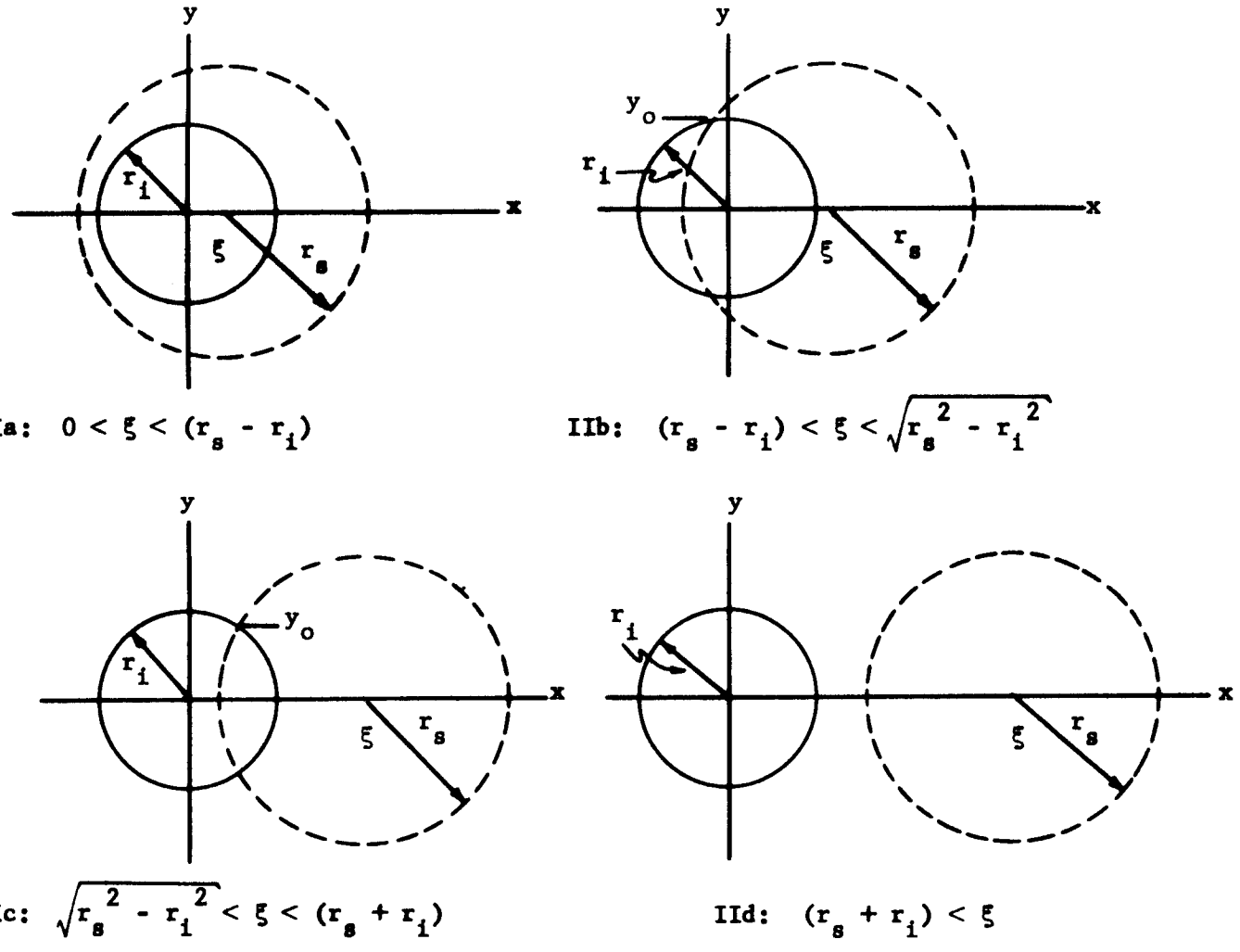

Figure A.2: Geometrical Relations for the Image - Spot Interaction Problem; $r_s > r_i$. A circular opaque image of radius r_i (solid circle) is "seen" by a circular spot of transmitted light of radius r_s (dashed circle). The image is centered at (x,y) = (0,0); the spot is centered at (x,y) = (ξ,0)

Case II, $r_s > r_i$:

$$T_a(\xi, r_s) = T_b + (T_i - T_b)\frac{r_i^2}{r_s^2}, \qquad 0 \le \xi \le (r_s - r_i);$$

$$= T_b + (T_i - T_b)\left(r_i^2 - \frac{A''}{\pi}\right)\frac{1}{r_s^2}, \quad (r_s - r_i) < \xi \le \sqrt{r_s^2 - r_i^2};$$

$$= T_b + (T_i - T_b)\frac{A}{\pi r_s^2}, \quad \sqrt{r_s^2 - r_i^2} < \xi < (r_s + r_i);$$

$$= T_b \qquad (r_s + r_i) \le \xi;$$

$$A'' = \xi\, y_0 - r_s^2 \sin^{-1}\frac{y_o}{r_s} + r_i^2 \sin^{-1}\frac{y_o}{r_i};$$

$$A = -\xi\, y_o + r_s^2 \sin^{-1}\frac{y_o}{r_s} + r_i^2 \sin^{-1}\frac{y_o}{r_i};$$

$$y_o = \frac{1}{2\xi}\sqrt{2\, r_i^2\, \xi^2 + 2\, r_s^2\, \xi^2 + 2\, r_i^2\, r_s^2 - \xi^4 - r_i^4 - r_s^4}.$$

(A-7)

It is clear from inspection of Equations (A-6) and (A-7) that the variable parts of $T_a(\xi, r_s)$ depend only on the difference $(T_b - T_i)$ and on the ratios ξ/r_i and r_s/r_i. Thus, a set of "universal" curves can be generated by choosing ($T_b = 1.0$, $T_i = 0.0$) and plotting $T_a(\xi/d_i)$ with d_s/d_i as a parameter. The image and spot diameters (d_i and d_s) were chosen rather than the corresponding radii because it was felt that it is somewhat easier to obtain a visual estimate of the total width of an image. A family of curves based on Equations (A-6) and (A-7) is presented as Figure 5 in the main text above.

Note there that the transmittance profile degrades very rapidly for $d_s/d_i > 1$. In effect, the image is then being used to interrogate the size of the scan spot.

B. Estimate of Scan Spot Size for the Engineering Test Model Scanner

A series of calibrated opaque circular dots on a clear field has been prepared by Franz Ucko using photoreduction techniques developed for semiconductor etching and photoetched circuit work. These images, which range in diameter from 10 microns to 160 microns, have been observed and measured under a microscope. Under sufficient magnification to show distinctly the fuzziness of a typical star plate image, the 10 micron dot appears as a sharp round image. The plate containing the series of dots was inserted in one channel of the engineering test model star plate machine and the x-axis position--governed by the lead screw--was adjusted manually to give a maximum signal for each dot as it was transited by the flying spot scanning in the y direction. The resultant amplified video output from the photomultiplier is shown in Figure A.3 for six of the dots. The microscopically measured diameters are given as d_i; the diameters as measured across the central graticle line of the video trace are given as d_v.

In light of the rather crude measurements obtainable from the oscillograms, the agreement between the d_i and corresponding d_v is excellent. The generally steep sides and sharp lower corners on the video traces of all but the smallest dots indicate that the system detects the details of the image with relatively little distortion. The positive going peaks on each side of the image are probably caused by diffraction.

Figure A.4 shows apparent transmittance profiles calculated on the basis of Equations (A-6) and (A-7) for a fixed scan spot diameter, $d_s = 22.5$ microns, and image diameters corresponding to those of Figure A.3. The match between these results is very good. Note that if d_s is increased to 25 microns, the predicted peak of the trace for the $d_i = 20$ micron dot would come at

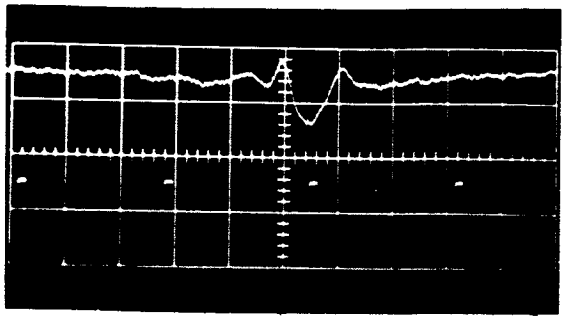

$d_i = 10\mu$

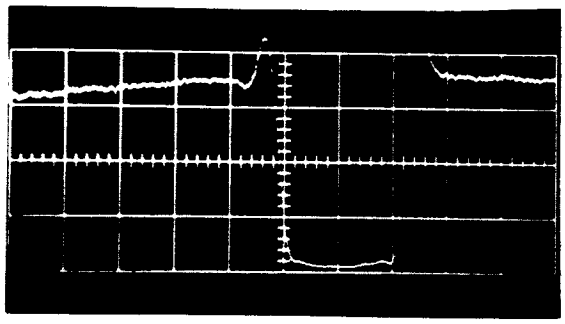

$d_i = 80\mu$; $d_v = 84\mu$

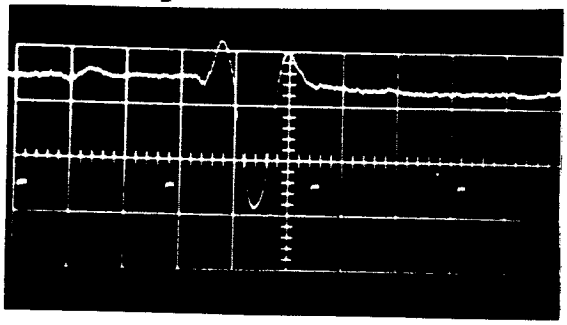

$d_i = 20\mu$; $d_v = 18\mu$

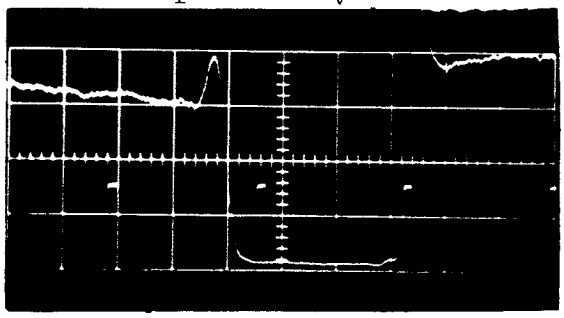

$d_i = 120\mu$; $d_v = 122\mu$

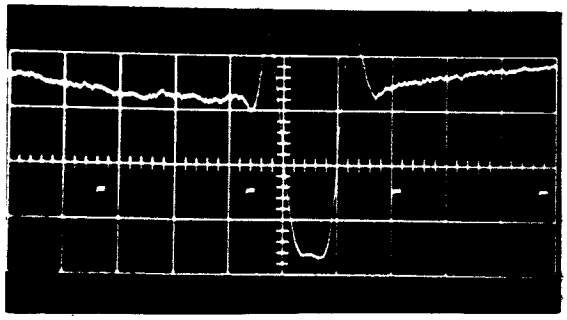

$d_i = 40\mu$; $d_v = 35\mu$

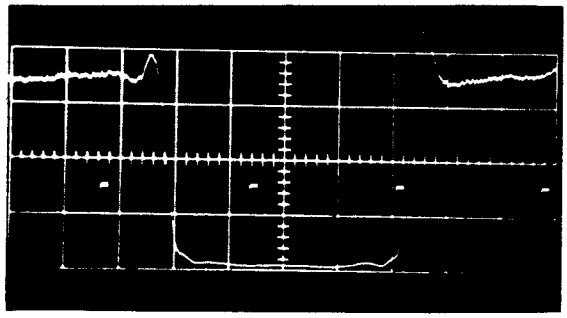

$d_i = 160\mu$; $d_v = 164\mu$

d_i = diameter of opaque circular image

d_v = image diameter measured on video trace

Figure A.3: Experimental Scans of Various Calibrated Opaque Circular Images. The oscillograms were obtained from the amplified video output of the photomultiplier in one channel of the engineering test model star plate scanner. The bright dashes are derived pulses from a reference reticle in the other channel of the scanner; the distance between the leading edges of successive dashes corresponds to a scan length of 100μ on the image plate.

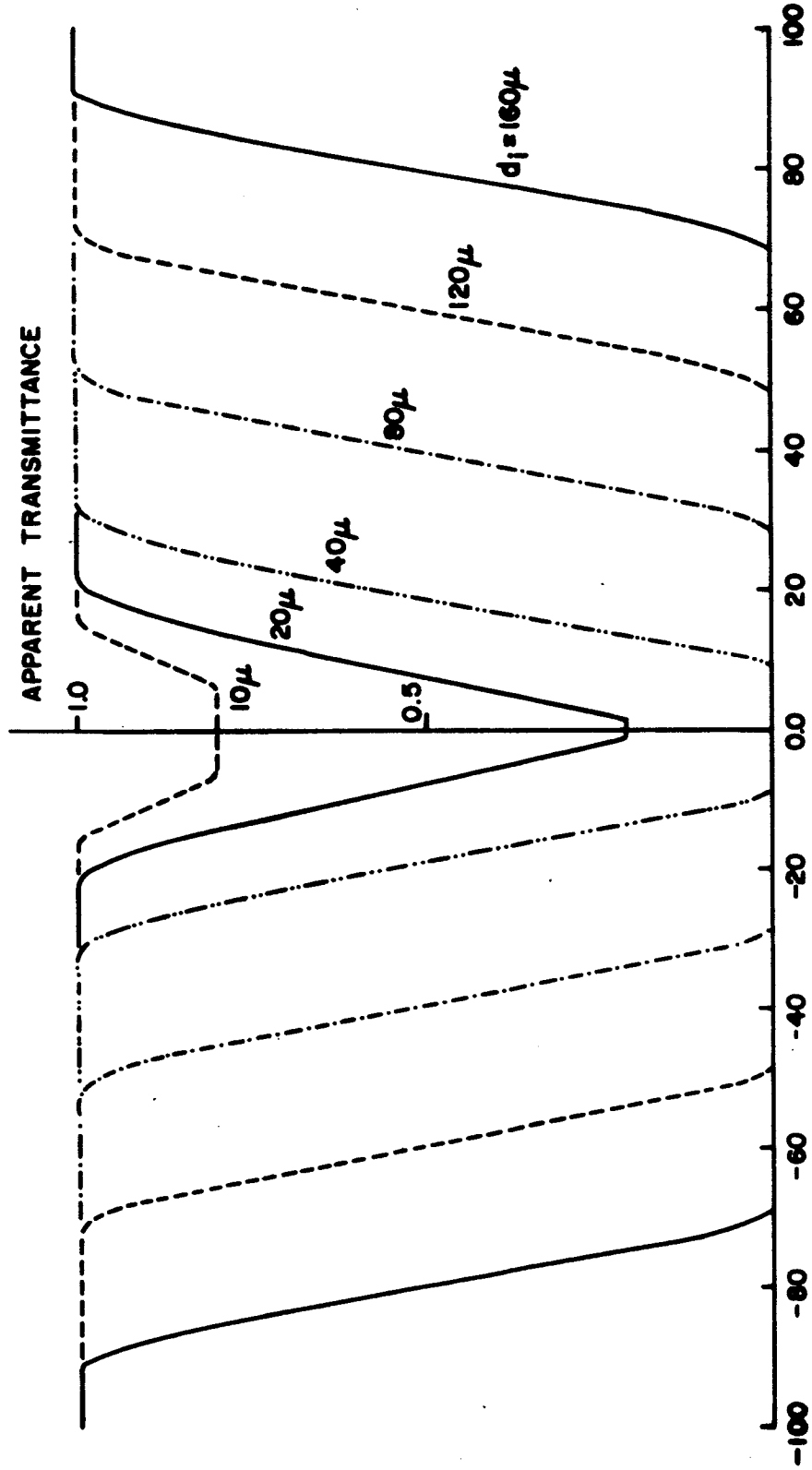

Figure A.4: Calculated Scan Profiles for the Calibrated Opaque Circular Images. The spot diameter is fixed at d_s = 22.5 microns. Compare with the experimental results in Figure A.3.

$T_a(0, 25) = 0.36$--a value somewhat too large to match the experimental trace. On the other hand, if $d_s = 20$ microns, the predicted peak would be $T_a(0, 20) = 0.0$--a value too small to match the observed video. Note also that the trace for the 10 micron dot shows a very shallow pulse coming down from the background and that the width at the base is just slightly less than that for the 20 micron dot--the scan spot is being interrogated by the image. Although a precise determination of the scan spot diameter from these traces would undoubtedly require a correction for diffraction and for minute photographic edge effects in the opaque dots, the present treatment does seem to give adequate and consistent results.

C. The Apparent Transmittance of a Star-Like Image Profile

In principle, the apparent transmittance of a star image as seen by a finite scan spot can be obtained by carrying out the integrations in Equation (A-4) with T(r) given by the expression in (A-2). However, the procedure is analytically intractable. Furthermore, it is not sufficiently certain that Equation (A-2) is correct to justify extensive and costly numerical calculations using this form of T(r) as a basis.

The photodensitometer studies of Evensen and Mohr* provide empriical image profiles for the Palomar-Schmidt plates and these curves can be approximated by simple combinations of polynomials whose integrals can be evaluated in closed form. The following functional form will be chosen, rather arbitrarily, to represent the transmittance of a starlike image:

$$T(r) = T_i + T_2 r^2 \qquad r < \rho,$$

$$= T_b + T_{-4} \frac{1}{r^4} \qquad r > \rho. \tag{A-8}$$

---

* See Appendix III, a proposal to the National Aeronautic and Space Administration for an Automatic Proper Motion Survey, Department of Astronomy, University of Minnesota.

It is clear that the transmittance is automatically equal to T_i at $r = 0$ and to T_b as $r \to \infty$. One would also expect a reasonably smooth profile (on a scale large compared with the grain size) and this can be achieved by requiring T and its first derivative to be continuous at $r = \rho$. Thus,

$$T(\rho) = T_i + T_2 \rho^2 = T_b + T_{-4} \frac{1}{\rho^4} \tag{A-9}$$

and

$$\frac{dT}{dr}\Big|_{\rho} = 2 T_2 \rho = -4 T_{-4} \frac{1}{\rho^5} \tag{A-10}$$

Together, these equations imply the following relations:

$$T_2 = \frac{2(T_b - T_i)}{3 \rho^2},$$

$$T_{-4} = \frac{(T_i - T_b)}{3} \rho^4 . \tag{A-11}$$

Hence,

$$T(r) = T_i + 2/3(T_b - T_i) \frac{r^2}{\rho^2}, \qquad r \leq \rho$$

$$T_b + 1/3(T_i - T_b) \frac{\rho^4}{r^4} . \qquad r > \rho \tag{A-12}$$

The transmittance T(r) from (A-12) can be substituted into the integral in (A-4) to obtain the apparent transmittance. The various cases which arise are again illustrated by Figures A.1 and A.2. In general, if the spot is centered a distance ξ from the image center (origin), then

$$T_a(\xi, r_s) = \frac{1}{\pi r_s^2} \left(\int\int_A T(r)\, d A_{spot} + \int\int_{A'} T(r)\, d A_{spot} \right) , \tag{A-13}$$

where A is the area of the spot in which $r \leq \rho$ (i.e., the overlap with the central portion of the image) and A' is the area of the spot where $r > \rho$. Direct evaluation of Equation (A-13) when both A and A' are non-zero is not obvious. However, Stoke's theorem,

$$\int_{A_o}\int (\nabla \times \bar{F}) \cdot \hat{n}\, dA = \oint_{C_o} \bar{F} \cdot \hat{t}\, d_s, \tag{A-14}$$

may be applied to transform each term from a surface integration over A_o to a line integral around the boundary C_o of the surface. The appropriate substitutions are as follows:

$$\bar{F} = \frac{r^3}{4}\hat{\theta}, \quad \nabla \times \bar{F} = r^2 \hat{k}, \quad r < \rho; \tag{A-15}$$

$$\bar{F} = -\frac{1}{2r^3}\hat{\theta}, \quad \nabla \times \bar{F} = \frac{\hat{k}}{r^4}, \quad r > \rho. \tag{A-16}$$

With the transformation given by Equations (A-14) with (A-15) and (A-16), all integrals encountered in the evaluation of (A-13) are changed into forms which are listed in a typical table of indefinite integrals. The procedure is then straightforward, but somewhat lengthy. It yields,

$$T_a(\xi, r_s) = T_i + (T_b - T_i)\frac{2\xi^2 + r_s^2}{3\rho^2}, \quad 0 \leq \xi \leq (\rho - r_s);$$

$$= T_b - (T_b - T_i)\left(\frac{\rho^2}{r_s^2} - \frac{1}{3}\frac{\rho^4}{(r_s^2 - \xi^2)^2}\right), \quad 0 \leq \xi \leq (r_s - \rho);$$

$$= T_i + (T_b - T_i)\left(\frac{2\xi^2 + r_s^2}{3\rho^2} + \frac{1}{\pi}F\right), \quad |\rho - r_s| < \xi < (\rho + r_s);$$

$$= T_b - (T_b - T_i)\frac{\rho^4}{3(\xi^2 - r_s^2)^2}, \quad (\rho + r_s) \leq \xi;$$

$$F = \left\{\left(1 - \frac{r_s^2}{\rho^2}\right) \cos^{-1} \frac{\rho^2 - 2r_s^2}{2 r_s^2} - \frac{\rho^2}{r_s^2} \cos^{-1} \frac{\rho}{2 r_s}\right.$$

$$\left. + \frac{\rho^4 + 5 \rho^2 r_s^2 - 6 r_s^4}{12 \rho r_s^4} \sqrt{4 r_s^2 - \rho^2}\right\} \quad \text{if } \frac{\rho}{2} < \xi \equiv r_s;$$

$$F = \left\{\frac{3\rho^2 - 2\xi^2 - r_s^2}{3 \rho^2} \cos^{-1}\left(\frac{\rho^2 - \xi^2 - r_s^2}{2 \xi r_s}\right) - \frac{\rho^2}{r_s^2} \cos^{-1}\left(\frac{\xi^2 + \rho^2 - r_s^2}{2\xi\rho}\right)\right.$$

$$- \frac{2 \rho^4}{3(\xi^2 - r_s^2)2} \tan^{-1}\left(\frac{\xi - r_s}{\xi + r_s} \sqrt{\frac{(\xi + r_s)^2 - \rho^2}{\rho^2 - (\xi - r_s)^2}}\right)$$

$$+ \frac{(5\rho^2 r_s^2 - 5r_s^4 - 2\rho^4) + (4r_s^2 - 5\rho^2)\xi^2 + \xi^4}{12\rho^2 r_s^2 (r_s^2 - \xi^2)}$$

$$\left. \times \sqrt{4\rho^2 r_s^2 - (\rho^2 + r_s^2 - \xi^2)^2}\right\} . \qquad \text{(A-17)}$$

A plot of the Evensen and Mohr data for the image of an 18^{th} magnitude star on an original plate is shown as the solid line in Figure A.5. These results were obtained using a microdensitometer with a spot diameter of 30 microns (r_s = 15 microns). It was also found that $T_b = 0.1$ on a typical original plate--i.e., the plate is heavily fogged. With these values for r_s and T_b, and an estimate of ρ = 45 microns, Equation (A-17) was used to find T_i. Comparison of the empirical curve with the curve resulting from Equation (A-17) with a 30 micron spot diameter (the dashed curve in Figure A.5)

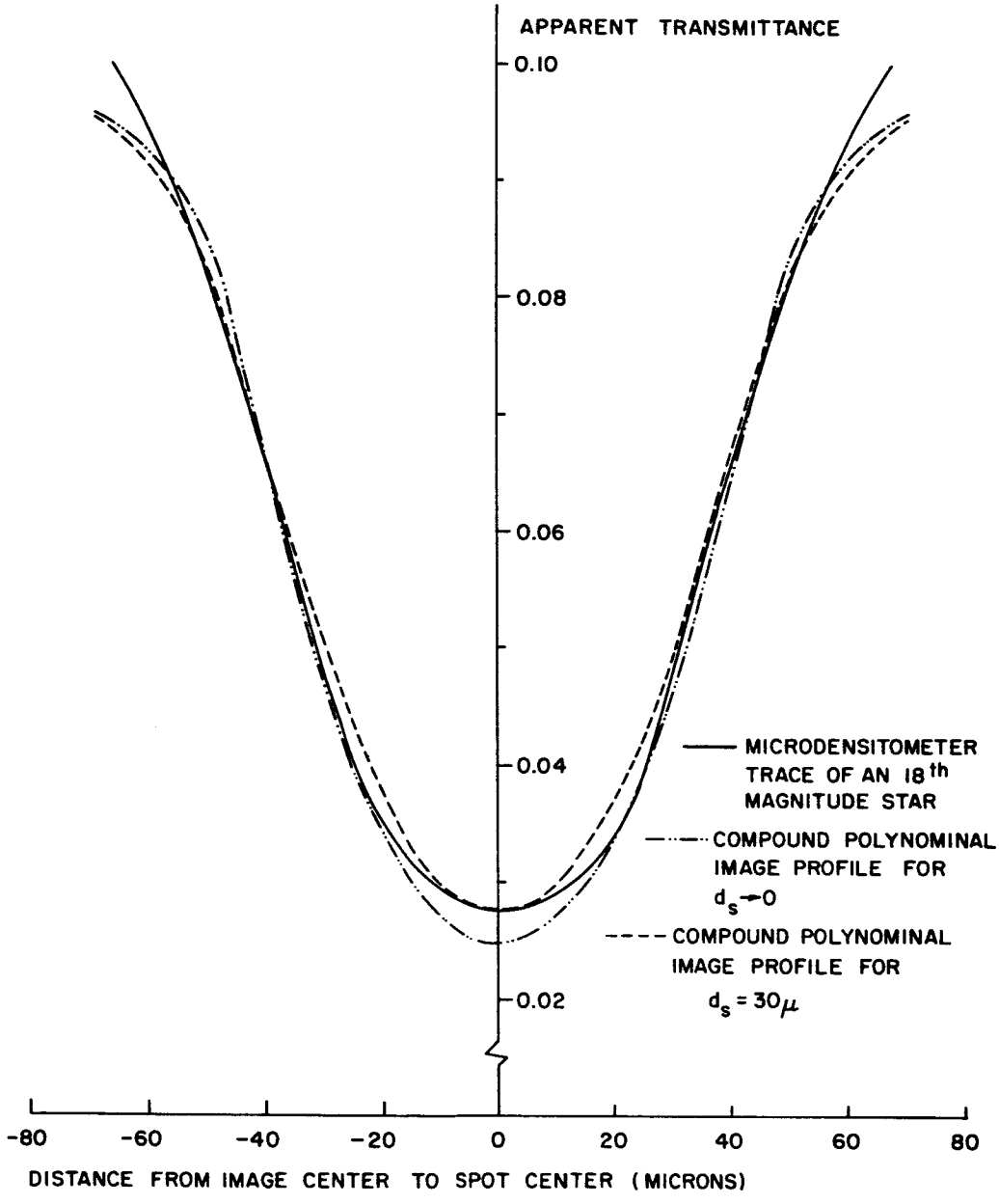

Figure A.5: Compound polynomial approximation to the transmittance profile of a photographic star image. The experimental microdensitometer trace corresponds to the image of an 18th magnitude star on a new original plate taken with the Palomar 48" Schmidt telescope. The parameters for the compound polynomial image are $T_b = 0.1$ (background transmittance), $T_i = 0.0248$ (transmittance at the image center), and $\rho = 45$ microns (the image "radius").

reveals reasonably good agreement. The transmittance profile for a zero diameter spot, $T_a(\xi, 0) = T(\xi)$, is also shown in Figure A.5.

This set of image parameters ($\rho = 45$ microns, $T_i = 0.0248$, $T_b = 0.1$) was then used to study the effect of varying the spot size for a given image. The results are presented as Figure 6 of the main text. Note particularly that the curve for $d_s/2\rho = 0.25$ corresponds to a spot diameter of 22.5 microns, the approximate value inferred from the video profiles of the calibrated opaque dots. The change in the transmittance profile of the star image due to the finite size of the spot is very small.

Even near the limiting magnitude for the red plates ($m_{red} = 20$) the images have diameters of the order of 30 microns. It is clear from the curves in Figure 6 and from the experimental results on the calibrated dots (Figure A.3) that the scanner should have the capability of consistently resolving images near this limit. Indeed, this system presents the possibility of varying the scan spot size (by changing the collecting aperture) and thereby tuning for a maximum ratio of the signal from a limiting magnitude star image to the "noise" from the grain background (see Figures 32 and 33 in the main text). The scanner appears to have the necessary margin of sensitivity; investigation of this attractive possibility is continuing.

DIGITAL DATA PROCESSING IN THE PROPER MOTION SURVEY: IMAGE RECONSTRUCTION

CDC TM-9564-4

Automatic Proper Motion Survey

May 16, 1966

Prepared by:

A. E. LaBonte

Aerospace Research
Research Division
CONTROL DATA CORPORATION
8100 34th Avenue South
Minneapolis, Minnesota 55440

DIGITAL DATA PROCESSING IN THE PROPER MOTION SURVEY: IMAGE RECONSTRUCTION

I. INTRODUCTION

The data processing problem for the proper motion survey--under the assumption that the raw data represents individual transits--can be divided into the following seven tasks:

1. Gathering of scan data (transit coordinates) in computer compatible form;
2. Transformation of data from sequencial order along scan path to group order by image;
3. Reduction of transit groups to "area" and "centroid" of corresponding images;
4. Pairing of images from old and new plates;
5. Computation of plate-to-plate alignment transformation from stars with negligible motion;
6. Calculation of proper motions;
7. Determination of stellar magnitudes for motion stars. Tasks 1 through 3 constitute a reconstruction of the plate patterns in the computer; tasks 4 through 7 represent the detection and measurement of proper motions.

It is obvious that the collection of raw transit data from the plate interrogation instrumentation (task 1) must be done with a digital system which is sufficiently fast to transfer the data from the scanner to magnetic tape without being saturated by the rates expected from a typical plate pair. However, because of (1) the variations in the data rate and (2) the idle time associated with plate setup, it seems clear that the digital portion of the real-time scanning system should otherwise be as small and inexpensive as possible. It would be very uneconomical to have a large, sophisticated computer system wait for data from the scanner. Furthermore, a premium is paid for machine time when a direct tie-in (instant turnaround) is required.

In contrast with the minimal system which is desirable for transit data gathering, the remaining tasks (2 to 7) should be done on the largest, fastest computer on which time is available. This assertion is based on two conditions. First, the computer has complete control over its data input rate (from tape) and can therefore operate very close to its maximum efficiency. Second, the cost per computation decreases as the size and speed of the computer system increases provided that the comparison among systems is made when each is operating at its full capability.

Under certain circumstances, however, these guidelines may be modified. In particular, there are some attractive alternatives for task 2--the scan-to-image data sort. The relations of this "sort" problem to the adjacent tasks--data gathering and image reconstruction--and a possible technique for handling the sort on a computer are the subjects covered by the remainder of this note.

II. RELATION BETWEEN THE SCAN-TO-IMAGE SORT AND THE TRANSIT-TO-IMAGE REDUCTION

The problems of sorting and grouping the transits by image (task 2) and of reducing each transit group to a star centroid and size (task 3) can be solved concurrently; each new transit is absorbed in the corresponding partial-image sums as soon as it is properly identified. Thus, the data is transformed directly from a sequence of transits ordered by their occurrence along the scan path to a set of sum triplets

$$\left\{ \sum_i x_{ij} \Delta y_{ij} \;,\; \sum_i (2y_{ij} + \Delta y_{ij}) \Delta y_{ij} \;,\; \sum_i \Delta y_{ij} \right\}$$

i = scan number, j = image number

where each triplet characterizes the location and magnitude of a "stellar"* image. If the entire process of image formation were to be done in digital form and in real time as the data is gathered, then this direct transformation

---

* In addition to individual stars, other astronomical objects which have somewhat star-like images--e.g. galaxies--and plate flaws will be represented in the set of triplets.

of raw scan data into images is probably the only approach which is remotely possible. However, the size and speed of the computer system required, even for this idealized procedure, appear to be economically prohibitive. It seems appropriate, therefore, to drop the requirement of real-time digital image formation.

Relaxation of the on-line constraints removes the physical limitations on the time available for reconstructing the images (although economic limitations remain). There are then a number of advantages to be gained by separating the scan-to-image transit sort from the area-centroid calculations. This separation permits, for example, the following operations to be interposed between the data sort and the image reconstruction.

1. The image group can be tested for "missed" transits and for systematic growth and decay of transit size as the image is swept out (through the group of transits).
2. Simple tests of image shape--intended primarily to differentiate between circular and non-circular images--may be carried out on the transit groups. This type of testing obviously cannot be done after the data has been reduced to centroids and isophotal areas.
3. The transit groups can be separated quickly according to size. This is significant because the structure of the larger images (star magnitude $m < 13$) can be quite complex; diffraction spikes and blazes are among the more common of these structural features.

It is hoped that most of the transit groups will be complete and will represent simple, nearly-circular images. Such "standard" groups may be reduced to areas and centroids directly by employing the corresponding discrete sum expressions:

$$\bar{A} = \Delta x \sum_{\substack{\text{transit} \\ \text{group}}} \Delta y_i \qquad (1)$$

$$\bar{x}_o = \sum_{\substack{\text{transit} \\ \text{group}}} x_i \Delta y_i \Big/ \sum_{\substack{\text{transit} \\ \text{group}}} \Delta y_i \qquad (2)$$

$$\bar{y}_o = \sum_{\substack{\text{transit} \\ \text{group}}} (2y_i + \Delta y_i) \Delta y_i \Big/ \sum_{\substack{\text{transit} \\ \text{group}}} 2\Delta y_i \,. \qquad (3)$$

The remaining image groups will require special treatment. If a group is missing a few transits (relative to the total number in the group) but is otherwise well behaved (i.e., represents a nearly circular image) then the image center and radius may be found by fitting the existing data to a circle in a least squares sense. Alternatively, the missing transits may be artificially generated; the augmented data (actual plus inferred transits) may then be used in Equations (1) to (3). If the data for a group fails to meet the criteria for a systematic variation of transit size across the image or the simple symmetry (circularity) checks, then the possibility of overlapping simple images (leading to "dumbbell", trefoil, or even higher order shape) should be tested. If the group cannot be resolved into a set of centers of two or more individual stars, then it should be deleted from the list with a brief output of its plate location and gross characteristics. This procedure should remove some spurious data from the star lists--information about such objects as non-circular galaxies, irregular emulsion flaws, plate scratches, and asteroid trails. Finally, images of bright stars which are known to be complex a priori can be given appropriate special treatment directly without first going through some of the initial tests which are used to classify the smaller images.

The main observations discussed in this section may be summarized in terms of the following two guidelines:

1. The "raw" data should first be reassembled so that all transits corresponding to a particular image are grouped together before any further processing is attempted.

2. The transit groups should then be reduced to star locations and sizes using a hierarchy of tests designed to distinguish between single stellar images, overlapping compound stellar images, and non-stellar images. In order to conserve machine time, the higher order (more complex) tests are to be applied to an image group only if it fails to meet criteria which designates it as complete and nearly circular--an isolated star-like image.

The second guideline is illustrated by the partial flow charts presented in Figure 1.

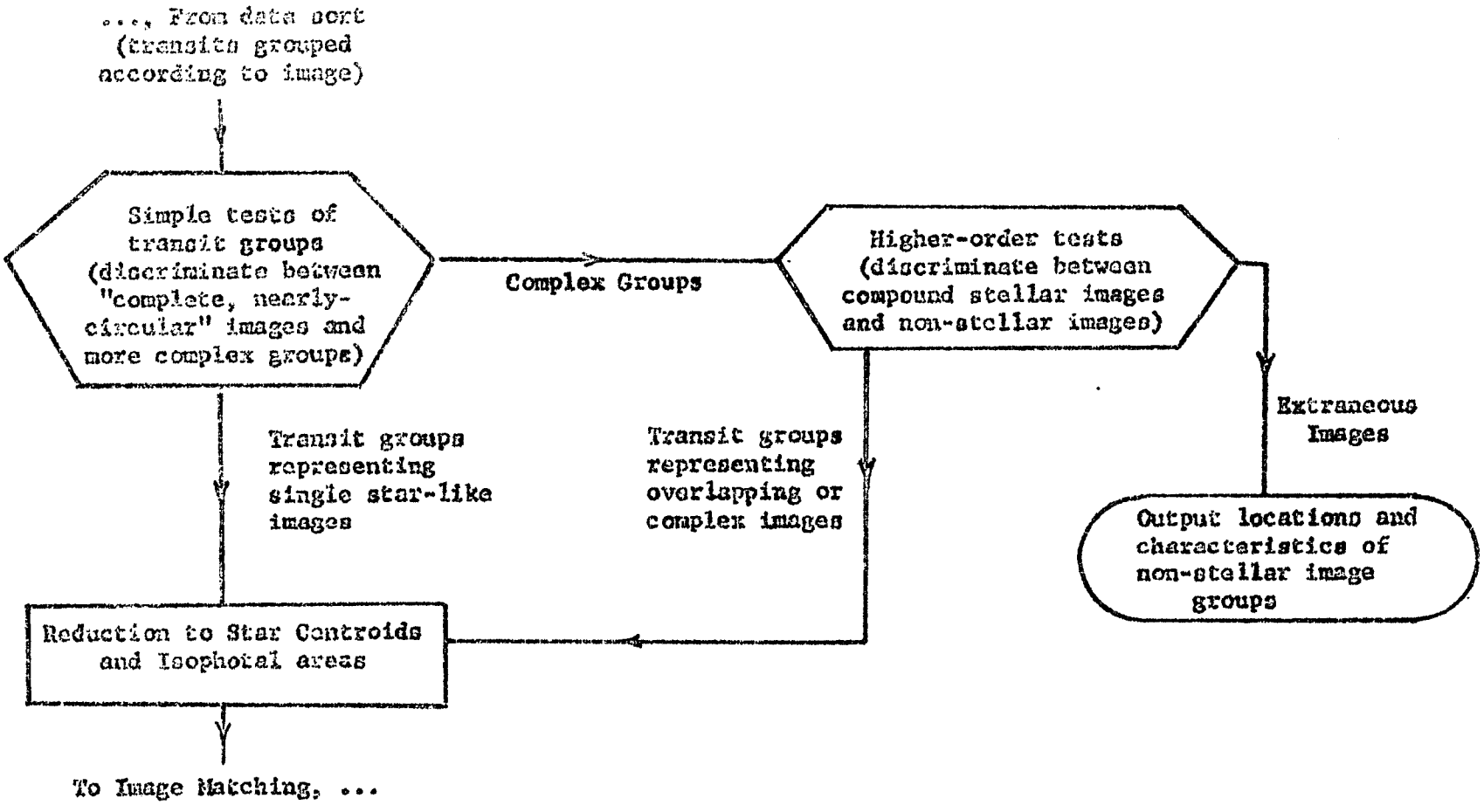

a. General Structure

Figure 1: Flow Charts for Reduction from Transit Groups to Image Centroids and Isophotal Areas

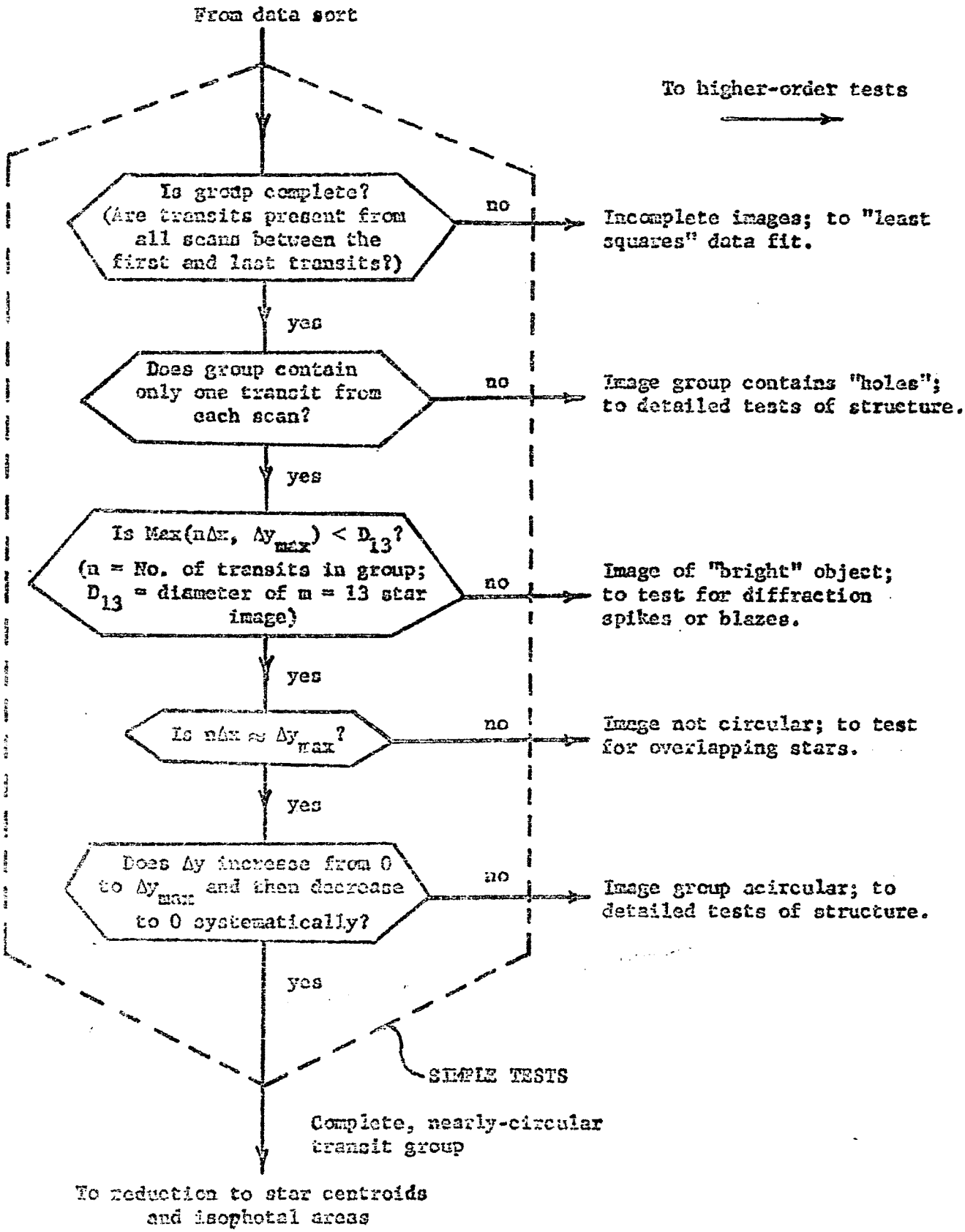

b. Some Representative "Simple" Tests of Transit Groups

Figure 1 (Continued)

III. RELATION BETWEEN TRANSIT DATA COLLECTION AND SCAN-TO-IMAGE TRANSIT SORT

The transits are collected from the star plates in the order in which they occur along the scan path. As was pointed out above, the digital data-gathering system must receive the transits from the scanner at a variable rate and dump them out on magnetic tape at a uniform rate. The buffer which is interposed between the scanner and the tape must contain, therefore, an extensive temporary memory and a fairly sophisticated control section to monitor both the input/output to this memory and the operation of the tape units. Indeed, the executive section must have the control capabilities of the central processor in small computer--a production item which can probably be obtained in less time and at less expense than would be involved in the design and fabrication of a special purpose executive. However, the processor from a small computer would automatically include arithmetic and logical capabilities along with its control functions. Thus, if such a computer is sufficiently fast and properly organized, it may be possible to sort the data into image groups before it is dumped to tape. A real-time sort of this form should result in a significant saving in computer time on the large system (probably the University's new 6600) which is to complete the reduction from transit data to proper motions.

It seems unlikely that a small system could undertake any of the remaining tasks (3 to 7) on a real time basis during the scan. (See the discussions of time requirements in TM-9564-3, where a large CDC 3600 is postulated). Figure 2, then, represents the two most probable alternatives for separating the processing tasks. The final section of this memo presents a scheme for sorting the data which is largely independent of this division. Hence, a selection between the Modes A and B in Figure 2 is not a critical point in the system development.

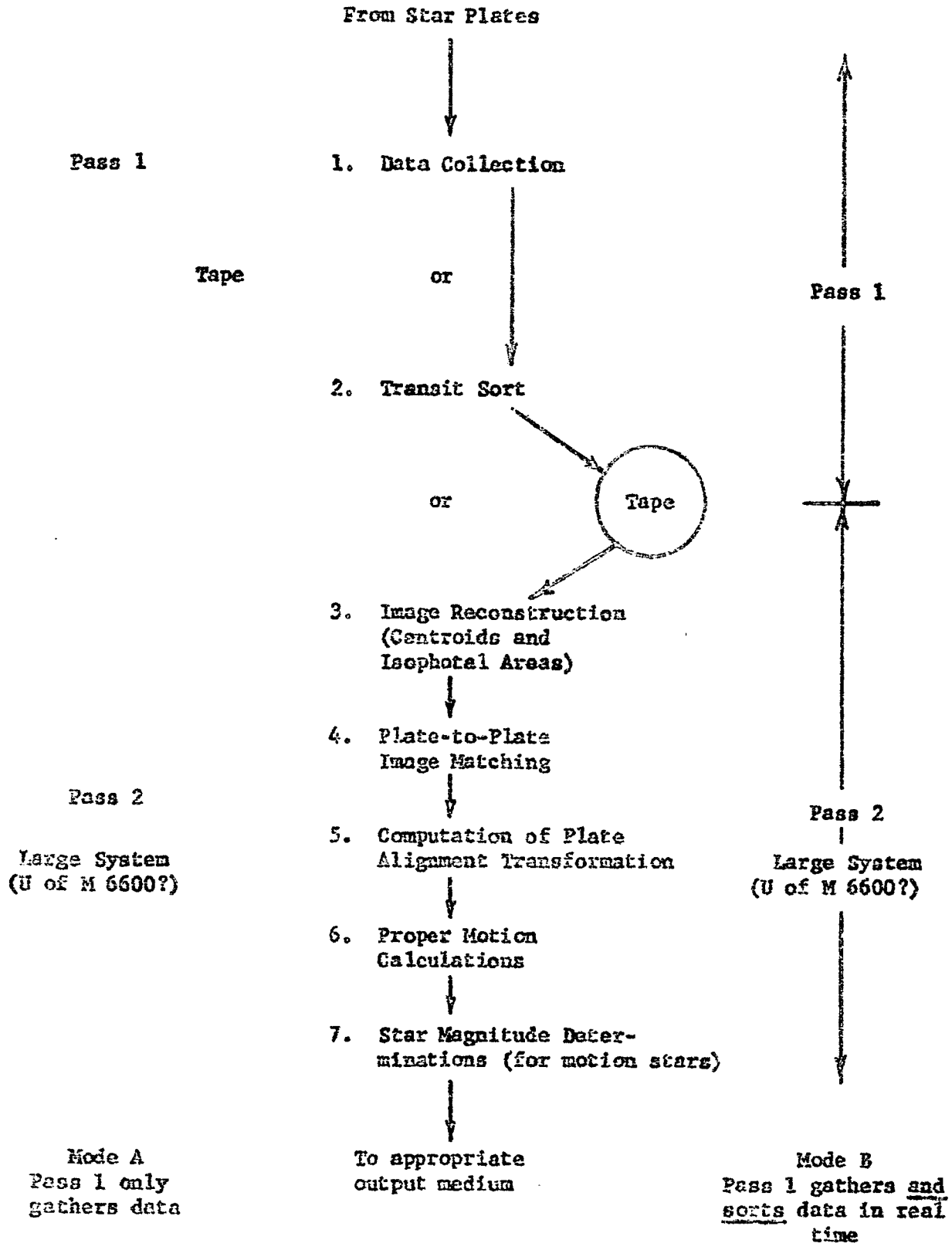

Figure 2: Most Probable Alternatives for the Division of the Digital Data Processing Tasks in the Proper Motion Survey

IV. OUTLINE OF A SCHEME FOR SORTING THE TRANSIT DATA FROM SEQUENTIAL SCAN-PATH ORDER INTO IMAGE GROUPS

A schematic representation of the scan pattern on a star plate is presented in Figure 3a. The scan path along each individual scan is from bottom to top and the scans are stepped sequentially from left to right. Each time an image is transited (and detected), the following data is sent to the collection system: $2y_{ingress}(s,i)$, $\Delta y(s,i)$, $x(s,i)$. Here (s,i) are indices which denote, respectively, the particular scan and the particular image to which the transit corresponds. The total data from each transit can be compressed into a single 47-bit word (a 48-bit word is more convenient for existing machines--see TM-9564-3, page 6) which will be denoted as $T(s,i)$.

The transits are stored into the "deep" memory of the computer in the serial order in which they occur along the scan path. In a smaller machine, each transit will require a number of computer words--e.g., four words per transit in a 12-bit machine such as a CDC 160A, three words per transit in a 16-bit machine such as a CDC 1700, etc.--where the address of the first word in $T(s,i)$ is denoted by $A(s,i)$. The transits will be stored such that there is an additional blank computer word following each $T(s,i)$. During the data sort, this blank word will be filled by a "chaining" address which gives the location--probably $A(s-1,i)$--of the transit which immediately precedes $T(s,i)$ in image i. In addition to the T's and corresponding blanks, a "start-of-scan" identifier will be sensed and stored each time a new scan begins. Figure 3b presents the conditions in "deep" memory after the data has been gathered from the scan pattern of Figure 3a.

The organization of computer memory during the scan-to-image transit sort is shown schematically in Figure 3c. The memory is broken into the following three types of sequential lists:

1. "Deep Memory" which contains the raw transit data in scan path order plus the associated cells for image "chain" addresses. This list occupies the majority of available memory space.

2. A pair of variable-length lists of partial images (PIL). The "active" PIL contains the most recent transit and its deep memory

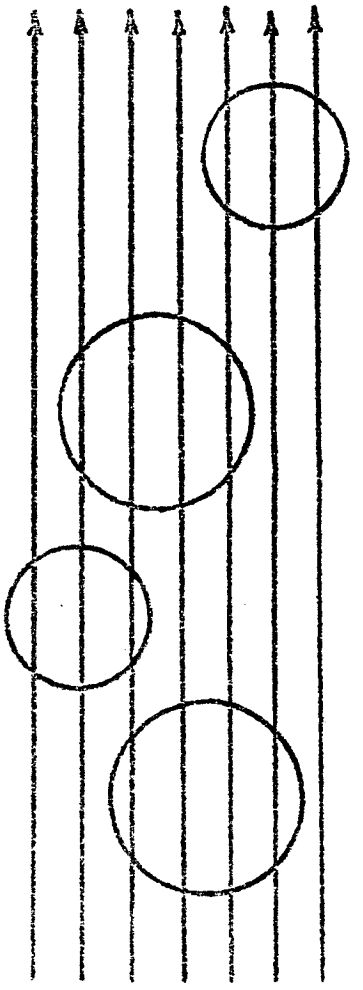

a. Schematic of Scan Pattern

T(s,i) represents the transit data obtained from image i during scan s. Each T is a 47-bit digital data word.

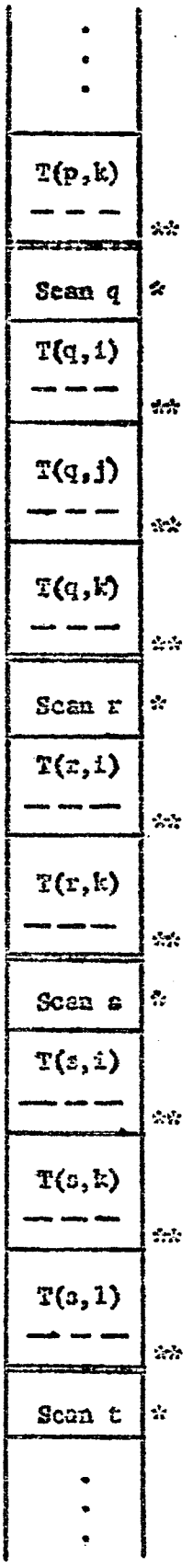

b. "Deep" memory with raw transits ordered sequentially along the scan path. Before the sort, the image index is unknown and the scan index is implied by * the start-of-scan identifier. The address of the start of data unit T(s,i) is denoted by A(s,i). A "data unit" in memory consists of a sequential group of words sufficient to contain the 47 bits of T plus a blank word** (in which a chaining address will be stored when the transits are sorted into image groups--See Figure 3c below).

Figure 3: Relations Between Scan Data, Computer Memory, and the Data Sort Procedure

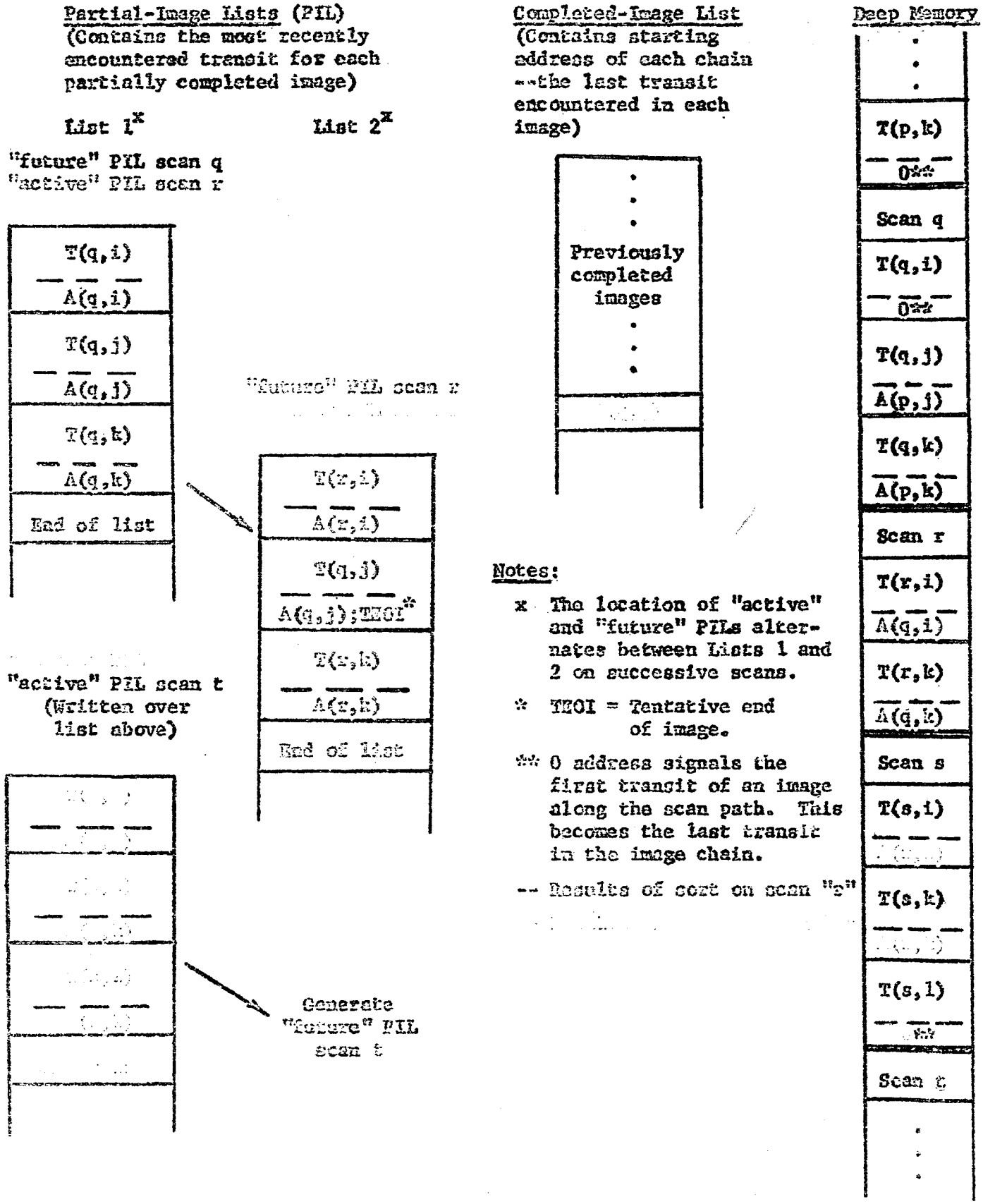

Figure 3 (Continued):
c. Schematic of Computer Organization for the Transit Sort From Sequential Scan-Path Order to Image Groups (Chains). Changes in the Computer State for Sorts on Scans "r" and "s" are Represented

address for each partially completed image chain; the transits are listed in order of increasing center ordinate. If s denotes the scan from which transits are currently being processed, the transits in the "active" PIL will be of the form T(s-1,i) or T(s-2,i). Here, transits from (s-2) will occur only if the corresponding transit of i on (s-1) was missed.

The "future" PIL contains transits (and addresses) from the current scan, T(s,i) or from the immediately previous scan, T(s-1,i). The "future" PIL from scan s becomes the "active" PIL for scan s+1; the "future" PIL for scan s+1 is then written over the old "active" PIL from scan s.

In summary, two sequential arrays (each of which is sufficiently long to absorb any anticipated partial-image list) are set aside in memory. The "active" and "future" PIL's then alternate between these two available list locations on successive scans.

3. A list of completed images which contains the "deep memory" addresses of the final transits encountered in each image. These addresses become the starting points for the image chains. For a particular image, each deep memory location in its chain contains a transit from the image and the address of the next location in the chain. The chaining process back through the transits of an image terminates when a "0" next address is encountered; the "0" is stored during the sort when the first transit of the image is encountered along the scan path.

The states of these various lists for three successive scans (q, r, and s of Figure 3a) are shown in Figure 3c. The process for generating these states is described by the flow charts in Figure 4. These charts are simplified to the extent that they presuppose that if a star transit is detected, it is approximately of the correct length and position and that it is not segmented into two or more parts along its length. However, the points at which more sophisticated tests may be inserted are indicated in the notes on the figure. The program as it stands does account for isolated, completely-missed transits of an otherwise complete image.

Although the process can be understood most thoroughly by tracing through the flow chart, a textual description of the basic decision processes is given below. The program attempts to match the next unaccounted-for (new) transit in deep memory with the next unmatched (comparison) transit in the "active" partial-image list. This attempted matching can have three possible outcomes.

1. The center of the new transit falls below the ingress of the comparison transit. The new transit is then interpreted as the start of a new image and a "0" is stored in the new transit's chaining address. The new transit and its own address are added to the "future" PIL. The next "new" transit is then brought up from deep memory; the comparison transit remains the same since it is still unmatched.

2. The center of the new transit falls between the ingress and egress of the comparison transit. The new transit is then interpreted as the continuation of the image to which the comparison transit corresponds. The address of the comparison transit is stored in the new transit's chaining address; the new transit and its own address are added to the "future" PIL. Both the next "new" transit and the next "comparison" transit are then brought up.

3. The center of the new transit falls above the egress of the comparison transit. This is interpreted as a missed transit in the image corresponding to the comparison transit. The comparison transit is tested to see if a transit was missed on the previous scan also--i.e. to see if it contains a tentative-end-of-image (TEOI) tag. If two successive transits are missed, the image is assumed to be complete and the address of the comparison transit is sent to the list of completed images. If only one transit has been missed, a TEOI tag is set with the comparison transit and this transit, its address, and the tag are transferred to the "future" PIL. The next "comparison" transit is then brought up from the "active" PIL; the new transit remains the same since it is still unaccounted for.

These three steps represent the major processing sequence. Additional branching arises when the end of the "active" PIL or the beginning of a new scan occurs. The treatment of these conditionals is included in Figure 4. Development of a more sophisticated sort procedure is not justified until some experience with actual scan data has been obtained.

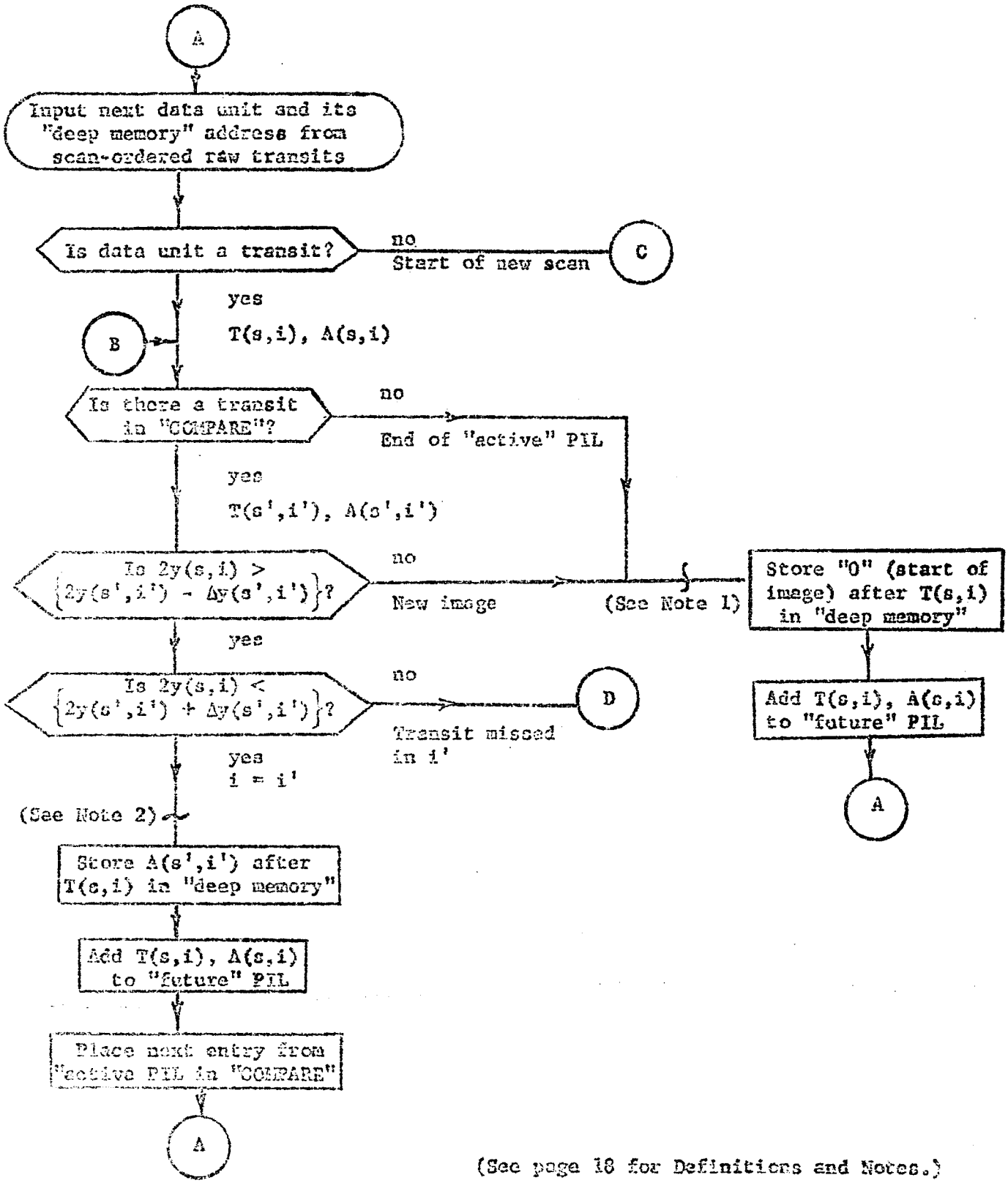

(See page 18 for Definitions and Notes.)

Figure 4: Flow Chart for Transit Sort From Scan-Path Sequential Order to Image Groups (Chains)

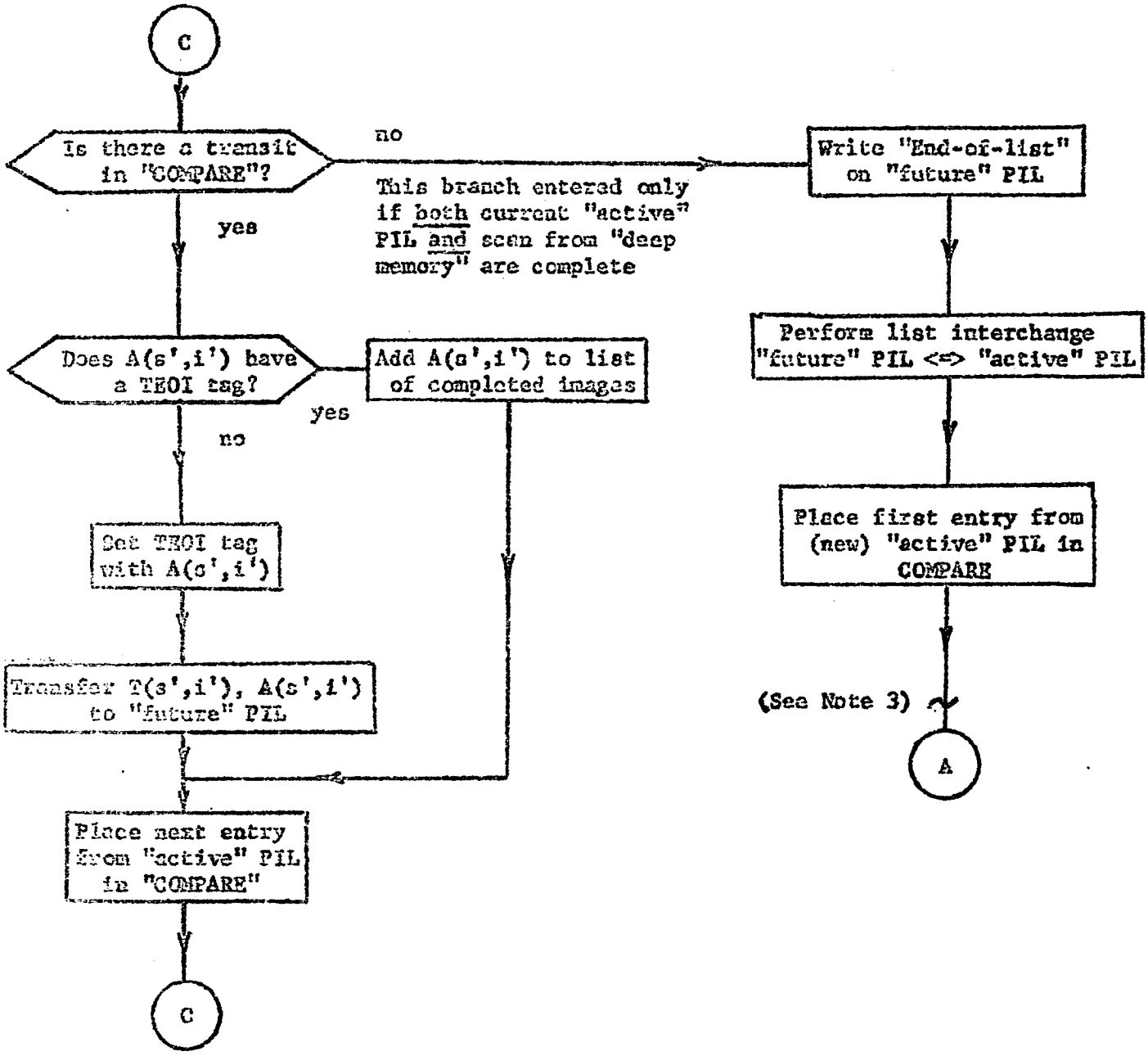

(See page 18 for Definitions and Notes)

Figure 4 (continued)

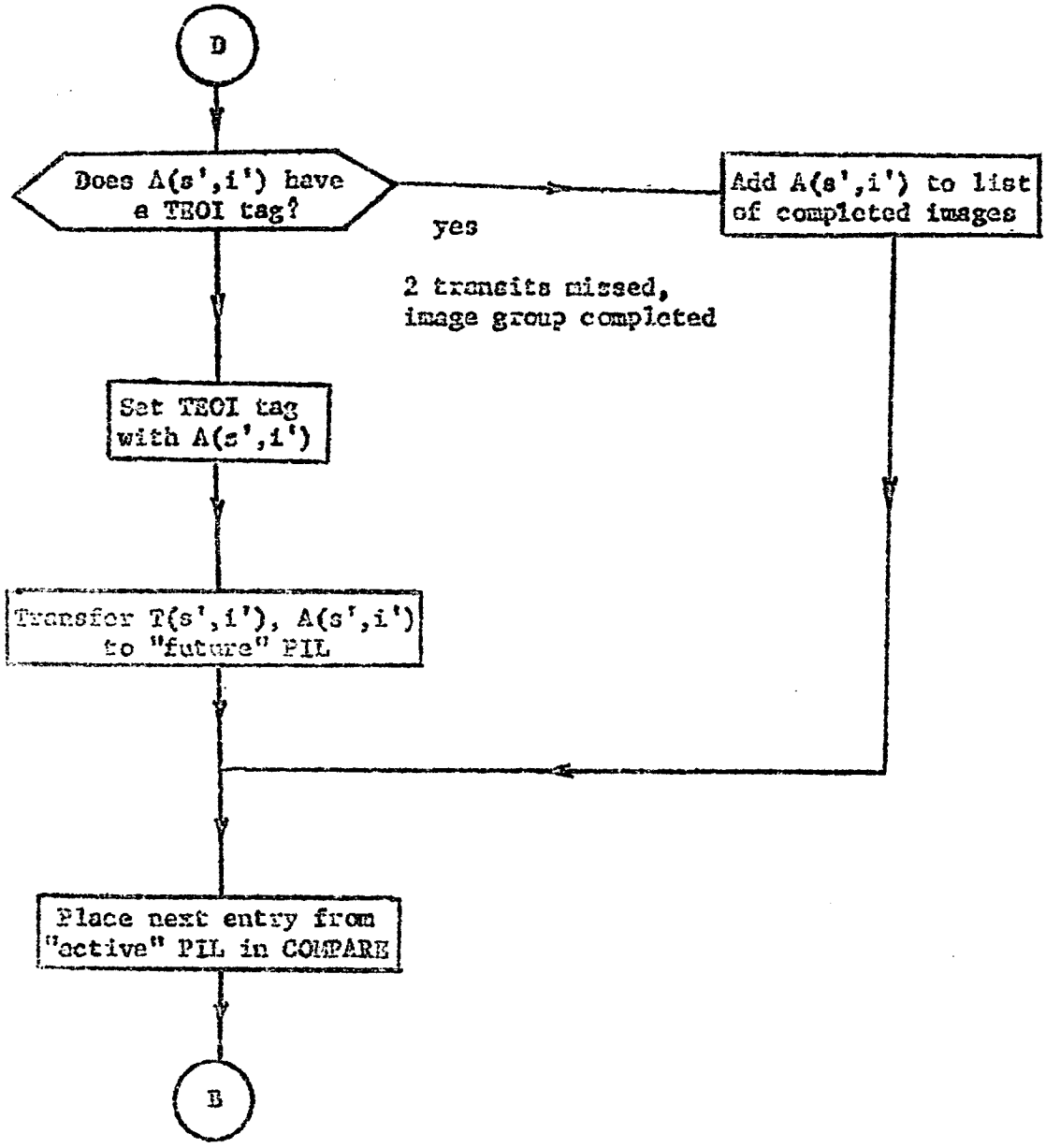

(See page 18 for Definitions and Notes.)

Figure 4 (concluded)

Definitions:

1. T(s,i): Data from transit of image i on scans
2. A(s,i): Address of start of T(s,i) in "deep memory"
3. 2y(s,i): $= 2y_{ingress}(s,i) + \Delta y(s,i)$ [Twice center ordinate of transit T(s,i)]
4. $\Delta y(s,i)$: Length of transit T(s,i)
5. "active" PIL: Active list of partial images. Contains transits from scan s-1 (and from s-2 if corresponding transits from s-1 were missed) where scan s is the current scan
6. "future" PIL: New list of partial images being generated from "active" PIL and current scan
7. COMPARE: Cell containing current entry from "active" PIL
8. TEOI: Tentative-end-of-image

Note 1: Tests for segmented transits should be inserted here.

Note 2: If a tag for missed transits is to be placed in the transit data, the following operation should be inserted here:

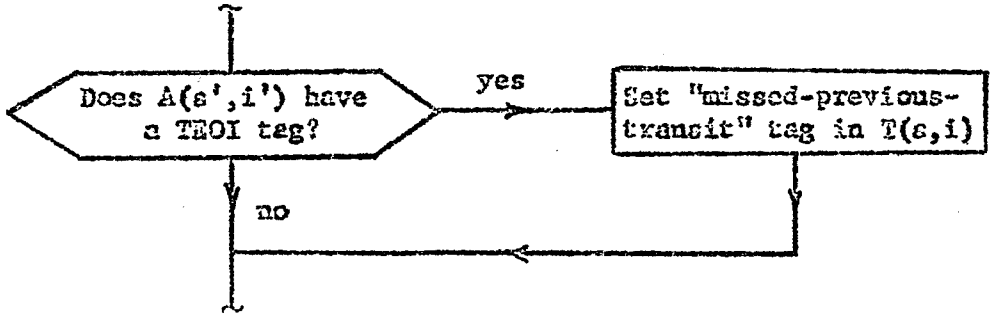

Note 3: Tests of length of list of completed images may be inserted here. Dump to tape if number exceeds some value.